Nanoscale Horizons

ROYAL SOCIETY OF CHEMISTRY

REVIEW

View Article Online
View Journal

Cite this: DOI: 10.1039/d5nh00429b

Exploring the potential of phosphorene and arsenene in plasmonic and 2D nanomaterial-based biosensing: from fundamentals to applications

Kalpana Devi P,[a] Melvin Jose K,[c] Krishna Kumar Singh,[a] Vilas H Gaidhane,[b] Neeru Sood [c] and Nikhil Bhalla *[d]

Two-dimensional nanomaterials such as phosphorene and arsenene have emerged as transformative platforms for next-generation biosensing, owing to their exceptional electronic, optical, and mechanical properties. Phosphorene, derived from black phosphorus, offers a tunable direct bandgap, high carrier mobility, and strong anisotropy, enabling highly sensitive and rapid detection of biomolecular interactions through variations in conductivity, photoluminescence, and strain. Arsenene, a structurally analogous 2D allotrope of arsenic, exhibits comparable advantages, including a direct bandgap and pronounced light–matter coupling, which facilitate precise and label-free detection across optical, electrochemical, and field-effect transistor platforms. Recent advances in plasmonic coupling, surface functionalization, and hybrid nanostructure engineering have further expanded their versatility, enabling the development of multimodal and sensor-fusion approaches that integrate electronic and photonic responses for enhanced signal transduction. This review provides a comprehensive overview of the fundamental properties, synthesis strategies, and biosensing mechanisms of phosphorene and arsenene, linking their structure–property relationships to device-level performance. We also discuss challenges related to stability, large-scale fabrication, and integration into practical diagnostic, environmental, and food-safety platforms. Overall, these 2D pnictogen nanomaterials hold immense potential to advance plasmonic and multimodal biosensing technologies, paving the way toward intelligent and adaptive next-generation diagnostic systems.

Received 20th June 2025,
Accepted 22nd October 2025

DOI: 10.1039/d5nh00429b

rsc.li/nanoscale-horizons

1. Introduction

A sensor is a piece of hardware that responds to an applied stimulus, the output of which is either electronically or optically read by the user.[1] A biosensor is a type of sensor that can detect a biochemical analyte and produce a measurable signal and the strength of the signal generated is usually proportional to the amount of analyte detected.[2,3] Biosensors can be classified based on the type of transducer used, such as electrochemical, optical, piezoelectric, thermal, field-effect transistor (FET)-based, magnetic, or acoustic wave biosensors.[3,4] Electrochemical biosensors detect electrical signals like current, voltage, or impedance,[5] while optical biosensors rely on light-based methods like fluorescence or surface plasmon resonance.[6] Piezoelectric and acoustic wave biosensors measure mass or frequency changes,[7] and thermal biosensors monitor heat variations during reactions.[8] FET-based sensors excel in charge detection, offering high sensitivity for applications like DNA and biomarker monitoring.[9] Magnetic biosensors use magnetic nanoparticles to identify analytes, ideal for immunoassays and cancer detection.[10] Biosensors are gaining prominence in diagnostic applications due to their miniaturization, which offers unique chemical and physical properties. These advancements improve the signal-to-noise ratio, enable the use of smaller sample volumes, and significantly reduce the overall cost of testing compared to traditional diagnostics.[11] Additionally, when dimensions of the biosensor are on the scale of micro/nano-length units, the surface-to-volume ratio of the sensing area increases. This makes the detecting electrode and the target biomarker of similar length

[a] Department of Physics, Birla Institute of Technology and Science, Pilani – Dubai campus, Dubai, UAE. E-mail: kalpana@dubai.bits-pilani.ac.in, singh@dubai.bits-pilani.ac.in
[b] Department of Electrical and Electronics Engineering, Birla Institute of Technology and Science, Pilani – Dubai campus, Dubai, UAE. E-mail: josemelvin1403@gmail.com, vhgaidhane@dubai.bits-pilani.ac.in
[c] Department of Biotechnology, Birla Institute of Technology and Science, Pilani – Dubai campus, Dubai, UAE. E-mail: sood@dubai.bits-pilani.ac.in
[d] Nanotechnology and Integrated Bio Engineering Centre (NIBEC), School of Engineering, Ulster University, Belfast, UK. E-mail: n.bhalla@ulster.ac.uk

scales,[12] leading to more specific and sensitive binding events.[13]

On the other hand, several nanomaterials such as nanoparticles, nanotubes, nanowires, and other nanoscale materials have been utilized to develop biosensor diagnostic devices[14–16] that are capable of detecting very minute quantities of the analyte of interest. Recently two-dimensional (2D) materials like graphene, Xenes, MXenes, transition metal dichalcogenides, and 2D pnictogens, which include group VA elements (P, As, Sb, and Bi), have gained wide consideration mainly due to their large surface-to-volume proportion and charge transfer properties.[14–17] In this review we discuss the development of biosensors using phosphorene and arsenene. Specifically, we discuss the synthesis methods of phosphorene and arsenene, presenting an in-depth discussion of their unique structural and physicochemical properties that make them promising candidates for biosensor applications. The existing applications of both phosphorene and arsenene are also provided, showing the potential of these nanomaterials to produce biosensors with exceptional sensitivity, specificity and versatility at low cost.

The 2D structures of phosphorene and arsenene provide a high surface area for biomolecule adsorption, hence increasing sensitivity. Both have tunable electronic characteristics for high-performance sensors because of their direct bandgap, which changes depending on the number of layers. These 2D sheets demonstrate outstanding carrier mobility, enabling sensitive and quick target analyte detection.[18] Functionalization is facilitated by the lone pair of electrons on phosphorus atoms,[19] which allows particular recognition components, such as DNA, enzymes, or antibodies, to attach. Arsenene's chemical reactivity makes it easier to functionalize with particular biomolecules, including enzymes, antibodies, or DNA strands, increasing the biosensor's selectivity.[20] Its direction-dependent characteristics increase its adaptability when creating extremely sensitive and targeted biosensors. Because of their relative biocompatibility, both these sheets can be used in medical diagnostics to detect biological analytes. Because of their special optoelectronic characteristics, including tunable direct bandgaps and significant light absorption throughout a broad range, from ultraviolet to near-infrared, they can respond to optical signals.[94,160] The reactive surface of phosphorene and arsenene improves biomolecule adsorption and permits accurate target analyte detection, contributing to their high sensitivity and specificity. Their superior electronic properties, such as their tunable bandgap and high carrier mobility,[96] enable quick signal transduction and a quick response time, which are crucial for real-time biosensing applications. Their adaptability also makes it possible to incorporate them into a variety of sensing platforms, including optical, electrochemical, and hybrid systems, increasing their applicability in the industrial, environmental, and medical fields.[122,170] In addition to their intrinsic electronic and optical advantages, phosphorene and arsenene can be integrated with plasmonic nanostructures, such as gold, silver, or hybrid metal–dielectric systems, to enhance local electromagnetic fields and improve biosensing sensitivity. Such plasmonic coupling enables label-free detection with enhanced signal amplification, bridging electronic and optical readouts in next-generation biosensors.

Nikhil Bhalla

In 2022, I published my first paper in Nanoscale Horizons, introducing a method to detect and generate localized surface plasmon resonance (LSPR) using frictional charges—without light or external power. I have also published three more papers in Nanoscale and was honored as a 2025 Emerging Investigator and a 2023 Outstanding Reviewer for Nanoscale Advances. Collaborating with the Nanoscale family of RSC journals has been a rewarding part of my early career. This review highlights the promise of phosphorene and arsenene in plasmonic and 2D biosensing. I look forward to continuing contributions. Congratulations to Nanoscale Horizons on its 10th anniversary!

2. Components and properties of biosensors

Biosensors comprise four major components – a bioreceptor, a transducer, signal processing electronics and a display unit as shown in Fig. 1.[3–9] A biosensor's functionality relies on its core components and performance properties. A bioreceptor is a critical element that detects and quantifies the target analyte, initiating a process called bio-recognition, where analyte binding triggers a measurable signal. This signal is then converted by the transducer into a quantifiable format. Following this, the signal undergoes amplification and digital conversion, allowing for accurate measurement and display.[4,13] The performance of a biosensor is determined by several key properties. Selectivity refers to the bioreceptor's ability to specifically recognize the target analyte amidst chemically similar compounds and contaminants, necessitating optimal selectivity for accurate detection.[5] Sensitivity, or the limit of detection, is crucial for identifying analytes present in trace amounts, especially for detecting biomarkers associated with certain medical conditions.[6] Linearity ensures that the concentration of the analyte correlates proportionally with the measurable signal. Stability reflects the biosensor's resistance to environmental perturbations, including temperature variations and bioreceptor degradation, which can negatively impact performance.[7,8,11] Finally, reproducibility determines the sensor's ability to deliver consistent and near-identical responses upon repeated exposure to the same analyte, relying on precision and accuracy.[8,9,12] These factors collectively influence a biosensor's effectiveness in detecting and quantifying target analytes.

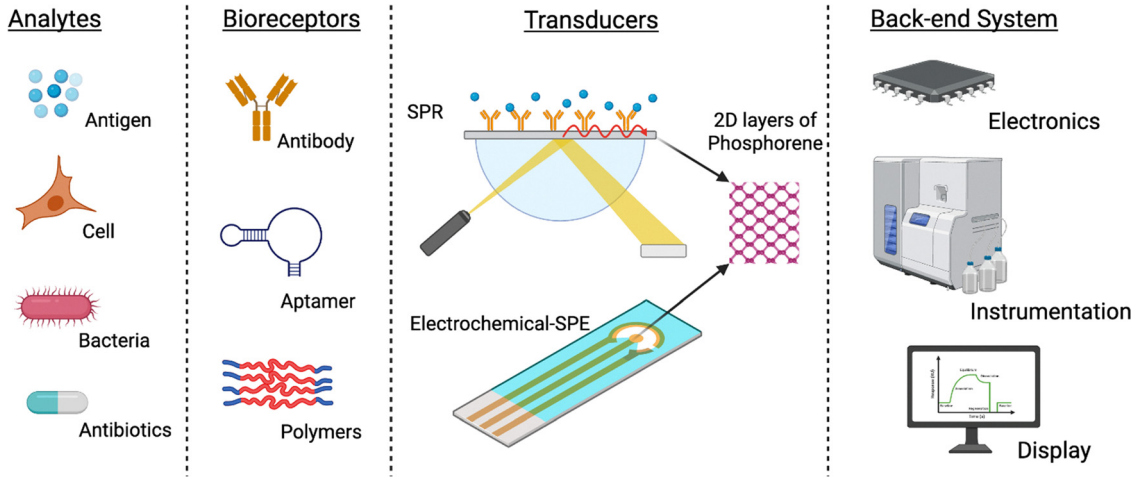

Fig. 1 Key components of biosensors showing analytes, bioreceptors, transducers and back-end systems.

3. Phosphorene

Phosphorus, the second element in Group 15 of the periodic table, is not found in pure elemental phosphorus form in the nature. Instead, phosphorus is present in minerals, mainly in the form of phosphates. Hennig Brandt discovered phosphorus in 1669 by distilling urine in a quest to find the philosopher's stone.[21] The name "Phosphorus" comes from the Greek word meaning "Light Bearer", referring to its property of glowing in the dark due to chemiluminescence. Phosphorus plays a vital role in biological systems as it forms the backbone of DNA and RNA, linking nucleotides through phosphodiester bonds.[22] Additionally, phosphorus is a key component of bones and teeth, where it is present as calcium phosphate, providing structure and strength. Its significance extends to energy transfer in cells, as it is part of ATP (adenosine triphosphate), the molecule that stores and transfers energy for biochemical processes.

Elemental phosphorus exists in several allotropes, each with distinct properties. White phosphorus is composed of P_4 tetrahedral molecules and it is highly reactive due to the angular strain in its 60° P–P bond angles. This angular strain makes it unstable and highly flammable in air; hence, it is stored under water.[23] Red phosphorus is amorphous, meaning it lacks a defined crystalline structure. Furthermore, the absence of angular strain makes it stable and less reactive than white phosphorus.[24] It is commonly used in safety matches and fireworks. Violet phosphorus, also known as Hittorf's phosphorus, has a crystalline structure formed by extended chain-like arrangements of phosphorus atoms. It is more stable than white phosphorus but less studied compared to the other allotropes.[25] Black phosphorus was discovered in 1914 by Percy Bridgman, synthesized by heating white phosphorus under high pressure. It has a layered, graphite-like structure, making it more stable than white phosphorus and red phosphorus as shown in Fig. 2.[26] It has also gained attention for its potential applications in electronics and optoelectronics due to its semiconducting properties.[27,28]

Black phosphorus known as phosphorene has structural features similar to graphite, where it is a layered material with weak van der Waals interaction between the layers, which facilitates phosphorene fabrication by exfoliation methods and micromechanical cleavage.[29] Each atom in monolayer phosphorene forms bond with three phosphorus atoms in a puckered honeycomb structure. The electronic properties of phosphorene are tunable and it is highly anisotropic along the zig-zag and armchair directions, which results in unique electrical and optical properties useful for sensing, thus making it better than the graphene layer.[29]

The first report on the successful isolation of monolayer black phosphorus using mechanical exfoliation was published in 2014 by Castellanos-Gomez *et al.*[30] Since then other techniques such as liquid exfoliation, pulsed laser deposition and plasma thinning have also been reported for black phosphorus isolation.[31–33] Its unique properties such as large hole mobility, high in-plane transport anisotropy, non-zero tunable band gap, anisotropic mechanical properties, high conductivity, and high photosensitivity contribute to different applications in sensing various biomarkers.[34,35]

3.1. Synthesis of phosphorene

The synthesis of phosphorene, however, presents unique challenges due to its instability under ambient conditions, including the natural, uncontrolled environmental factors like atmospheric composition, temperature, light exposure, and humidity, and the difficulty in achieving controlled, large-scale production. Phosphorene synthesis typically involves techniques that aim to exfoliate or thin bulk black phosphorus into individual or few-layered sheets. Several methods have been developed, including liquid-phase exfoliation, mechanical exfoliation, chemical vapor deposition (CVD), and electrochemical exfoliation. Each approach has its advantages and limitations in terms of quality, yield, and scalability. The primary goal in phosphorene synthesis is to obtain high-quality, structurally and chemically stable monolayers or few-layer phosphorene sheets while overcoming its sensitivity to

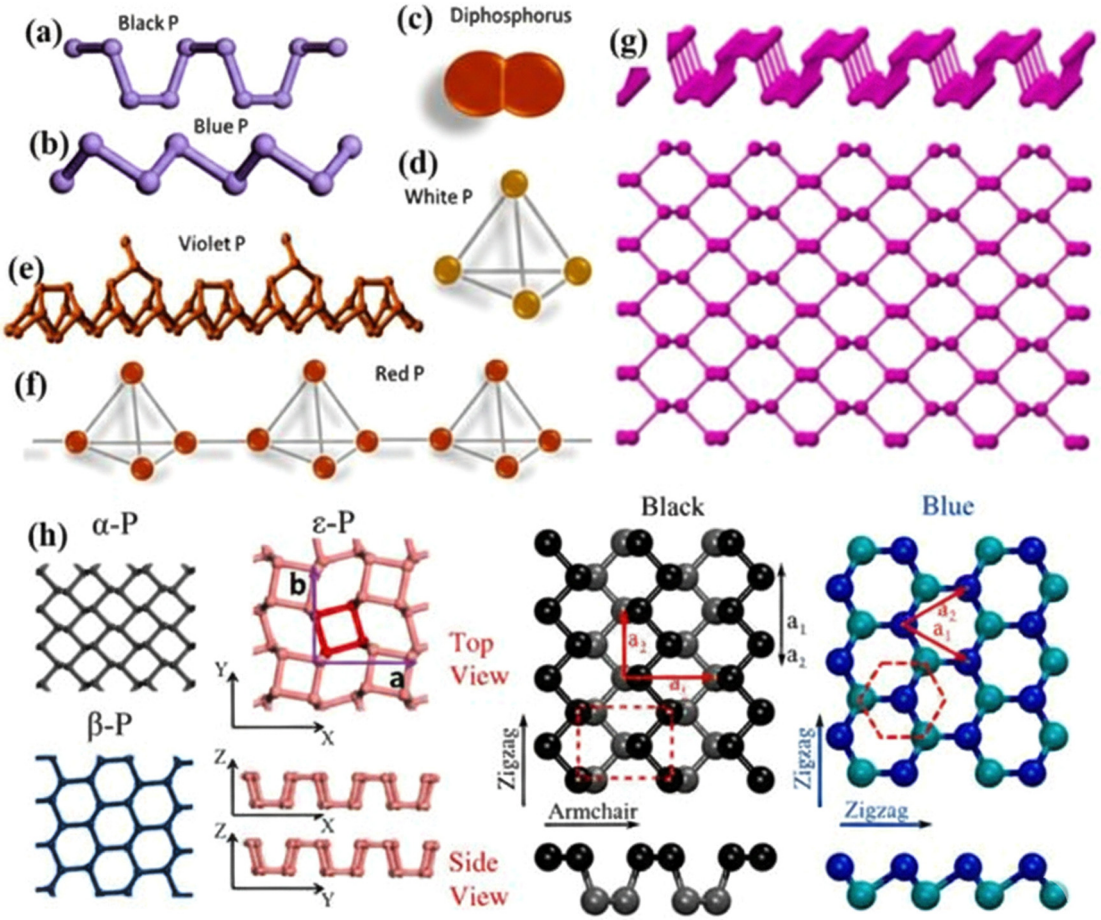

Fig. 2 (a)–(f) Various allotropes of phosphorus; this figure has been reproduced from ref. 31 with permission from Elsevier, copyright 2017. (g) Top and side views of the phosphorene crystal structure. (h) Predicted structural polymorphs of phosphorene; these figures have been reproduced from ref. 72 and 74 with permission from ACS Publications and Springer Nature, copyright 2015.

oxygen and moisture, which can lead to rapid degradation. Efforts are ongoing to refine these synthesis methods, with a focus on enhancing material stability and scalability for many practical applications.

3.1.1. Mechanical cleavage. Since bulk black phosphorus is composed of stacked layers of monolayer black phosphorus that were bound together by weak van der Waals' forces, it was theoretically possible to create 2D layers of black phosphorus from bulk black phosphorus. High-quality black phosphorus crystals are essential for successful exfoliation, typically obtained through chemical vapor transport (CVT) or high-pressure synthesis. The bulk crystal is characterized to ensure it is free of significant structural and chemical defects and has the desired properties for exfoliation. A technique similar to the "Scotch tape method" used for graphene can be employed.[37] Li *et al.* used this scotch tape-based mechanical exfoliation method for obtaining thin flakes of phosphorene, from their bulk crystals. In this process, adhesive tape is applied to the surface of a bulk crystal to adhere to its layers. When the tape is peeled away, it removes a thin layer of the material due to the weak van der Waals forces between adjacent layers in the crystal. The tape, now carrying the thin flakes, is then pressed onto a target substrate, typically a degenerately doped silicon wafer coated with a layer of thermally grown silicon dioxide (Fig. 3). This SiO_2 layer provides a high-contrast background, making it easier to identify the exfoliated flakes under an optical microscope. Additionally, the degenerately doped silicon beneath the oxide layer acts as a back gate for potential electronic measurements. The adhesive properties of the tape and the transfer process are carefully optimized to ensure that the flakes remain intact and are deposited uniformly on the substrate, resulting in high-quality monolayer or few-layer phosphorene sheets. Few layer black phosphorus can then be obtained from the tape with a thickness of 1–10 nm. These few layers of black phosphorus have the potential to be built into FETs, and when tested, they displayed a carrier mobility of 1000 $cm^2 V^{-1} s^{-1}$.[38]

Protecting few-layer BP from degradation during and after exfoliation remains challenging, as exposure to air can cause rapid oxidation. To counter this, researchers have employed several protective measures. For example, Saito *et al.* applied a resist (ZEP 520 A) immediately after exfoliation, which they later removed using *N*-methyl-2-pyrrolidone (NMP) at 323 K, followed by acetone and isopropyl alcohol rinses.[38] Luo *et al.* used a 1-μm-thick poly vinyl alcohol (PVA) layer, coated with

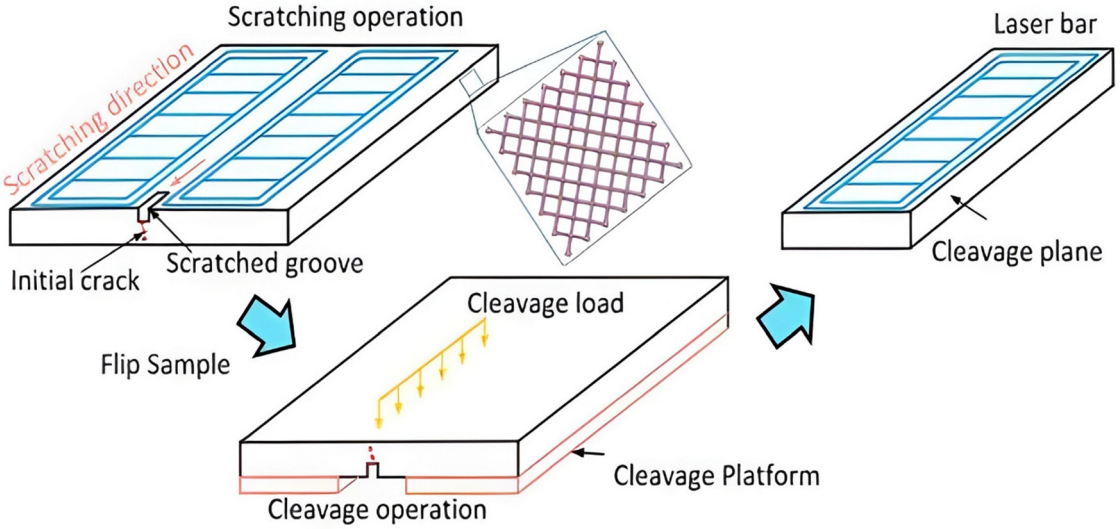

Fig. 3 Schematic sketch of mechanical cleavage, reproduced from ref. 36 with permission from Elsevier, copyright 2022.

200-nm-thick poly methyl methacrylate (PMMA), as a protective stack. The exfoliated BP was transferred to this stack, then cleaved and flipped for mounting on a glass plate. After transferring the BP to the target substrate, PMMA/PVA was dissolved in acetone and dried with nitrogen, with no baking involved to avoid oxidation.[39] The phosphorene produced through mechanical exfoliation is often of high quality by persevering its layered arrangement of atoms, with consistent thickness, minimal defects such as vacancies, dislocations, or grain boundaries, and a pristine crystal structure. The method is relatively simple and does not require sophisticated equipment, making it accessible in research laboratories. The disadvantage with this method is that it gives low yield and the fabricated black phosphorus has uncontrollable shape, thickness, and size.[40]

Castellanos-Gomez *et al.* introduced a modified approach to mechanical exfoliation to improve the deposition quality of atomically thin BP flakes. Traditional exfoliation using adhesive tape often results in a low yield of few-layer BP flakes and leaves adhesive residues, which diminishes flake quality. To enhance exfoliation results, an intermediate viscoelastic surface, such as poly-dimethyl siloxane (PDMS), was used. Bulk BP was initially cleaved multiple times with blue Nitto tape, and the tape containing thin BP crystallites was then gently pressed onto a PDMS substrate before being peeled off. Finally, the flakes on the PDMS were transferred to the target substrate by bringing the PDMS in contact with the new substrate and slowly peeling it away over 5–10 minutes.[30] Island *et al.* employed a viscoelastic stamp (Gelfilm from Gelpak) as an intermediate substrate during exfoliation, instead of traditional Scotch tape, which often leaves residues. They observed that prolonged exposure of BP flakes to air results in gradual layer-by-layer etching, thinning down to monolayer phosphorene ($\approx$0.7 nm). They concluded that, initially, air exposure induces n-type doping in BP flakes, while extended exposure leads to p-type doping due to water absorption.[41]

3.1.2. Liquid phase exfoliation. Liquid-phase exfoliation is a scalable method for producing phosphorene by dispersing bulk black phosphorus in a liquid medium and using mechanical forces to separate the layers into few-layer or monolayer phosphorene sheets. In liquid phase exfoliation (LPE), solvents are used to insert layered materials by sonicating or vortexing them, which ultimately results in the exfoliation or expansion of nano-materials and their suspension in the solvent. The choice of solvent is critical for successful exfoliation. Common solvents used include *N*-methyl-2-pyrrolidone (NMP), dimethylformamide (DMF), and isopropyl alcohol (IPA), or a mixture of these.[31,42,43] The solvent must have a surface energy close to that of phosphorene to facilitate effective exfoliation and stabilization of the exfoliated layers in suspension. The solvent should be degassed or prepared in an inert atmosphere to minimize exposure to oxygen and moisture, which can degrade phosphorene. Bulk black phosphorus is added to the selected solvent in a suitable container. The concentration of black phosphorus in the solvent typically ranges from 1 to 10 mg mL^{-1}.[44] The dispersion is subjected to sonication, where ultrasonic waves create cavitation bubbles in the liquid. The collapse of these bubbles generates localized high-pressure conditions that break apart the bulk black phosphorus into thinner layers. Sonication is usually performed using a probe sonicator or a bath sonicator, depending on the desired scale and control over the process. The sonication time can vary from a few minutes to several hours, depending on the required degree of exfoliation and the properties of the final product.[45,46,177]

After sonication, the dispersion contains a mixture of exfoliated phosphorene layers and unexfoliated or partially exfoliated black phosphorus. The dispersion is subjected to centrifugation to separate the thinner, exfoliated layers from the thicker, unexfoliated material as shown in Fig. 4.

The speed and duration of centrifugation are carefully controlled. Lower speeds (*e.g.*, 1000–5000 rpm) help separate thicker flakes, while higher speeds (*e.g.*, 10 000–20 000 rpm)

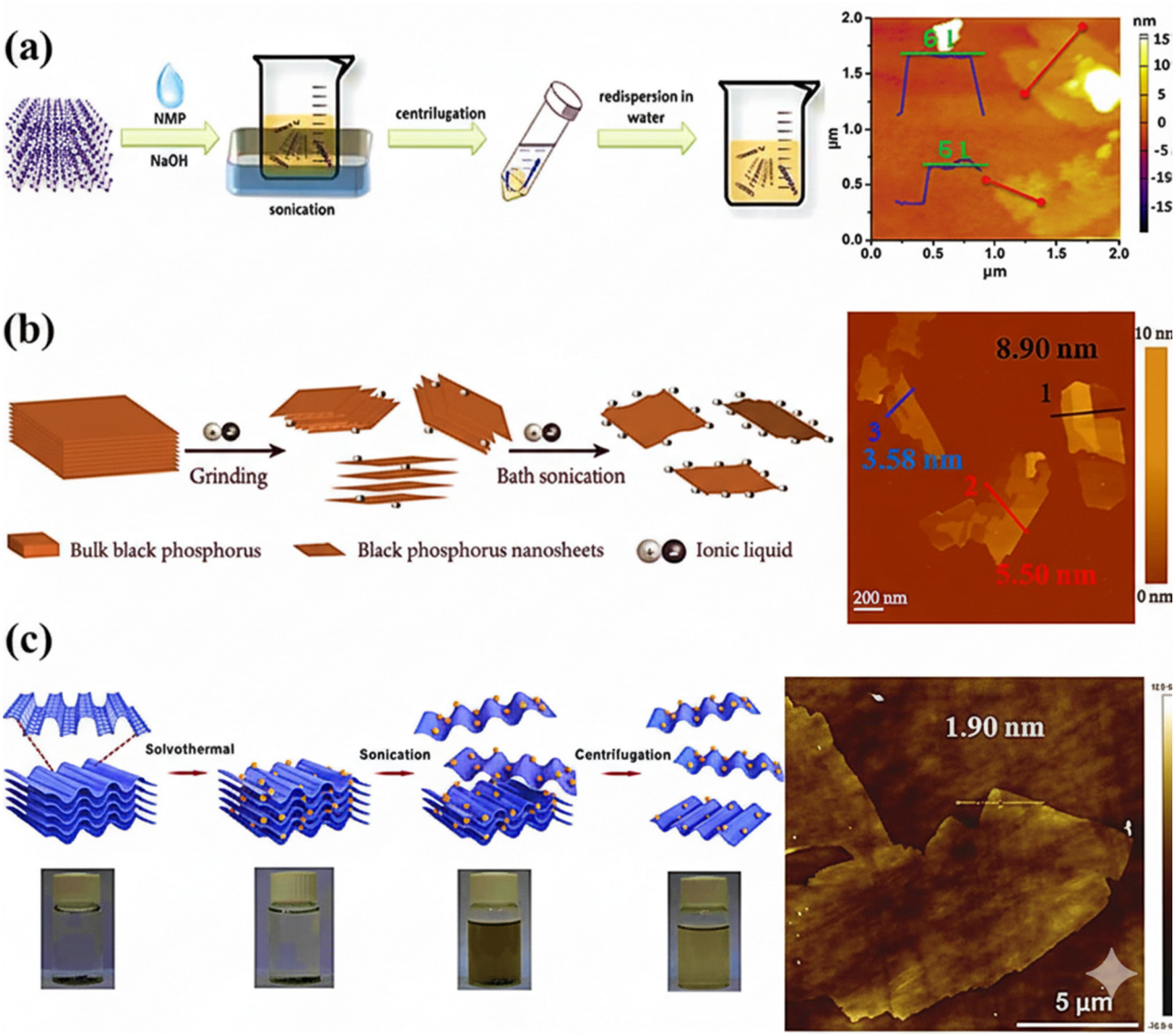

Fig. 4 (a) Schematic representation of liquid exfoliation of black phosphorus (BP) into phosphorene nanosheets in *N*-methyl-2-pyrrolidone (NMP), with NaOH as an assisting agent, and the corresponding atomic force microscopy (AFM) image of the resulting nanosheets, reproduced from ref. 43 with permission from John Wiley and Sons, copyright 2015. (b) Liquid exfoliation of BP in an ionic liquid and the corresponding AFM image of the phosphorus nanosheets. Reproduced from ref. 51 with permission from ACS Publications, copyright 2015. (c) Schematic of solvothermal-assisted liquid exfoliation of BP in acetonitrile and the corresponding AFM image of the nanosheets reproduced from ref. 48 with permission from Elsevier, copyright 2018.

isolate monolayer or few-layer phosphorene.[47,48] Various protocols of LPE that were used are listed below: Brent *et al.* suggested that it is feasible to manufacture few layer black phosphorus using bath ultrasonication of bulk black phosphorus utilizing *N*-methyl-2-pyrrolidone (NMP) as an exfoliating solvent. However, it is quite challenging to stabilize the prepared few layers of black phosphorus in any of the more common solvents.[49] Hanlon *et al.* showed that the exfoliation of bulk black phosphorus may be accomplished with the use of *N*-cyclohexyl-2-pyrrolidone (CHP) as a solvent and these few layers demonstrated stability for around 200 hours under ambient conditions.[50]

Zhao *et al.* suggested that phosphorene could be manufactured by using ionic liquids as solvents, followed by gentle grinding and sonication.[51] Bat-Erdene *et al.* presented a microwave-based two-step exfoliation method. First, bulk black phosphorus is submerged in NMP, and then the mixture is transferred to a microwave system and heated for time intervals ranging from four minutes to twenty minutes. After receiving a second treatment in the microwave for three minutes, it is then centrifuged.[52] The bulk black phosphorus is first crushed into a fine powder, then it is dissolved in acetone, and finally it is added to a wet jet mill. A piston pass and a nozzle with an aperture of 0.3 millimetres may provide forces that are sufficient to exfoliate the majority of the distributed black phosphorus. Exfoliation may be accomplished in a matter of minutes using this technique that has been presented by Castillo *et al.*[53]

3.1.3. Electrochemical exfoliation. Electrochemical exfoliation (ECE) is another method used to prepare phosphorene, involving the application of an electric potential to bulk black phosphorus in an electrolyte solution. This method can produce few-layer phosphorene sheets with a controllable number of layers and relatively high yield.[54] The basic principle here is that an electrode is fixed onto the bulk material. The electrochemical cell typically consists of a two-electrode or three-electrode setup. The working electrode is usually a piece of bulk black phosphorus. The counter electrode is often a platinum wire or carbon rod.[54,55] In a three-electrode setup, a reference electrode (like Ag/AgCl) is added to monitor the potential accurately.[56] The electrolyte solution is chosen based on its ability to facilitate the exfoliation process. Common electrolytes include aqueous solutions of acids (*e.g.*, sulfuric acid), alkali metal salts (*e.g.*, KCl and NaCl), or ionic liquids.[56,57] The concentration of the electrolyte is optimized to ensure efficient ion intercalation and exfoliation. A suitable voltage is applied between the working electrode (black phosphorus) and the counter electrode. Positive or negative ions from the electrolyte intercalate into the layered structure of black phosphorus, causing the layers to expand and weaken the van der Waals forces holding them together.[58] Counter ions are driven to the interlayer space in black phosphorus and reduce van der Waals forces. This leads to the separation of layers, as illustrated in Fig. 5.

Erande *et al.* came up with an ECE approach in which bulk black phosphorus would be used as an anode in a solution of 0.5 M sodium sulfate. The lateral diameters of the resulting nanosheets range from 5 to 10 m, while their thickness ranges from 1 to 5 nm. The ions of sulfate operate as counter ions in this situation. A mobility of 7.3 $cm^2 V^{-1} s^{-1}$ was obtained with a yield of 80%[59] Tang *et al.* demonstrated that IL-assisted anodic ECE, in conjunction with simultaneous fluorination, may yield fluorinated phosphorene. Even after seven days, the phosphorene that was synthesized exhibited a high degree of stability.[60] Huang *et al.* demonstrated that it is also feasible to perform cathodic exfoliation of bulk black phosphorus in *N*,*N*-dimethylformamide (DMF) electrolyte by using tetrabutylammonium hexafluorophosphate (TBAP). By altering the voltage, it is possible to control the final amount of black phosphorus layers that are produced. The nanosheets that were generated did not have any surface functional groups.[61] In their research, Yang *et al.* demonstrated that by using tetra-*n*-butylammonium bisulphate as an intercalating agent, they were able to obtain a yield of 78% and construct nanosheets with a lateral dimension of up to 20.6 micrometres and a thickness of 3.7 nm. The FETs that were built based on it demonstrated a hole mobility of 270 $cm^2 V^{-1} s^{-1}$ at a very cold temperature of 143 K.[62]

Zu *et al.* showed that black phosphorus layers could be generated by cathodic exfoliation in a propylene carbonate solution containing tetraethylammonium perchlorate as an intercalating agent. This method may be used to manufacture phosphorene. The yield is around 93.1%.[63] Luo and colleagues demonstrated that it is also feasible to perform cathodic exfoliation in a solution of hexadecyltrimethylammonium chloride (CTAC). Phosphorene layers that are 5–8 nm in thickness may be created in a matter of twenty seconds.[64] According to Mayorga-Martinez *et al.*, bipolar exfoliation is also conceivable, and it has a lower cost compared to anodic and cathodic

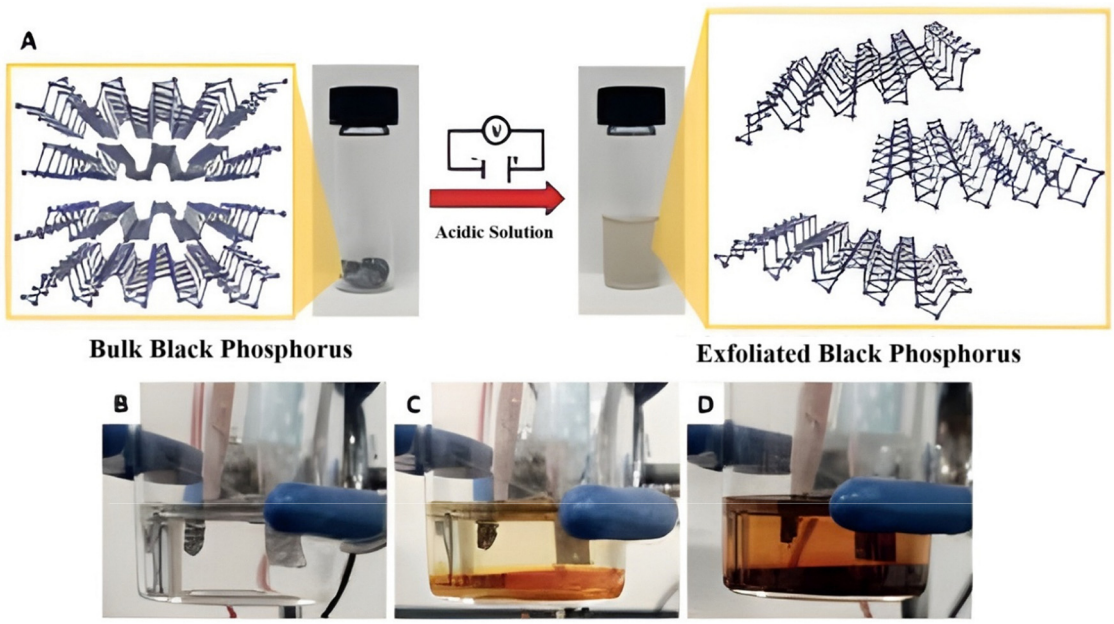

Fig. 5 (A) Schematic and photographic illustration of the electrochemical exfoliation of bulk black phosphorus (BP) in an acidic aqueous solution under an applied DC voltage, leading to controlled anodic oxidation and the formation of exfoliated BP nanosheets dispersed in DMF. (B–D) Sequential images of the exfoliation process: (B) initial bulk BP in solution, (C) intermediate stage showing gradual color change as exfoliation progresses, and (D) final stage with a homogeneous brown dispersion indicating successful formation of BP nanosheets.

exfoliation. Excellent capacitive energy storage capabilities may be observed for the obtained few-layer black phosphorus, which can have a lateral dimension of only a few hundred nanometres.[65]

3.1.4. Vapor-phase deposition techniques. Bottom-up methods for synthesizing phosphorene include chemical vapor deposition (CVD), hydrothermal synthesis, and pulsed layer deposition, but none of these techniques have proven effective for large-scale production of phosphorene. While CVD is effective for growing graphene and TMD monolayers, it is less suitable for phosphorene because non-toxic phosphorus-based precursors are unavailable. However, Li *et al.* pioneered a CVD-like synthesis approach for creating BP thin films on flexible substrates. They began with red phosphorus (RP) powder, depositing it on a flexible substrate through thermal evaporation at 400 °C. Following the deposition, the film was exposed to a multi-anvil press at 10 GPa, which converted RP into BP, resulting in a BP film with a thickness of approximately 40 nm.[66] Smith *et al.* later synthesized few-layer phosphorene with an area ranging from 0.35 to 100 μm^2. In their process, RP was first deposited on a SiO_2/Si substrate at 600 °C in a vacuum tube furnace. After forming a uniform RP thin film, the sample was combined with Sn and SnI_4 mineralizing agents in a pressure vessel reactor filled with argon at 27.2 atm and heated to 900 °C.[67] Xu *et al.* reported the growth of highly crystalline few-layer phosphorene on a gold-coated SiO_2/Si substrate. This method utilized intermediate polyphosphate species (Au_3SnP_7) as a nucleating layer, enabling controlled growth of phosphorene. This approach allowed for precise control over thickness from a few nanometers to hundreds of nanometers and scalability in lateral size, producing nanosheets ranging from a few microns up to sub-millimeter dimensions.[68]

Pulsed laser deposition (PLD) is a technique that might be used to manufacture ultrathin films composed of black phosphorus. Films that have been developed are capable of being deposited in Si/SiO_2 substrates as well as graphene/copper. According to the findings of Yang *et al.*, FETs created using this methodology and having a thickness of just 2 nm may have a carrier mobility of 14 $cm^2\ V^{-1}\ s^{-1}$. Amorphous BP, a highly disordered form of black phosphorus with thicknesses ranging from 2 to 10 nm, has been achieved using PLD at a relatively low temperature of 150 °C, compared to traditional high-temperature and high-pressure methods. The bulk BP crystal target was positioned 4 cm from the substrate within a chamber evacuated to approximately 1.5×10^{-7} Torr before starting the PLD process. During deposition, the BP target was ablated by a KrF pulsed laser (λ = 248 nm) at a 5 Hz repetition rate while maintaining the substrate temperature at 150 °C. For uniform film growth, both the BP target and the substrates were rotated continuously. Following deposition, the system was naturally cooled to room temperature under high vacuum.[69] Optimizing the parameters of the PLD allowed Yu *et al.* to demonstrate that phosphorene films were grown on a mica wafer in an ultrahigh vacuum chamber using bulk monocrystalline BP as the source, achieving centimetre-scale films as shown in Fig. 6. The as-grown BP films exhibited a distinct reflective color, with a uniform sheen across the 1 cm^2 surface of the mica wafer, indicating the potential for large-scale device fabrication. The thickness (or the layer number) of the BP films could be precisely controlled by adjusting the number of laser pulses during deposition, with a growth rate of approximately 1.3 Å s^{-1}. The use of an ultrahigh homogeneous mica surface and uniform BP cluster distribution enabled unidirectional growth, leading to the merging of monolayer BP flakes and the formation of continuous films. The elemental purity of the BP films was established, and potential contamination from oxidation was ruled out. These films have a thickness of less than 5 nm, and their mobility in FETs is measured at 213 $cm^2\ V^{-1}\ s^{-1}$.[70]

3.2. Properties of phosphorene

Phosphorus may often be found in one of these four allotropic forms: red, white, purple, and black. Because of its orthorhombic structure, black phosphorus has a high degree of stability. The structure of black phosphorus consists of several monolayers of phosphorene, which are held together by weak van der Waals' forces. Monolayer black phosphorus, also known as phosphorene, is made up of sp^3 hybridized atoms, which results in a non-planar hexagonal structure.[71] Phosphorene exhibits two distinct crystal directions: the armchair orientation along the *x*-axis with a lattice parameter of 4.43 Å, and the zigzag orientation along the *y*-axis with a lattice parameter of 3.27 Å, as shown in Fig. 7.

3.2.1. Structural properties. Phosphorene, having a puckered honeycomb lattice, possesses a layer numbered finite band gap that varies from 0.3 eV to 1.5 eV when the flake thickness is reduced from bulk to a single layer.[72] The puckered honeycomb structure in phosphorene is due to sp^3 hybridization. Due to the puckered structure, each layer of honeycomb lattice contains two atomic layers with the interatomic distance between the two nearest atoms as 2.224 Å and between top and bottom atoms as 2.244 Å. Black phosphorus has a variety of bond lengths in its structure. Atoms that are located inside the same layer have a bond length of 2.16 Å, while atoms that are located between layers have a bond length of 2.21 Å.[73] Phosphorene can be exfoliated into monolayers or few-layer sheets, with each monolayer being about 0.8 nm thick. Due to its puckered structure, phosphorene exhibits anisotropic properties, meaning its mechanical, electrical, and optical properties differ depending on the direction (zigzag *vs.* armchair directions) in the plane of the material. Unlike hexagonal graphene, phosphorene has an orthorhombic unit cell, displaying distinct armchair and zigzag orientations along the *x* and *y* axes, respectively, leading to pronounced structural anisotropy. Strong in-plane anisotropy is mainly due to the unique topological structure and the differences between zigzag and armchair directions.[74]

The arrangement and coordination of phosphorus atoms can be altered due to changes in external conditions or intrinsic instabilities, resulting in distinct bond angles, bond lengths, and puckering patterns. It exhibits a variety of allotropes due to its unique bonding and structural flexibility. These allotropes

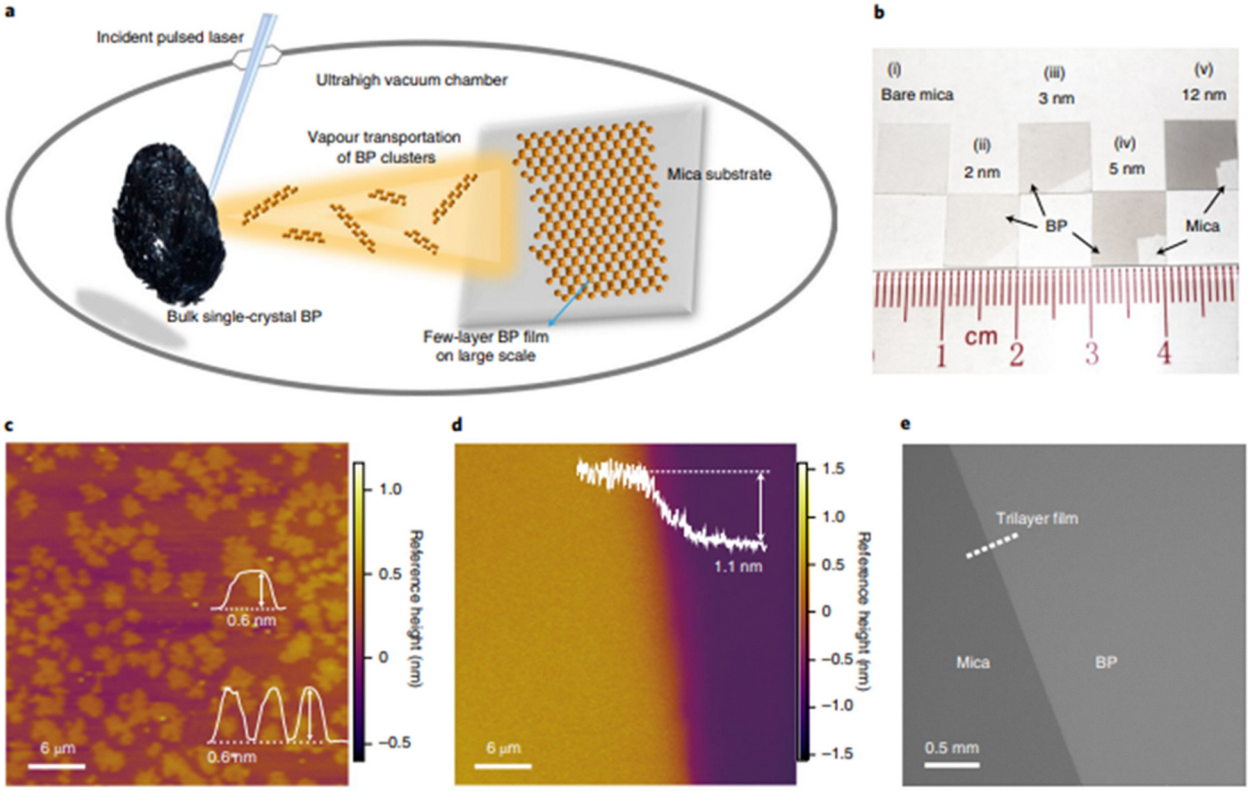

Fig. 6 (a) Schematic picture of a controlled PLD process used to fabricate few-layer BP films; (b) photographs show: (i) the bare mica substrate, (ii)–(v) as-deposited BP films with varying thicknesses, covering centimetre-scale areas. (c) An atomic force microscopy (AFM) image illustrates the topography of monolayer BP flakes synthesized with a few laser pulses, with the corresponding monolayer thickness indicated in the height profile. (d) Another AFM image presents the thickness of a bilayer BP film. (e) An electron back-scatter diffraction (EBSD) image reveals a trilayer BP film on the mica substrate, demonstrating the film's uniformity and continuity extending beyond the millimetre scale, reproduced from ref. 70 with permission from Springer Nature, copyright 2021.

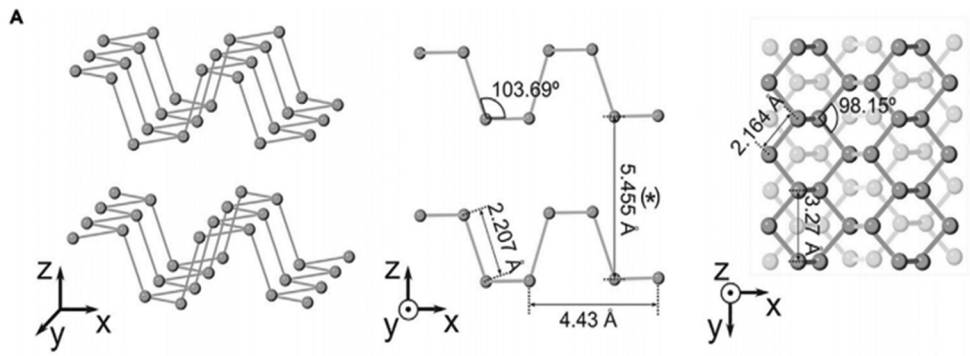

Fig. 7 Crystalline structure of black phosphorus observed in *x*, *y* and *z* directional views, reproduced from ref. 77 with permission from IOP Publishing, copyright 2014.

arise from different arrangements of phosphorus atoms in the lattice and exhibit distinct electronic, mechanical, and thermal properties. Allotropes arise due to the flexibility in bonding patterns of phosphorus atoms, including tri-coordinate sp^3 hybridization and lone pair interactions. The structural versatility of phosphorus atoms, facilitated by their ability to form various bonding configurations, gives rise to numerous allotropes of phosphorene. These allotropes, with varying atomic arrangements and unit cell geometries, display diverse properties, including distinct band gaps, carrier mobilities, and thermal conductivities. The crystal structures of various phosphorene allotropes are illustrated schematically in Fig. 8. These allotropes are identified as α-phosphorene (Fig. 8a), β-phosphorene (Fig. 8b), γ-phosphorene (Fig. 8c), δ-phosphorene (Fig. 8d), and ζ-phosphorene (Fig. 8e), following the established notation for phosphorene variants. All these phases share a

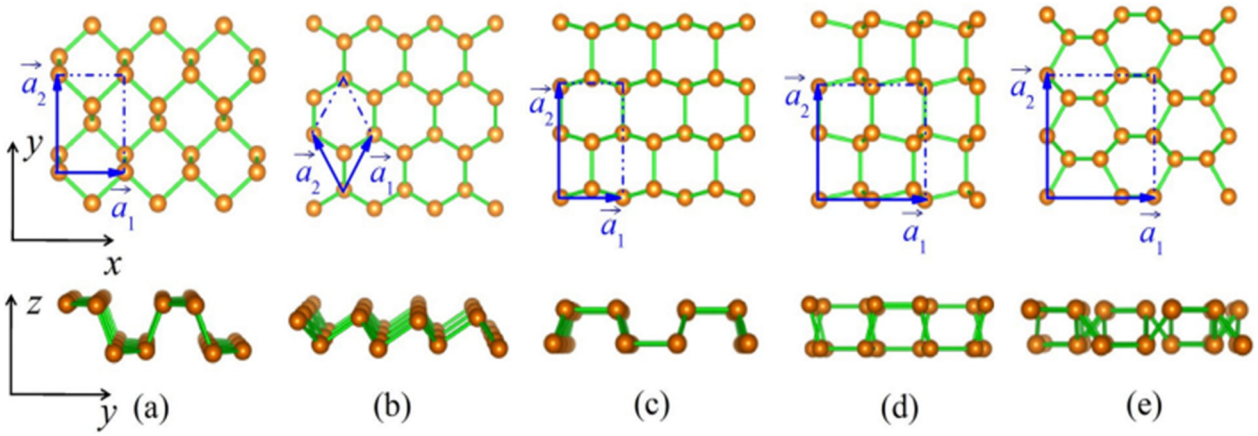

Fig. 8 Top and side views of the following phosphorene allotropes are shown: (a) α-phosphorene, (b) β-phosphorene, (c) γ-phosphorene, (d) δ-phosphorene, and (e) ζ-phosphorene with coordinate axes (x, y, z) and lattice vectors (a_1, a_2) reproduced from ref. 75 with permission from Springer Nature, copyright 2017.

common structural motif of threefold-coordinated phosphorus atoms, forming a non-planar honeycomb atomic layer.[75] The α- and γ-phosphorene allotropes have four atoms in their rectangular unit cells, while the δ- and ζ-phosphorene structures feature eight atoms per unit cell. In contrast, the β-phosphorene allotrope, characterized by isotropic properties, has only two phosphorus atoms in its hexagonal unit cell. Wu *et al.* presented a novel class of monolayer phosphorus allotropes, namely ε-P, ζ-P, η-P, and θ-P, distinct from the well-known other allotropes. Unlike the buckled honeycomb lattice observed in earlier phosphorene structures, these new allotropes feature unique arrangements composed of P_4 square or P_5 pentagon units, optimized for tri-coordinated phosphorus atoms. This discovery significantly expands the diversity of phosphorene structures. First-principles calculations confirm the stability of these four polymorphs, alongside five additional hybrid structures.[74] Recent advancements in synthesis techniques, such as epitaxial growth and topological modeling, have enabled the exploration of novel phosphorene forms, including porous structures, diatomic layers, and helical configurations.

3.2.2. Electronic properties. Regardless of the layers that are present, black phosphorus always exhibits very different bandgap characteristics. The bandgap is subject to change by the layers that are now present. Bulk black phosphorus has a bandgap that falls anywhere between 0.1 and 0.35 eV, whereas monolayer black phosphorus has a bandgap that falls anywhere between 1.0 and 1.7 eV.[71,76] The band gap is tunable and directly dependent on the thickness of the material. As the number of layers rises, the bandgap will decrease because of the increased interlayer interactions, particularly the interlayer hybridization near the top of the valence band and the bottom of the conduction band, which reduces the energy required to excite an electron across the gap.[77] In monolayer BP, the absence of this interlayer hybridization results in a larger band gap as shown in Fig. 9, making it suitable for applications where higher energy gaps are necessary, such as in high-performance electronic devices. The tunability of the band gap with layer thickness is a key advantage of phosphorene for state-of-the-art applications in nanoelectronics and optoelectronics.[78]

The bandgap may be altered using a variety of techniques, including doping, strain engineering, chemical functionalization, and application of an external electric field. Doping phosphorene with a suitable molecule can enhance the conductivity in phosphorene, *i.e.*, doping with transition metals such as Fe, Co, Cr, or Mn can induce localized magnetic moments, and the type of transition metal dopant can also influence the electronic conductivity by creating impurity levels that allow for enhanced electron transport.[79,80] Replacing a phosphorus atom with nonmetallic elements like Si, S, and Cl can also introduce local magnetic moments. This implies that both metallic and nonmetallic doping can potentially induce magnetism in phosphorene, making it tunable for applications in spintronics or magnetoelectronic devices.[81,82] Furthermore, current in phosphorene can be increased by creating a vacancy. Theoretical studies, such as those conducted by Srivastava *et al.*, have shown that the removal of a single atom creates localized magnetic moments in the material, leading to magnetic behavior. This defect-driven magnetism is interesting because pristine phosphorene is normally nonmagnetic. A divacancy defect, on the other hand, does not induce magnetism, and phosphorene remains nonmagnetic in this case. This suggests that the type of vacancy plays a crucial role in determining the magnetic nature of phosphorene.[83]

Other methods to alter conductivity are by applying a perpendicular electric field and introducing strain as shown in Fig. 10.[84–86] Experimental and computational studies have shown that applying a gate voltage or vertical electric field can significantly modulate the electronic properties of few-layer phosphorene, including its drain current, conductance, and even its topological phase. DFT/PBE (Density Functional Theory/Perdew–Burke–Ernzerhof) computations performed by Liu *et al.* have predicted a transformation of few-layer phosphorene (1–4 layers) from a normal insulator to a topological insulator

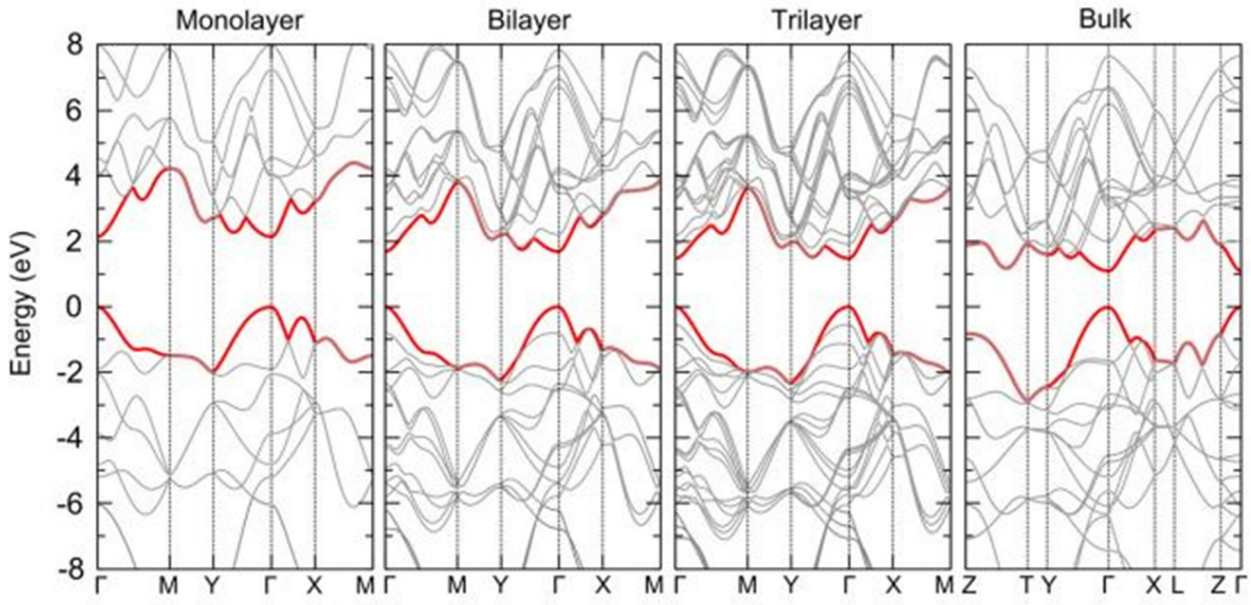

Fig. 9 The calculated electronic band structures for monolayer, bilayer, trilayer, and bulk black phosphorus (BP) reveal how the electronic properties evolve as the thickness increases, from a single layer to the bulk material, reproduced from ref. 77 with permission from IOP Publishing, copyright 2014.

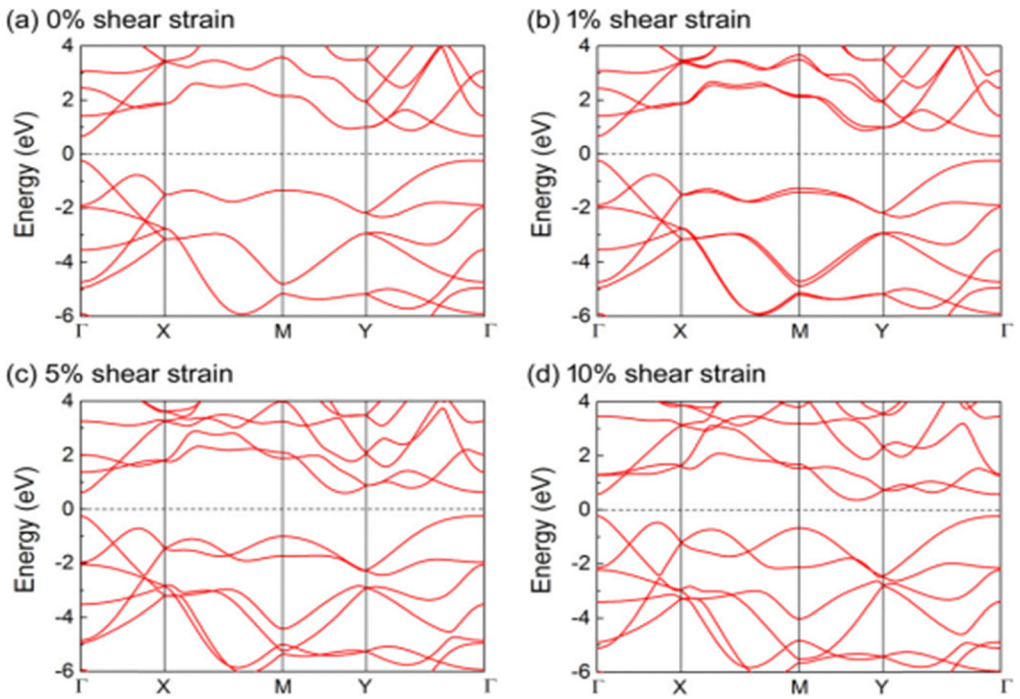

Fig. 10 Band structures of phosphorene calculated under different applied shear strains: (a) 0% shear strain, (b) 1% shear strain, (c) 5% shear strain, and (d) 10% shear strain.

under the influence of a vertical electric field. As the external electric field increases, 4-layer phosphorene can transition from a semiconducting state to a metallic state. For instance, at an electric field strength of 0.6 V $Å^{-1}$, the band structure of 4-layer phosphorene becomes metallic, as shown in computational studies.[87] Kim *et al.* have provided experimental evidence confirming that the band gap of few-layer phosphorene can be effectively tuned by applying a vertical electric field.[88] Their measurement demonstrated that at a critical electric field, the semiconducting few-layer phosphorene can transition to a Dirac semimetal, supporting the theoretical predictions of Liu *et al.*[87]

The value of the band gap decreases when strain applied along the zigzag direction increases. When phosphorene is subjected to an axial strain, the band gap undergoes a direct–indirect–direct transition. This can be achieved by a −2% compression in the zigzag direction. An expansion of +11.3% or a compression of −10.2% strain can again tune the gap from indirect to direct.[89] A possibility of inducing a band gap by achieving a topological state is also reported. Because of its tunable bandgap, black phosphorus is capable of absorbing light throughout the spectrum, from ultraviolet to infrared. It also exhibits a high mobility when compared to other similar elements.[90] At room temperature, the carrier mobility of phosphorene is approximately 300 $cm^2\ V^{-1}\ s^{-1}$, which can increase by up to a factor of 5 at low temperatures. This indicates that phosphorene's electronic performance improves significantly in colder environments.[91] Such mobility is beneficial for use in field-effect transistors (FETs), where phosphorene FETs have demonstrated an ON/OFF ratio ranging from 10^3 to 10^5, indicating excellent switching behavior between conductive (ON) and non-conductive (OFF) states. This tunability and high responsiveness make phosphorene an excellent candidate for biosensors, when biomolecules such as proteins, DNA, or other target molecules bind to the phosphorene surface. They induce shifts in the material's electronic structure, causing measurable changes in conductivity or current in a field-effect transistor (FET)-based sensor with high precision, fast response times, and the ability to detect low concentrations of biomolecules.

3.2.3. Optical properties. Phosphorene's physical properties vary depending on the crystallographic direction. Its anisotropy leads to direction-dependent optical behavior. Light absorption varies with polarization; light polarized along the armchair direction is absorbed, while light polarized along the zigzag direction is forbidden due to the specific electron wave function symmetry.[92] Phosphorene, like other 2D materials, has a strong exciton binding energy (∼800–900 meV). This high value is due to reduced dimensionality and screening, which enhances the Coulomb attraction between electrons and holes. This strong binding stabilizes excitons and trions (charged excitons) against thermal fluctuations, which is essential for applications in light transport and quantum computing.[93] This strong exciton binding energy results in more stable and pronounced photoluminescence emissions, which can be used for detecting biomolecular interactions. When biomolecules bind to the surface of phosphorene, they can alter the exciton dynamics, causing shifts in the photoluminescence intensity or wavelength. These changes can be used as a sensitive readout for biosensing. The anisotropic nature of phosphorene extends to its excitons. Excitons exhibit directionally dependent behavior, with their wave functions stretched along the armchair direction due to the mass anisotropy of charge carriers (lighter along the armchair, heavier along the zigzag direction) (Table 1). This anisotropy impacts how excitons and trions behave and propagate in the material.[94] Experiments using polarization-resolved photoluminescence have confirmed these highly anisotropic excitons in monolayer phosphorene, providing key insights into the exciton binding energy through the difference between the excitonic emission peak and the quasi-particle bandgap. The stability of excitons in phosphorene enhances its ability to engage in optical biosensing techniques like fluorescence-based detection. Since the excitons can be easily manipulated by external stimuli (*e.g.*, light and electric fields), interactions with biomolecules can be detected through shifts in the optical properties of the material, such as changes in absorption or emission spectra. The exciton binding energy facilitates stronger interactions with the target biomolecule, leading to more significant optical signals that improve sensor sensitivity. The strong light–matter interactions of phosphorene and arsenene can be further leveraged through plasmonic enhancement, where coupling with localized surface plasmon resonances (LSPR) in metallic nanostructures amplifies optical signals and sensitivity. This synergy between 2D materials and plasmonic nanostructures underpins hybrid photonic–plasmonic biosensor designs (Fig. 11).

Table 1 Effective masses of holes and electrons depending on the crystal direction

Phosphorene	Effective mass of holes	Effective mass of electrons
Zigzag	6.35 m_0	1.12 m_0
Armchair	0.15 m_0	0.17 m_0

As additional layers are added to phosphorene, increased screening reduces the exciton binding energy, slightly diminishing the excitonic effects observed in the monolayer.[95] The high exciton binding energy, combined with spatial anisotropy, suggests that phosphorene has strong potential for use in optoelectronic devices and quantum applications where long-lived excitons and trions are advantageous.[96] The spatial distribution of excitons changes with the number of layers. In a three-layer phosphorene, holes remain confined to a single layer, while the electron distribution extends across all layers. The binding energy of excitons significantly decreases in bulk black phosphorus (∼30 meV), due to increased screening from interlayer interactions, unlike in monolayers where it is much higher (∼800–900 meV).[97] The observation of quantum oscillations in phosphorene is significant because it demonstrates the high purity and crystal quality of the material. When a magnetic field is applied to a 2D electron gas, it causes the formation of Landau levels (quantized energy levels), and sweeping the Fermi level through these levels leads to oscillations in resistance. This phenomenon, observed in encapsulated phosphorene, underscores its suitability for high-performance electronic applications.[98] Phosphorene shows distinct Landau levels under a magnetic field, and Zeeman splitting (the splitting of energy levels due to the magnetic field) is observed at magnetic fields greater than 8 T. The ability to observe these fine features in the resistance measurements indicates the cleanliness and low disorder in encapsulated phosphorene systems.[99]

3.2.4. Mechanical properties. Phosphorene exhibits strong anisotropy in its mechanical properties, meaning its behavior differs significantly along different crystallographic directions: the armchair and zigzag directions. This is a direct result of its

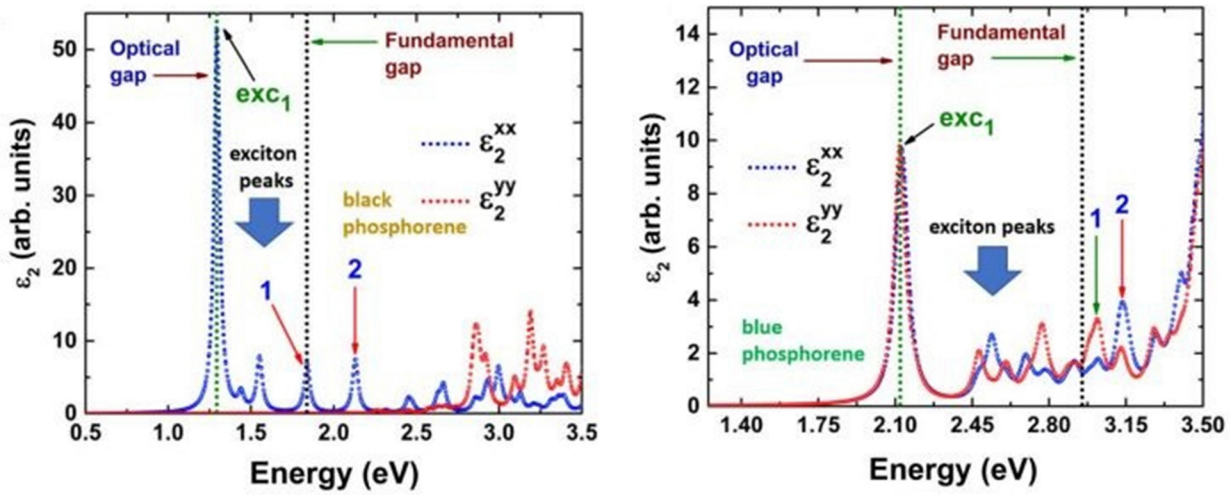

Fig. 11 Imaginary part of the dielectric function for black and blue phosphorenes, highlighting the values of the optical and fundamental gaps along with exciton peaks reproduced from ref. 96 with permission from Springer Nature, copyright 2022.

puckered structure, where atomic bonds are stronger along the armchair direction compared to the zigzag direction. Along the armchair direction, phosphorene has a higher Young's modulus, making it stiffer, while in the zigzag direction, the modulus is lower, reflecting greater flexibility (for the armchair direction: ~166 GPa and for the zigzag direction: ~44 GPa).[100] The tensile strength also shows directional dependence, being higher in the armchair direction than in the zigzag direction. Phosphorene is relatively brittle along the armchair direction compared to the zigzag direction. Phosphorene can withstand strain up to about 30% before fracturing. This makes it a suitable candidate for applications requiring mechanical flexibility.[101] Phosphorene's mechanical properties degrade at high temperatures, which poses challenges for some applications. The material is stable under ambient conditions, but careful consideration of environmental factors (such as oxygen and moisture) is necessary as phosphorene can degrade when exposed to air.[102] Phosphorene exhibits a negative Poisson's ratio in some directions, meaning that it can expand in one direction when compressed in another, a behavior that's unusual in most materials. This negative Poisson's ratio makes phosphorene of particular interest in the design of materials with auxetic behavior, where the material becomes thicker when stretched.[103] Phosphorene's puckered structure makes it highly flexible out-of-plane, which means it can bend significantly without breaking, a property that is useful in flexible electronics. These mechanical deformations make phosphorene particularly valuable in sensors that detect biomolecular binding events based on mechanical changes at the nanoscale, providing high sensitivity and real-time detection.

3.3. Applications of phosphorene

Phosphorene-based biosensors influence the unique electronic, optical, and mechanical properties of phosphorene for highly sensitive and selective detection of biomolecules. Their tunable electronic properties, anisotropic structure, and high surface area enable the creation of versatile biosensors with applications ranging from medical diagnostics and environmental monitoring to personalized healthcare and wearable devices. Moreover, in comparison to other prevalent 2D nanomaterials, phosphorene demonstrates reduced cytotoxicity and favorable biodegradability within the organism.[104] These traits piqued the curiosity of scientists seeking novel materials with highly adaptable properties for diverse biomedical applications. However, its practical applications, particularly in biosensing, are hindered by its susceptibility to oxidative degradation when exposed to environmental factors such as oxygen and moisture. To mitigate this limitation and enhance its stability and functionality, surface functionalization strategies have been extensively explored. A smaller number of works report actual experimental results on the use of phosphorene in biomedical applications, despite the high volume of papers that address theoretical studies on the potential interaction of phosphorene with biomolecules (Fig. 12).[105]

3.3.1. Electrochemical biosensors. Biosensors that quantify alterations in electrical properties (such as current, voltage, or impedance) upon the interaction of an analyte with a biological recognition element (*e.g.*, an enzyme or an antibody) are classified as electrochemical biosensors. The development of very sensitive biosensors for medical applications was necessitated by the normally low concentrations of specific biomarkers in clinical blood samples.

Myoglobin detection. The inherent redox properties of BP allowed for efficient electron transfer, enhancing the sensitivity of the biosensor compared to other 2D materials, such as reduced graphene oxide (rGO). BP's electrochemical properties facilitate the direct oxidation of myoglobin, ensuring a strong and measurable signal. Myoglobin is a cardiac biomarker that can indicate a heart attack or other heart-related conditions when present at abnormal levels in the blood. By utilizing aptamer-functionalized black phosphorus electrodes, Kumar *et al.*'s electrochemical sensor has the potential to offer a rapid

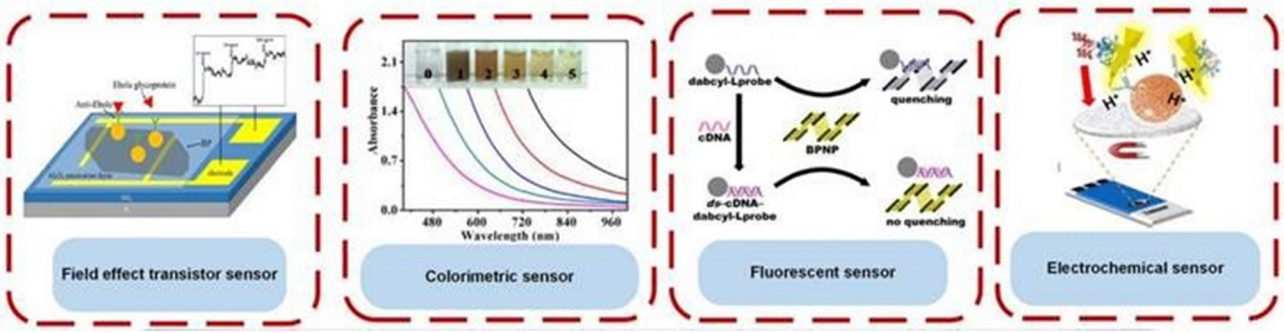

Fig. 12 Various applications of biosensing reproduced from ref. 105 with permission from RSC publication, copyright 2020.

and precise diagnosis of such conditions. The few layer black phosphorus prepared and used for this sensor was fabricated by using a surfactant-mediated liquid exfoliation technique. The few layer black phosphorus prepared was functionally modified by the addition of poly-L-lysine so that it can interact with the anti-myoglobin DNA aptamers. The positively charged amino groups of PLL interact electrostatically with the negatively charged phosphorene surface, improving adhesion and stability. PLL provides anchoring sites for biomolecules such as DNA or aptamers, ensuring stable and oriented immobilization. The aptamers were created using nanostructured electrodes. The functionalized sensor with poly-L-lysine showed strong affinity for binding with myoglobin when tested with a cross-reactivity test. Using the previously developed reduced graphene oxide sensor which also targets myoglobin, this BP biosensor showed a linear detection range of 1 pg mL^{-1} to 16 g mL^{-1}. This biosensor also has a very low detection limit of 0.524 pg mL^{-1} and a sensitivity of 36 A mL pg^{-1} cm^{-2} (Fig. 13).[106]

Glucose sensing. The first non-enzymatic H_2O_2 sensor based on black phosphorus has been created by Yan *et al.* The synthesis of phosphorene often presents challenges, such as prolonged time requirements and issues with material stability. In this study, the use of supercritical carbon dioxide ($scCO_2$)-assisted exfoliation allowed for the rapid production of few-layer BP within 5 hours, a significant improvement over traditional methods. The $scCO_2$-assisted process offers a more efficient and scalable approach to producing high-quality few-layer BP, making it a promising technique for large-scale applications. The developed sensor exhibited an impressively low detection limit of 1×10^7 M for H_2O_2, which is significantly more sensitive than the general detection limits of other electrochemical sensors.[107] This study demonstrates a breakthrough in the rapid synthesis of few-layer BP using supercritical CO_2 and its application in developing a highly sensitive non-enzymatic H_2O_2 sensor. The results not only provide experimental verification of BP's theoretical chemical sensing capabilities but also highlight the material's potential for future biosensing technologies and large-scale applications. Phosphorene has also been explored as an electrochemical platform for glucose sensing.

Phosphorene nanosheets were integrated into an enzymatic glucose biosensor, demonstrating high sensitivity and a detection limit down to 0.5 μM. The exceptional electron mobility of phosphorene allowed for rapid electron transfer between

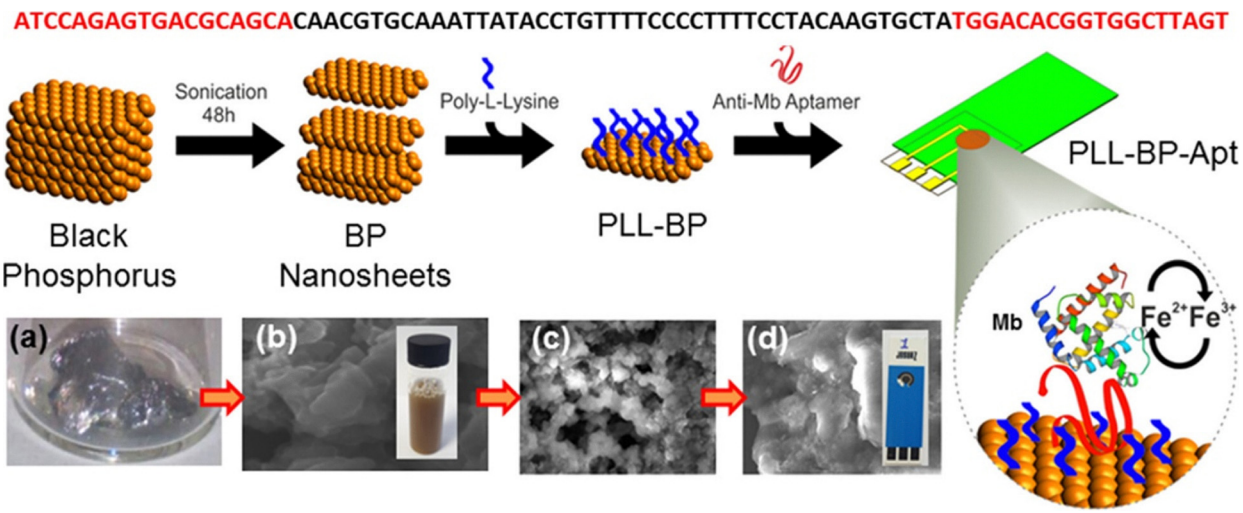

Fig. 13 Workflow showing using liquid phase exfoliation to produce nanosheets of black phosphorus and showing the detection of myoglobin *via* a label free electrochemical sensing method, reproduced from ref. 106 with permission from ACS Publications, copyright 2016.

glucose oxidase and the electrode, leading to accurate glucose detection in biological fluids. The study examined the performance of phosphorene in two different enzymatic reactions: one based on glucose oxidase (GOx) for glucose detection and the other based on horseradish peroxidase (HRP) for H_2O_2 detection. The study underscores phosphorene's potential in biosensing, particularly in reductive electrochemical environments. In this system, horseradish peroxidase (HRP) catalyzed the oxidation of FcMeOH to Fc^+MeOH in the presence of H_2O_2. The oxidized mediator (Fc^+MeOH) was then electrochemically reduced back to FcMeOH at the phosphorene-modified electrode, producing a measurable reduction signal corresponding to the concentration of H_2O_2. In the case of glucose detection, the presence of phosphorene did not significantly enhance the recorded signal from FcMeOH oxidation compared to control experiments without phosphorene. Phosphorene showed promise as an electrochemical platform in reductive systems, particularly in the HRP-based H_2O_2 detection, where the applied potential favored its stability and maintained its excellent electron transfer capabilities.[108]

DNA sensing. DNA sensing using phosphorene-based electrochemical sensors typically involves the immobilization of DNA probes onto the phosphorene-modified electrode. When a target DNA strand hybridizes with the immobilized probe, changes occur in the electrochemical properties, such as conductivity or capacitance, which are detected as a signal. Phosphorene's ability to interact with DNA *via* π–π stacking and coulombic interactions makes it a suitable material for DNA sensors. The innovative approach combines advanced materials and electrochemical techniques to detect the specific DNA sequences of pathogens, with potential applications in food safety and public health. The sensor utilizes nitrogen-doped carbonized polymer dots (N-CPDs) grown *in situ* on few-layer black phosphorus (FLBP) as a functional material for the modification of the sensor's surface. The N-CPDs@FLBP nanocomposite enhances the electrochemical properties of the biosensor, improving sensitivity and conductivity. The analytical performance was evaluated using complementary single-stranded DNA (ssDNA), with the sensor showing a linear detection range from 1.0×10^{-19} to 1.0×10^{-6} mol L^{-1} and a low detection limit of 3.33×10^{-20} mol L^{-1} (3σ), making it highly sensitive for detecting minute amounts of bacterial DNA. The portable nature of the sensor makes it suitable for on-site food safety monitoring, reducing the need for complex and time-consuming lab-based testing.

Electrochemical detection of cancer biomarkers. Phosphorene has also been applied in detecting cancer biomarkers like the carcinoembryonic antigen (CEA) and the prostate-specific antigen (PSA). In one study, a phosphorene-modified electrode was used to detect the CEA in serum samples, achieving a detection limit of 0.1 ng mL^{-1}. The high affinity of phosphorene for biomolecules, combined with its electrochemical activity, resulted in accurate and reliable detection.[109]

Cancer cell sensing. A novel approach to detecting cancer cells using a cytosensing platform based on supramolecular recognition has been developed. The platform utilizes a nanocomposite formed using a *p*-sulfonated calix[8]arene (SCX8), polydopamine (PDA), and black phosphorene (BPene). The BPene@PDA nanocomposite was functionalized with SCX8, creating the final BPene@PDA-SCX8 nanocomposite. SCX8 plays a crucial role in recognizing folic acid (FA) molecules through host–guest interactions. The cancer cells are captured by the BPene@PDA-SCX8·FA modified electrode *via* the interaction between FA and folate receptors (FR) on the cancer cells' surface. This binding forms an SCX8-FA-FR sandwich-type conjugate. The presence of cancer cells increases the impedance at the electrode, which can be measured. The change in impedance is directly proportional to the concentration of cancer cells. The cytosensor was able to detect LNCaP cells (a type of cancer cell) within a concentration range of 2×10^2 to 1×10^5 cells per mL, with a detection limit of 36 cells per mL. This demonstrates the high sensitivity of the sensor for early-stage cancer detection. The cytosensor described in this paper shows great promise for use in cancer recognition and diagnosis due to its high sensitivity, specificity, and ability to detect low concentrations of cancer cells (Fig. 14).[110]

Antigen detection. Another study presents a novel electrochemical immunosensor using black phosphorene (BPene) and magnetic covalent organic frameworks (COFs) for the detection of the prostate specific antigen (PSA). Magnetic COFs have traditionally been employed for enrichment and separation of analytes, but their application in electrochemical immunosensors is relatively new. Au nanoparticles (Au NPs) were deposited onto BPene to form a nanocomposite (Au@BPene), which was used as an immunosensing platform for capturing primary antibodies and enhancing electron transfer. The sensor exhibited excellent performance with a wide linear detection range (0.0001 ng mL^{-1} to 10 ng mL^{-1}) and a detection limit of 30 femtograms per milliliter (fg mL^{-1}) for PSA. The sensor demonstrated high specificity, stability, and reproducibility when tested with real samples.[111]

Detection of immunoglobulin G (IgG). The black phosphorus based field effect transistors have performed well when used for gas sensing. In the field of biosensing, there has been a lot of attention focused on these FETs. Functionalization of the dielectric component of the FET biosensor was accomplished by using specific bio-receptor molecules. The bio-receptor molecules bind with the analyte biomolecules and, as a result, changes the channel conductance when the FET device is exposed to the analyte (Fig. 15).

Chen *et al.* created a similar biosensor for the detection of human immunoglobulin G. As a target bio-receptor in this case, anti-human IgG-conjugated gold nanoparticles were put on the surface of the dielectric layer, and the device was then coated with aluminium oxide for surface passivation. Gold nanoparticles are used to enhance bioreceptor immobilization by providing a large, conductive, and biocompatible surface for stable and oriented attachment of biomolecules. The Al_2O_3 layer provides chemical stability, protecting the underlying

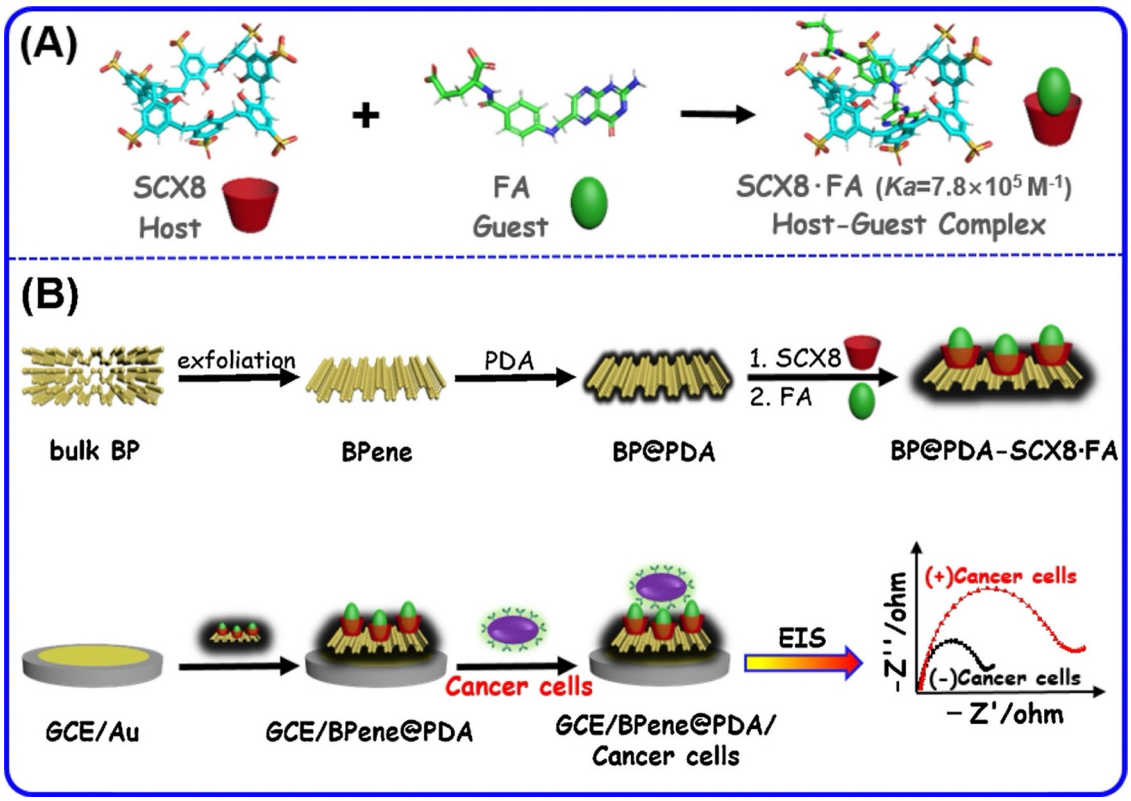

Fig. 14 (A) Host–guest complex formation between SCX8 and FA. (B) Cancer cell sensing mechanism using the (black phosphorene) BPene@PDA-SCX8·FA nanocomposite reproduced from ref. 110 with permission from Elsevier, copyright 2020.

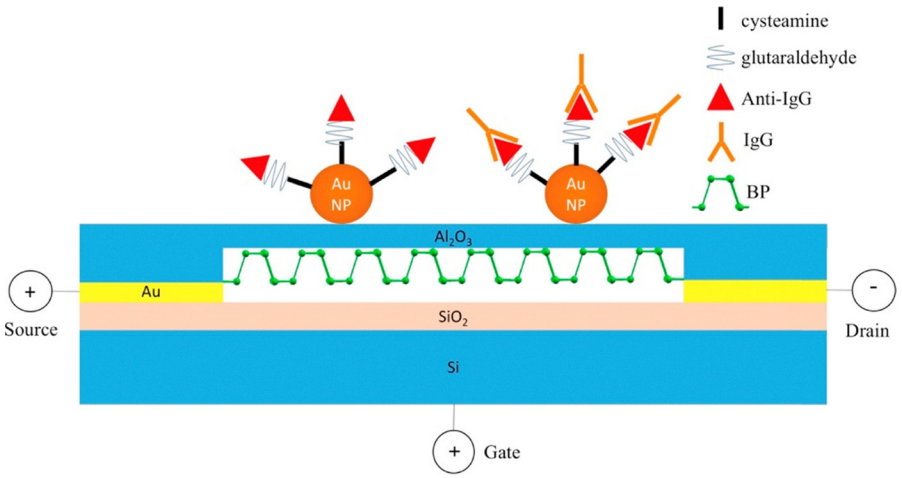

Fig. 15 Black phosphorene based FET sensor, reproduced from ref. 112 with permission from Elsevier, copyright 2017.

electrodes and dielectric from oxidation or degradation in aqueous or biological environments. The human immunoglobulin G could be detected by the FET biosensor as shown in Fig. 16, which had a reaction time on the order of seconds and a detection limit of 10 mg mL^{-1} while showing high sensitivity.[112]

Heavy metal ion detection. Phosphorene-based electrochemical sensors have been developed for the detection of heavy metal ions such as lead (Pb^{2+}) and mercury (Hg^{2+}). In one study, phosphorene-modified electrodes exhibited enhanced sensitivity due to their large surface area and excellent charge transfer properties. The detection limits for Pb^{2+} and Hg^{2+} were below 1 ppb, making these sensors highly effective for environmental monitoring.[113]

Pesticide detection. Another application of phosphorene in environmental sensing is in detecting pesticides. Phosphorene-modified electrodes showed high sensitivity and selectivity for

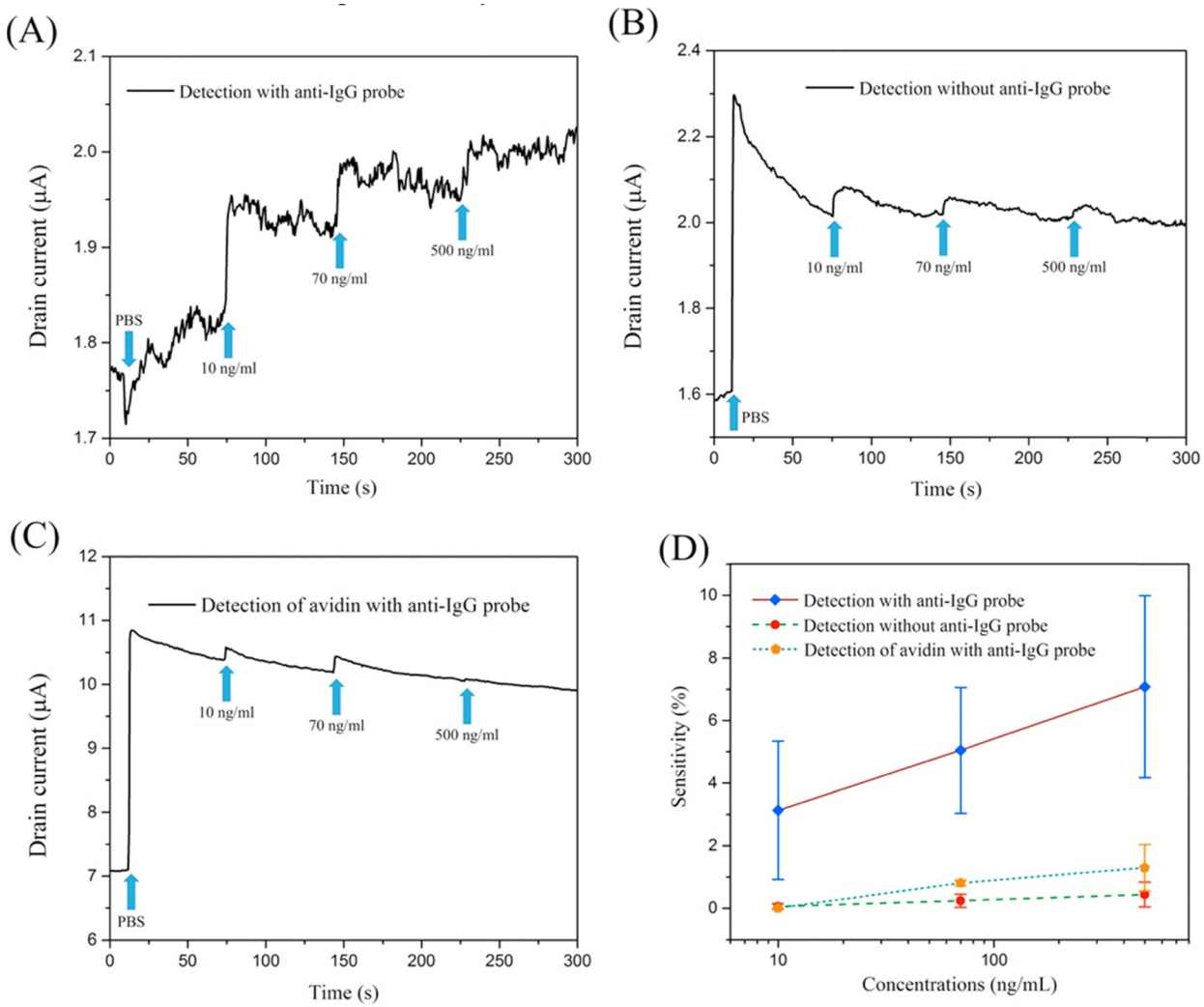

Fig. 16 (A) Dynamic response of the BP FET biosensor to varying IgG concentrations. (B) Control experiment showing non-specific binding on the BP sensor without antibody probes. (C) Control experiment detecting a non-specific protein (avidin). For all measurements (A)–(C), the source–drain voltage was maintained at 0.01 V. (D) Sensitivity plotted against target protein concentration, demonstrating that specific IgG binding yields the highest sensitivity compared to sensors without probes or with non-specific proteins, reproduced from ref. 112 with permission from Elsevier, copyright 2017.

detecting carbaryl pesticides. An electrochemical aptamer sensor based on black phosphorene nanosheets (BPNPs) modified with poly(3,4-dioxyethylenethiophene)-poly(styrene sulfonate) (PEDOT) and gold nanoparticles (Au NPs) was fabricated. A carbaryl-specific aptamer, modified with sulfhydryl groups (-SH), was attached to the Au NPs. This enabled the selective recognition and capture of carbaryl molecules. The binding of carbaryl to the aptamer caused detectable changes in the interfacial electrochemical signal. These changes were characterized using cyclic voltammetry. It achieved a detection range of 0.01 ng mL^{-1} to 10 μg mL^{-1} and a limit of detection of 7.0 pg mL^{-1}, showcasing high sensitivity. The sensor is highly suitable for detecting trace levels of carbaryl, a pesticide, in various samples. Its combination of high sensitivity and specificity makes it a promising tool for environmental monitoring and food safety.[114]

3.3.2. Optical biosensors. Phosphorene-based optical biosensors rely on the interaction of light with the material's surface, where the binding of target molecules changes their optical properties (*e.g.*, fluorescence, absorbance, or refractive index). This shift can be detected and correlated with the concentration of the target analyte. Phosphorene's band gap can be adjusted depending on the number of layers, enabling detection in different wavelength regions, including visible, ultraviolet (UV), and near-infrared (NIR). Its optical properties, such as absorption and photoluminescence, make phosphorene sensitive to small changes in its environment, useful in optical sensing.

DNA sensing. In a study based on fluorescence, Yew *et al.*, proposed using black phosphorus for detecting nucleic acid molecules, especially single stranded and double stranded DNA nucleotides. This detection approach takes advantage of the fact that labelled single strand and double strand DNA oligonucleotides have different affinities when it comes to self-assembly with black phosphorus. Quenching of

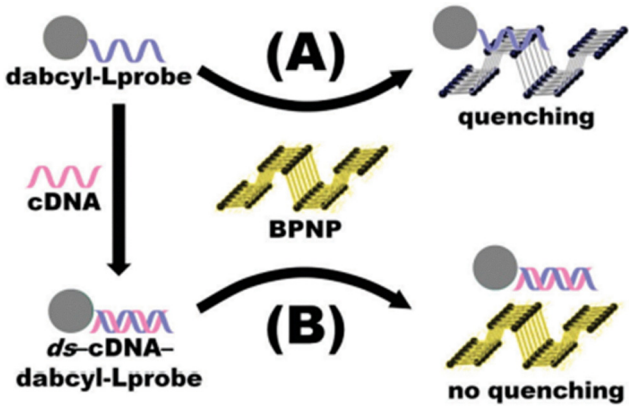

Fig. 17 Schematic illustration of the proposed DNA detection strategy using BPNPs as a fluorescence-quenching platform: (A) Without complementary DNA (cDNA), the single-stranded dabcyl-labeled probe binds to BPNPs, leading to fluorescence quenching. (B) Upon addition of cDNA, hybridization forms a double-stranded complex (ds-cDNA–dabcyl-Lprobe) that cannot adsorb onto BPNPs, resulting in no quenching and fluorescence recovery.

photo-luminescence in black phosphorus occurred due to adsorption of single stranded DNA by using the dactyl label. A complex was formed when complementary DNA was further added to the probe resulting in the formation of a ds-cDNA-dabcyl-L-probe which enhanced the hybridization of both single-stranded oligonucleotide sequences. The complex had a low affinity for nanoparticles used here; therefore, it did not adsorb onto the fluorophore surface and interfere with the photoluminescence signal given by black phosphorus. This detection assay has a detection limit of 5.9 pM L^{-1} and a linear detection range of 4 pM L^{-1} to 4000 pM L^{-1} (Fig. 17).[115]

Protein sensing. Due to the high level of specificity it has and the improved catalytic characteristics it possesses, Pumera *et al.* conducted research on the potential use of black phosphorus for the identification of proteins. In addition to this, they made use of black phosphorus as a platform for fluorescence-based sensing of DNA. As a result, they were able to accomplish a broad detection range with a low limit of detection and quantification. They also made the discovery that the catalytic influence of the black phosphorus NPs on the hydrogen evolution reaction mechanism was much higher. As a consequence of this, black phosphorus nanoparticles were used as tags in the immunoassay for the purpose of detecting rabbit IgG through the hydrogen evolution reaction mechanism itself. In the case of rabbit IgG, the detection system showed a low detection limit of 0.98 ng mL^{-1} in addition to a linear concentration range that extended from 2 to 100 ng mL^{-1}.[116] In order to assess the activity of acetylcholinesterase (AChE) with an outstanding level of sensitivity, Gu *et al.* developed a sensing technique that did not need the use of labels by combining BP-QDs with TNB anions. They measured the performance of the AChE using acetylthiocholine on the same platform that they had previously used. The acetylcholinesterase activity of the BP NPs was also tested using the fluorescence exhibited by phosphorene nanoparticles, which was based on the inner filter effect between the BP NPs and 2-nitro-5-thiobenzoate anion (TNB). For AChE, the biosensor developed has a low detection limit of 0.04 units per L, with a range of 0.2 units per L to 5 units per L.[117]

Detection of cancer biomarkers. Peng *et al.* have presented an innovative method for locating cancer biomarkers by making use of the electrical properties of FL-BP. In order to convert 4-nitrophenol into 4-aminophenol (4-AP), they used a catalyst with outstanding catalytic efficiency called BP–Au that was functionalized with gold. After that, they immobilized the carcinoembryonic antibody, also known as anti-CEA, on BP–Au. This led to the ''switching off'' of the catalytic activity, which was caused by the adsorption of anti-CEA to the surface of the Au. On the other hand, when CEA was added, it attached to anti-CEA, which led to the development of an antigen–antibody complex. This caused anti-CEA to desorb from the BP–Au surface, which in turn reactivated the catalytic capacity. Because of this, it was possible to design a colorimetric method, which is highly selective and sensitive towards the detection of CEA. This colorimetric detection of CEA showed a very broad linear detection range of 1 pg mL^{-1} to 10 g mL^{-1}, better sensitivity of 0.2 pg mL^{-1} and stronger sensitivity. The technique was used in order to identify CEA in the biological samples acquired from individuals suffering from breast and colon cancer (Fig. 18).[118]

It was shown that PEGylated 2D phosphorene nanoparticles tagged with fluorescein isothiocyanate could enter HeLa cells by early endocytosis *via* caveolae, as well as late endosomes *via* macropinocytosis, and lysosomes pathways. Additionally, it was discovered that these nanoparticles could enter HeLa cells *via* macropinocytosis. The results of this work provide important new insights into the way that manufactured nanoparticles behave within cells. In a second study, Cy7-attached PEGylated 2D-P NSs were used for *in-vivo* imaging. These NSs showed substantial accumulation in a mouse model of cervical cancer xenograft, which demonstrates that they have a significant amount of promise for usage in *in vivo* therapeutic research.[119]

Glucose sensing. According to the findings of Sarswat *et al.*, alpha-hydroxybutyrate (AHB) may be identified by using a black phosphorus coated fluoride doped tin oxide. Further studies increasingly show that the AHB metabolite in blood is a reliable marker of impaired glucose tolerance, which could potentially be a precursor for diabetes mellitus. The assay proposed showed a linear detection range of 0.8 g L^{-1} to 8.75 g L^{-1}.[120]

Bioimaging. Photoluminescence lifetime imaging, also known as PLTI, is a technology that is frequently used for the purpose of dynamically monitoring how environmental conditions influence the physiological advancement of pathogens and biological cells. Researchers like Meng *et al.* have used PLTI to generate 2D-P NPs with a typical size of around 35 nm. These NPs have shown to be useful for imaging biological cells, especially when environmental conditions are taken into

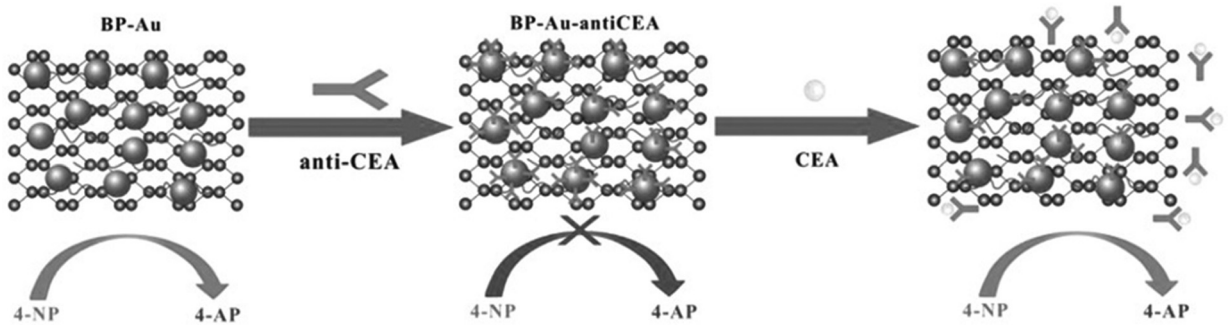

Fig. 18 Immunological detection of CEA using black phosphorene, reproduced from ref. 118 with permission from John Wiley and Sons, copyright 2017.

consideration. Photoluminescence (PL) emission was seen from the 2D-P NPs at a wavelength of about 690 nm, with a lifespan of 110.5 ps.[121] It was shown that this emission was sensitive to variations in ionic strength as well as the intracellular milieu. This finding highlights the potential of these nanoparticles for detecting variances in cellular microenvironments as well as cells with varied cytosolic contents. Lee *et al.* demonstrated that 2D-P NMs, which have a diameter of around 10 nm on average, are capable of functioning as a fluorescent mediator for live organisms.[122] In addition to this, they looked at the possibility of using BP NMs for the bioimaging of live organisms. They generated highly fluorescent BP NMs by using LPE, and they noticed that the strength of the fluorescence depended on the wavelength of the excitation light. They saw green fluorescence after the light was excited at 488 nm, and they saw blue fluorescence after the light was excited at 358 nm. When compared to other forms of NMs, BP NMs showed much lower levels of toxicity to organisms and good fluorescence properties; as a result, these nanoparticles offer a great deal of promise for use in bio-imaging applications.

Cancer treatment. PEGylated black phosphorus was produced using a basic mechanical milling method by Sun *et al.*, and this compound was then evaluated in 4T1 mice. Within only five minutes of 808 nm laser irradiation, the photothermal data indicated a considerable rise in tumor temperature, going from 34 to 59 °C. In contrast, the temperature of the non-FL-BP group barely rose by 6 °C.[123] Shao *et al.* came up with the idea of coating BP-QDs with poly(lactic-*co*-glycolic acid), also known as PLGA, in order to increase the stability of photothermal mediators. They showed that after exposing the tumor to NIR laser light for ten minutes, the temperature rapidly climbed by 26.3 °C, reaching a maximum temperature of 58.8 °C.[124]

The material's high surface area, tunable electronic properties, and excellent redox behavior make it a versatile platform for sensitive and selective detection of analytes. However, challenges like environmental stability still need to be overcome for wider commercial applications. With ongoing research focused on improving phosphorene's stability and integration into sensor devices, phosphorene is likely to play a pivotal role in the next generation of electrochemical sensing technologies (Table 2).

4. Arsenene

Arsenic (As) is a chemical element with the atomic number 33 and belongs to group 15 of the periodic table, classified as a metalloid due to its properties that are intermediate between metals and non-metals. Arsenic has been known and utilized for centuries, both for its useful properties and its infamous toxicity. In nature, arsenic exists in various forms and is commonly found in minerals combined with sulfur and metals, as well as in trace amounts in water, air, and soil. Arsenic exists in several allotropes that differ in color, structure, and stability. The most commonly recognized allotropes of arsenic are gray arsenic, yellow arsenic, and black arsenic. These different forms arise due to varying arrangements of arsenic atoms in their solid states.[125] Gray arsenic, also known as β-phase arsenic, adopts a rhombohedral structure (space group *R*3*m*) and is the most common and stable allotrope. Its crystal structure is layered, similar to graphite, with honeycomb arrangements of atoms. Unlike graphene, where the layers are flat, gray arsenic consists of buckled hexagonal rings of six arsenic atoms per layer. These layers are stacked in an ABC stacking mode, resulting in a 3D crystal structure. Gray arsenic exhibits semimetal behavior and high conductivity due to strong interlayer binding energy, which is much higher than that of graphene. This is attributed to the cross-layer orbitals in gray arsenic. Owing to the weaker interlayer forces compared to in-plane chemical bonds, gray arsenic is brittle and can be easily exfoliated into 2D layers using sonication or mechanical exfoliation techniques.[126] These few-layer 2D arsenene flakes exhibit properties useful for various electronic applications. They exhibit layer-dependent electrical properties, meaning that the electrical characteristics of the material change based on the number of layers (Fig. 19).[127]

Black arsenic adopts an orthorhombic structure (space group *Bmab*), similar to black phosphorus. Its structure consists of puckered atomic layers held together by van der Waals forces. In contrast to gray arsenic, black arsenic is semiconductive with a direct bandgap of around 0.3 eV.[128] Black arsenic displays extreme in-plane anisotropic electronic and thermal properties, which makes it promising for applications in fields like thermoelectrics and electronics. Black arsenic is a metastable phase, meaning it is less stable than gray arsenic. It is primarily found in the naturally occurring mineral arsenolamprite, and its

Table 2 Summarizing black phosphorus applications in biosensing

No.	Biosensor/imaging type	Material/modification	Target analyte/application	Sensitivity/LOD	Key property/advantage	Ref.
1	Electrochemical aptasensor (label-free)	Few-layer black phosphorus + poly-L-lysine + anti-myoglobin aptamer	Myoglobin (cardiac biomarker)	LOD: 0.524 pg mL^{-1}	High surface area and conductivity enabling stable aptamer immobilization and efficient charge transfer	Kumar *et al.*, 2016[106]
2	Non-enzymatic electrochemical sensor	Few-layer black phosphorus (supercritical CO_2 exfoliated)	Hydrogen peroxide (H_2O_2)	LOD: 0.1 μM	High surface area and conductivity enabling efficient electron transfer for H_2O_2 detection	Yan *et al.*, 2016[107]
3	Mediator-based enzymatic electrochemical sensor	Black phosphorus with mediators (FcMeOH) + GOx/HRP	Oxidoreductase enzymatic reactions	Not specified	Differential electrochemical stability and redox behavior—efficient charge transfer under reductive conditions, prone to oxidation in oxidative systems	Mayorga-Martínez *et al.*, 2019[108]
4	Electrochemical DNA biosensor	Black phosphorus + *in situ* grown N-doped carbonized polymer dots + AuNPs	DNA sequence of *E. coli* O157:H7	LOD: 3.33 × 10^{-20} M	High conductivity and large surface area enhanced with N-CPDs for electron transfer, stability, and DNA probe immobilization; semiconducting behavior gives strong hybridization signals	Shi *et al.*, 2022[109]
5	Electrochemical cytosensor	Black phosphorus + polydopamine + calix[8]arene	Cancer cells (*via* folic acid–receptor recognition)	LOD: 36 cells per mL	Conductive, functionalizable platform; semiconducting properties enable efficient electron transfer and enhanced sensor sensitivity and stability	Xu *et al.*, 2020[110]
6	Electrochemical immunosensor	Phosphorene platform + magnetic covalent organic framework (COF)	Prostate-specific antigen (PSA)	Not specified	Conductive and functionalizable phosphorene enables efficient electron transfer; magnetic COFs amplify signal, enhancing sensitivity and stability	Liang *et al.*, 2019[111]
7	Field-effect transistor (FET) biosensor	Few-layer black phosphorus nanosheets + AuNP-antibody conjugates + Al_2O_3 passivation	Various biomolecules (antigens)	Not specified	High carrier mobility, tunable bandgap, and functionalizable surface enable sensitive, label-free FET biosensing with improved stability	Chen *et al.*, 2017[112]
8	Ion-sensing FET device	Few-layer black phosphorus + ionophore encapsulation	Metal ions (*e.g.*, Pb^{2+})	LOD: 1 ppb	High carrier mobility and tunable bandgap for sensitive ion detection; ionophore encapsulation enhances air stability and preserves semiconducting properties	Li *et al.*, 2015[113]
9	Electrochemical aptasensor (label-free)	Few-layer black phosphorus + poly-L-lysine functionalization	Carbaryl (pesticide)	Not specified	High surface area and conductivity for sensitive detection; poly-L-lysine enhances stability and surface adhesion	Zhang *et al.*, 2022[114]
10	Fluorescent DNA sensor	Black phosphorus nanoparticles (BPNPs)	Nucleic acids (DNA)	LOD: 5.9 pM	Act as fluorescent nanoprobes offering high sensitivity, wide linear range, and low LOD/LOQ	Yew *et al.*, 2017[115]
11	Electrochemical immunoassay	Black phosphorus nanoparticles (BP NPs)	Rabbit IgG	Not specified	Act as electrocatalytic labels *via* the hydrogen evolution reaction for sensitive detection	Mayorga-Martínez *et al.*, 2016[116]
12	Fluorescent enzyme activity sensor	Black phosphorus quantum dots (BP QDs)	Acetylcholinesterase (AChE)	Not specified	Fluorescent probes providing high photostability, pH resistance, and label-free sensitive detection	Gu *et al.*, 2017[117]
13	Colorimetric biosensor	Few-layer black phosphorus (FL-BP) + AuNP hybrid	Carcinoembryonic antigen (CEA)	LOD: 0.20 pg mL^{-1}	FL-BP acts as an electron donor/reservoir enhancing catalytic activity; wide detection range and label-free detection	Peng *et al.*, 2017[118]
14	Theranostic platform	PEGylated black phosphorus nanosheets	Cancer cells (general)	Not specified	BP nanosheets provide drug delivery and NIR imaging; PEGylation enhances stability and biocompatibility	Tao *et al.*, 2017[119]
15	Electrochemical metabolite sensor	Black phosphorus-coated fluoride-doped tin oxide (FTO)	Alpha-hydroxybutyrate (AHB)	Linear range: 0.8–8.75 g L^{-1}	Enables rapid assessment of impaired glucose tolerance; BP coating enhances electron transfer and sensor performance	Sarswat *et al.*, 2017[120]
16	Photoluminescence imaging	Black phosphorus nanoparticles (BPNPs), optionally mesoporous silica coated	Live cell imaging	Not specified	Photoluminescent BPNPs with tunable lifetime responsive to the cellular microenvironment; surface modification extends PL lifetime	Meng *et al.*, 2018[121]
17	Fluorescent nanodot imaging	Black phosphorus nanodots	Biomedical imaging, drug delivery, cellular tracking	Not specified	Tunable bandgap, minimal cytotoxicity, effective blue/green fluorescence; suitable for imaging and drug delivery	Lee *et al.*, 2016[122]

Table 2 (*continued*)

No.	Biosensor/imaging type	Material/modification	Target analyte/application	Sensitivity/LOD	Key property/advantage	Ref.
18	Photothermal & photoacoustic theranostics	PEGylated black phosphorus nanoparticles	Cancer cells (photoacoustic imaging and photothermal therapy)	Not specified	High NIR light-to-heat conversion, excellent photostability, PEGylation enhances biocompatibility; scalable solventless synthesis	Sun *et al.*, 2016[123]
19	Photothermal therapy	PLGA-coated black phosphorus quantum dots (BP-QDs)	Cancer cells (photothermal therapy)	Not specified	PLGA coating enhances stability and biocompatibility; efficient NIR light-to-heat conversion enables effective tumor ablation	Shao *et al.*, 2019[124]

artificial synthesis remains challenging. Studies suggest that pure black arsenic is difficult to stabilize, though it can be stabilized by impurities.[129] It shows anisotropic electronic and thermal properties, which make it suitable for applications where direction-dependent conductivity or heat transfer is desired.[130] Yellow arsenic exists as tetrahedral As_4 molecules, similar to the structure of white phosphorus (P_4). Yellow arsenic is the least stable allotrope and tends to transform into gray arsenic over time, particularly under ambient conditions. Its instability and high reactivity make it useful as an arsenic source in chemical reactions. Unlike the other arsenic allotropes, yellow arsenic is an insulator and has a waxy texture.[125] The reduction of bulk arsenic to the 2D limit results in significant changes to its electronic, optical, and transport properties, making it a promising material for advanced applications in nanoelectronics and optoelectronics.[126,127]

The quest for new materials with extraordinary properties has led to the discovery of various 2D materials beyond graphene, including transition metal dichalcogenides and phosphorene. Arsenene, the monolayer form of arsenic, has emerged as a promising candidate due to its intriguing properties. As a member of the 2D materials family, arsenene exhibits unique structural characteristics and potential for advanced applications in nanoscale devices. The theoretical foundation for arsenene was laid out in the early 2010s, following the success of graphene and other 2D materials. In 2015, researchers began exploring the potential of 2D materials made from heavier group-V elements, including arsenic.[131,132] Theoretical predictions indicated that arsenene would have a tunable bandgap, high carrier mobility, and exceptional mechanical flexibility, all of which made it an intriguing candidate for applications that require semiconductors with controllable properties.[132,133] Key studies predicted that arsenene could exhibit both direct and indirect bandgaps, depending on the number of layers, and that its electronic properties could be tuned by applying mechanical strain or modifying its structure. These theoretical predictions laid the groundwork for experimental efforts to isolate arsenene and study its properties in detail. The ideal structure of arsenene shares a basic element with silicene with clasped honeycomb structures, showing inclination of sp^3 hybridization. Like black phosphorus, arsenene has transporter mobilities as high as a few thousand $cm^2\ V^{-1}\ s^{-1}$.[134] Taking these particular electronic properties into account, arsenene might be a promising candidate for detection applications. Arsenene represents a novel and promising platform for biosensing applications, leveraging its unique electronic and optical properties to develop sensitive, selective, and versatile sensors. Continued research into its synthesis, functionalization, and integration with existing technologies will be crucial in advancing the field of arsenene-based biosensing. With the potential to improve early disease detection and monitoring, arsenene may play a significant role in the future of biomedical diagnostics.

4.1. Synthesis of arsenene

Arsenene can be prepared through several methods, mainly involving techniques like mechanical exfoliation, chemical

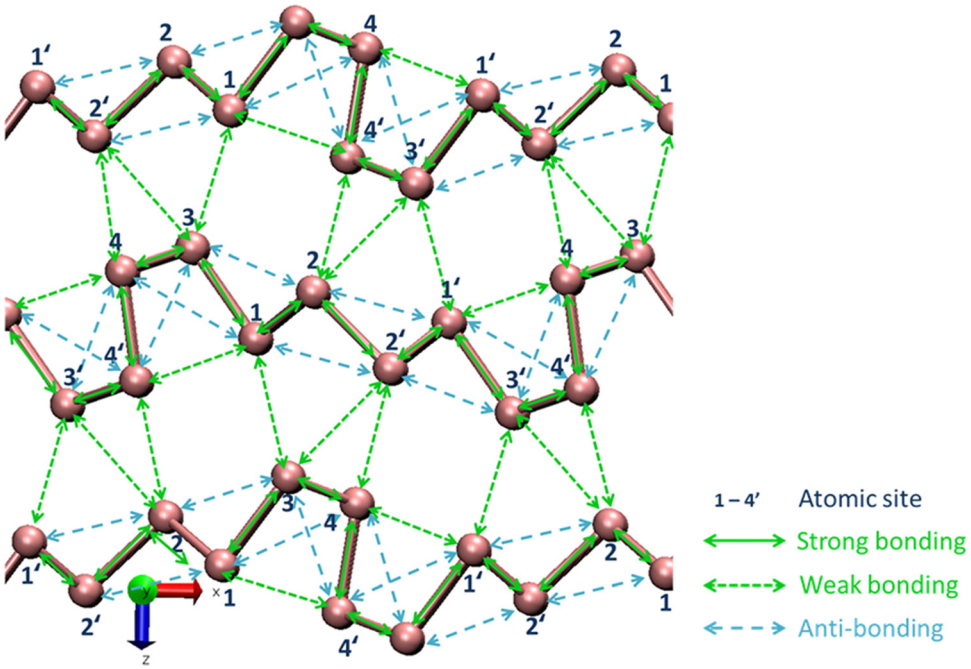

Fig. 19 Bonding nature of arsenic: covalent bonding (strong), van der Waals bonding (weak), and anti-bonding interactions in Pnm_{21}-phase arsenic, reproduced from ref. 130 with permission from Springer Nature, copyright 2019.

vapor deposition (CVD), and liquid-phase exfoliation.[135] Below is a detailed description of these methods: due to the fact that it is composed of piled up 2D monolayers of arsenic atoms, 3D arsenic is an excellent starting point for its preparation techniques. Fabrication often involves exfoliation as a technique due to the high level of covalent connection that exists between arsenic atoms in a monolayer. There are several different kinds of exfoliation, including liquid phase, chemical, mechanical, and surface-based exfoliation. Synthesis of 2D arsenene is possible by liquid phase exfoliation in either aqueous or organic solution environments.[136]

4.1.1. Mechanical exfoliation. Mechanical exfoliation of arsenene is a relatively new area of research, and specific studies focusing solely on mechanical exfoliation are limited compared to other 2D materials like graphene or phosphorene. Several methods fall under this category, each offering different advantages in terms of layer control, scalability, and material quality. The most common is the Scotch tape method, which uses adhesive tape to peel layers from bulk crystals, ideal for high-quality small-scale samples. Atomic force microscopy (AFM)-assisted exfoliation employs precise forces *via* AFM tips for controlled layer removal. Ultrasonic cleaving applies ultrasonic vibrations to exfoliate layers gently. Laser-induced exfoliation uses localized thermal or mechanical stress from a laser to separate layers. Thermal expansion-assisted exfoliation relies on heating to create stress that peels layers. The blade-based shear method uses sharp edges to apply direct force for exfoliation. Lastly, nanoparticle-assisted exfoliation employs nanoparticles in a matrix to propagate stress for uniform layer removal. It has been shown that it is difficult to manage the number of layers that are generated when exfoliation is used, despite the fact that exfoliation is a promising method for fabricating a variety of arsenene nanostructures.

Mechanical exfoliation is especially effective for black arsenic, which has a weaker interlayer force, making it easier to peel off thin layers. The first successful mechanical exfoliation of 2D black arsenic was performed by Chen *et al.*, who used natural black arsenic minerals. The atomic force microscopy (AFM) image from Fig. 20 showed thin black arsenic nanoflakes with a step size of 0.6 nm, indicating the presence of thin, few-layer flakes.[137] Zhong *et al.* successfully exfoliated monolayer black arsenic flakes with a thickness of 0.7 nm from bulk natural minerals onto Si/SiO_2 (300 nm) substrates.[138] Yun *et al.* used commercially available black arsenic crystals (from 2D Semiconductors Inc.) and successfully exfoliated thin nanoflakes using the Scotch tape method. They confirmed the quality of the 2D black arsenic nanoflakes with images of exfoliated layers showing successful transfer and preservation of the nanoflake structure.[139] The method preserves the intrinsic crystal quality of black arsenic, making it suitable for studying its fundamental physical, optical, and electrical properties. For materials like gray arsenic and other allotropes, the stronger interlayer forces make it difficult to obtain thin films using this method.

4.1.2. Liquid-phase exfoliation. Liquid-phase exfoliation is a prominent method for the large-scale production of arsenene, the monolayer form of arsenic. In this process, a liquid medium (solvent) is used to suspend and exfoliate the bulk material into thin nanosheets, such as monolayers or few-layer structures. This method applies external forces, such as sonication or shear force, to break the interlayer bonds in bulk materials, resulting in the exfoliation of thin 2D nanosheets. Organic solvents with higher boiling points and surface tension, like

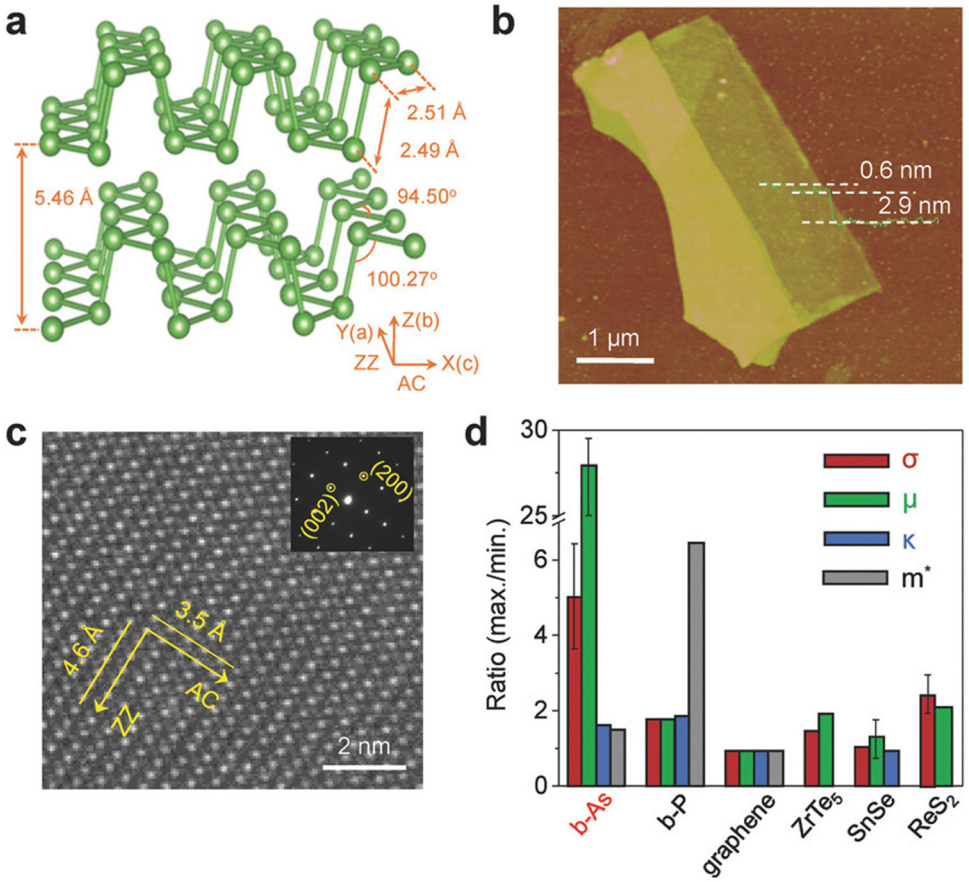

Fig. 20 Anisotropic lattice structure and properties of layered black-arsenic. (a) Its 3D structure, modeled *via* DFT, reveals a 5.46 Å interlayer spacing. (b) Mechanically exfoliated b-As flakes, imaged by AFM, show monolayer thickness around 0.6 nm. (c) HRTEM with atomic resolution identifies lattice parameters of 4.6 Å (AC direction) and 3.5 Å (ZZ direction), with an inset displaying the indexed SAED pattern. (d) Electrical conductivity (σ), mobility (μ), thermal conductivity (κ), and effective mass (m^*) exhibit significant in-plane anisotropy between AC and ZZ directions, compared with other 2D materials, reproduced from ref. 137 with permission from John Wiley and Sons, copyright 2018.

N-methyl-2-pyrrolidone (NMP) and dimethyl sulfoxide (DMSO), are typically used. For example, Vishnoi *et al.* isolated arsenene sheets from gray arsenic crystals in NMP, while arsenene nanodots were achieved in nonpolar toluene solvents. DMSO was employed for direct exfoliation due to its high polarity and thermal stability. The exfoliated nanosheets can be functionalized, for instance, with 4-nitrobenzenediazonium salts, enhancing their properties and stability.[140] Beladi-Mousavi *et al.* systematically studied the effect of different solvents, including hexane, isopropyl alcohol (IPA), acetone, methanol, and others, on the productivity of arsenene. They found that solvents with higher boiling points and surface tensions, like NMP and DMSO, yielded the highest concentrations of gray arsenene nanosheets as shown in Fig. 21. Additionally, the interaction between monolayer arsenene and solvents was shown to influence yields. For example, stronger interactions between solvents (like cyclohexane and chloroform) and arsenene lead to higher exfoliation efficiency.[141] In shear exfoliation, mechanical force is applied externally to break the interlayer bonds. Pumera *et al.* used an everyday kitchen blender, in combination with sodium cholate as a surfactant, to exfoliate arsenene, antimony, and bismuth nanosheets. This method produced nanosheets with reduced thickness and scale. Further modification of exfoliated arsenene is possible using chemical agents like dichloromethane and butyllithium, introducing functional groups into the nanosheets.[142]

The insertion-assisted exfoliation method utilizes intercalation agents (*e.g.*, ions and molecules) to expand the interlayer distance in bulk arsenic, facilitating easier exfoliation. For instance, Kovalska *et al.* performed electrochemical exfoliation using ammonium hexafluorophosphate (NH_4PF_6) as the intercalating agent. Low-voltage electrochemical treatment of black arsenic enabled the exfoliation of layers, resulting in nanosheets with a thickness of ~0.6 nm.[143] In photo-assisted exfoliation, light irradiation is used to assist the exfoliation process. For instance, Sturala *et al.* employed UV light and chromium hexacarbonyl to exfoliate and covalently functionalize gray arsenic crystals simultaneously.[144] Zhao *et al.* provided computational insights into a light-driven method for exfoliating arsenene, potentially leading to the development of single or few-layer arsenene. Azobenzene, known for its ability to switch between *trans* and *cis* conformations upon exposure to light, can induce structural changes in the layered material. DFT results show that the *trans*-to-*cis* transition in azobenzene

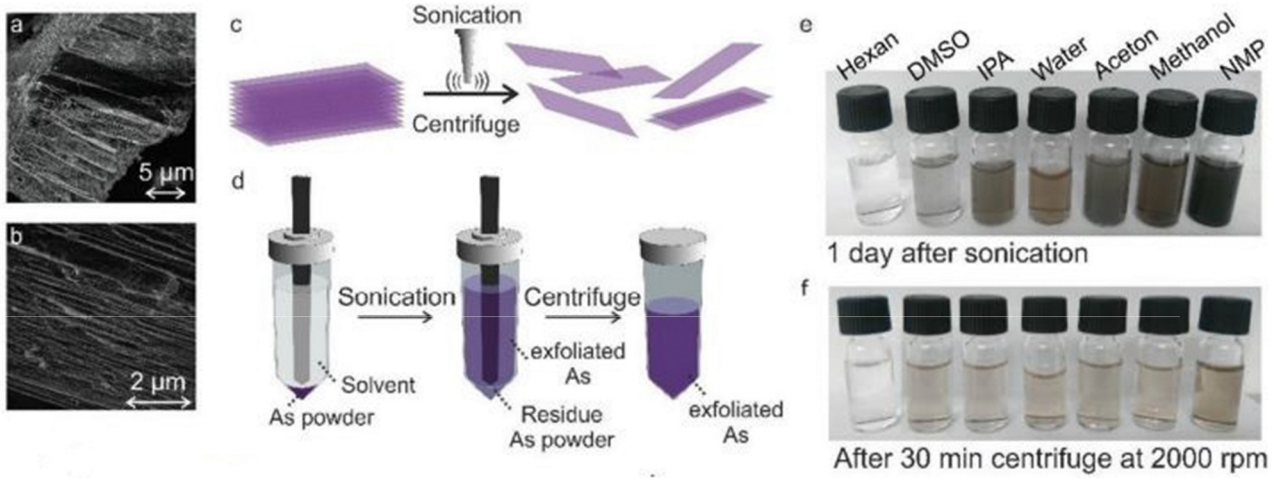

Fig. 21 Solvent exfoliation of arsenic *via* tip ultrasonication: (a) and (b) SEM images showcase the layered structure of bulk arsenic crystals. (c) The exfoliation process involves tip ultrasonication and subsequent centrifugation to isolate thin layers. (d) A schematic illustrating the tip ultrasonication setup designed to minimize exposure to ambient air, preserving material quality. (e) A photograph shows arsenene dispersions in various solvents one day post-ultrasonication, and (f) the dispersions after centrifugation at 2000 rpm, reproduced from ref. 141 with permission from John Wiley and Sons, copyright 2018.

can increase the interlayer spacing of arsenene from 6.59 Å to 11.07 Å. This conformational shift may weaken the van der Waals forces between layers, promoting exfoliation.[145] Another method was sonicating grey arsenic in either NMP or toluene in order to create regular arsenene nanosheets and nanodots. Using photoluminescence (PL) studies, the blue luminescence of arsenene nanodots was seen. It was feasible to validate the predicted shape and interlayer spacing of rhombohedral arsenic by employing TEM and selected area electron diffraction (SAED) on the few-layer arsenene that was produced. In addition, AFM was used in order to examine monolayer and bilayer arsenene nanosheets with a thickness of less than 1 nanometer. The few-layer arsenene was given a treatment with 4-nitrobenzene-diazonium tetrafluoroborate, which resulted in the chemical functionalization of the compound.[146]

4.1.3. Epitaxy method. When fabricating 2D nanostructures using bottom-up methods, the arrangement of atoms is influenced by their intrinsic characteristics. This approach is particularly suited for nanomaterials lacking a layered geometric structure. The primary techniques employed in this process are physical vapor deposition (PVD) and chemical vapor deposition (CVD). The performance and functionality of the resulting nanostructures depend significantly on the choice of substrate used in the fabrication. Due to arsenic's low melting point and high volatility, PVD techniques like molecular beam epitaxy (MBE) are commonly employed. MBE allows for the growth of high-quality arsenene monolayers at low temperatures, which is essential for maintaining the material's structural integrity. In 1993, Boca *et al.* demonstrated how molecular beam epitaxy enables precise control over deposition to form thin, flat layers of grey arsenic, making it an effective method for fabricating arsenene layers for future nanoelectronic and optoelectronic applications.[131] CVD methods utilize chemical reactions to deposit materials onto substrates. In the context of arsenene, CVD can involve using arsenic precursors that react to form arsenene nanostructures. This approach can yield uniform films with good crystallinity but typically requires careful control of deposition conditions due to the volatility of arsenic. The use of an InAs substrate and nitrogen ions led to the production of a stack of arsenene nanoribbons that was both complicated and multi-layered. In order to produce arsenene, the substrate was subjected to a treatment with nitrogen plasma at a temperature of 450 °C for a period of thirty minutes. By exposing the substrate to nitrogen plasma for thirty minutes at a power of one hundred watts, it was possible to regulate the nanoribbons' thickness and prevent flaws from occurring. Transmission electron microscopy (TEM) and secondary ion mass spectrometry (SIMS) were utilized to verify the successful production of multilayer arsenene, which also included an InN buffer layer and an InAs substrate.[147] According to the findings of Shah *et al.*, it is also feasible to synthesize homogeneous arsenene on an Ag substrate by subjecting a heated piece of InAs to an atmosphere of As pressure that is two times 10^{-7} Torr at temperatures ranging from 250 to 35 °C. Low-energy electron diffraction (LEED) was able to verify the well-ordered geometry of arsenene. Scanning tunnelling microscopy (STM) was able to identify line and triangle flaws in the material. The results of an experiment known as angle resolved photo electron spectroscopy (ARPES) demonstrated an indirect band gap with a value of 1.47 eV. These results are consistent with theoretical predictions.[135]

4.2. Properties of arsenene

Arsenic atoms have five valence electrons in the $4s^2$ $4p^3$ orbitals, allowing them to form different bonding patterns. The nature of bonding within arsenic, particularly involving p-orbitals, enables flexibility in how arsenic atoms arrange themselves, resulting in different atomic structures. In the case

of arsenene, the surface-to-volume ratio becomes critical due to the small size of the arsenic atom. As the size of the nanostructure decreases, more atoms are located at the surface relative to the bulk. This increased surface area can significantly impact properties like electrical conductivity, chemical reactivity, and mechanical strength, making arsenene highly suitable for advanced applications in nano-electronics, sensors, and optoelectronic devices.[148] Furthermore, the number of arsenic atoms in arsenene nanostructures also influences their physical behavior. In nanoscale systems, the collective behavior of a smaller number of atoms can alter fundamental properties, such as bandgap, due to quantum effects. The electronic configuration and the hybridization of orbitals in the arsenic atom lead to various forms of allotropes.[149] Bandgaps seen in arsenene vary depending on the allotrope of arsenene.

4.2.1. Structural properties. The monolayer allotropes of arsenene are categorized into three main types of structures based on their atomic arrangements: honeycomb, non-honeycomb, and porous structures. α-As and β-As are the most common honeycomb structured allotropes consisting of six-membered rings and exhibiting hexagonal symmetry, with armchair and zigzag edges, similar to phosphorene in structure. These allotropes are composed of six-membered (As) rings, and both puckered (α-As) and buckled (β-As) forms exist. γ-As, δ-As, and Tricycle (T)-As allotropes also have honeycomb symmetry but differ in their ring connectivity. Tricycle-As, for example, combines features of α-As and β-As through in-plane connections, refer to Fig. 22. Non-honeycomb allotropes involve square and octagonal arrangements of arsenic atoms. A square-octagon ((O)-As) allotrope is made up of alternating squares and octagons (4–8 structure), giving it a non-honeycomb configuration. The structure leads to unique electronic properties due to its geometry. ε-As and ξ-As allotropes include As_4 square units. Their puckered side views resemble armchair and zigzag edges similar to those found in honeycomb structures like α-As and β-As. They are notable for their (4–6–10)-As arrangements, incorporating four, six, and ten-membered rings in non-honeycomb patterns. Porous structures are characterized by more open, lattice-like arrangements of arsenic atoms. η-As and θ-As structures feature As_5 pentagonal units connected by As–As bonds. They differ from the honeycomb-type allotropes in terms of their open, porous nature. A Hex-Star (HS-As) allotrope forms a hexagonal lattice that looks like the star of David (Magen-David) when viewed from above as shown in Fig. 22.[134]

The openness of the lattice makes it a unique porous structure among arsenene allotropes. Arsenene primarily exhibits sp^3 hybridization due to the involvement of both s and p orbitals in bonding. This hybridization leads to a mix of sigma bonds and lone electron pairs, creating the distinctive buckled or puckered structures.[150] In the β-phase, for instance, the buckling is driven by sp^3 hybridization, which prevents a planar honeycomb structure, thereby making the material stable. The lattice constants of different arsenene allotropes vary. In α-arsenene, the in-plane As–As bond distance is approximately 2.5 Å, while in β-arsenene, the distance between atoms in different layers is slightly larger due to the buckling. The lattice constants of arsenene are typically in the range of 3.6 Å to 4.2 Å, depending on the specific allotrope, and contribute to its electronic properties, including band gaps.[151] The stability of arsenene depends on factors such as temperature and environmental exposure (*e.g.*, to oxygen). DFT calculations confirm the dynamical stability of α- and β-arsenene phases, especially at low temperatures, making them suitable for nano-electronics applications. Most arsenene allotropes have a relative formation energy less than 100 meV per atom, making them energetically stable and relatively easy to form.[152] The structural tension caused by smaller rings increases the formation energy and reduces stability, while allotropes with five- or six-membered rings are more energetically favorable. Each allotrope has distinct structural and electronic properties, making arsenene a versatile material for applications in optoelectronics and nanotechnology. The variety of bond configurations and atomic arrangements give rise to different physical characteristics, such as stability, band gaps, and reactivity.[153]

4.2.2. Electrical properties. The electronic properties of 2D arsenene are strongly influenced by various external factors such as the layer number, strain, electric field, doping, and functionalization. These factors not only affect the magnitude of the energy band gap but also its nature, leading to transitions between semimetallic and semiconducting behavior. The energy band gap in arsenene nanomaterials showed a notable decrease with increase of layers in the nanomaterial. Bulk gray arsenic is a semimetal. However, when the thickness is reduced, it undergoes a semimetal-to-semiconductor transition.

A monolayer of gray arsenene shows an indirect bandgap of 2.49 eV and a bilayer has an indirect bandgap of 0.37 eV. The electronic band structures of arsenic differ across its trilayer, bilayer, and monolayer forms due to variations in interlayer interactions and quantum confinement, refer to Fig. 23. Trilayer arsenic exhibits a smaller band gap with moderate interlayer coupling, influenced by its stacking arrangement. Bilayer arsenic shows a larger band gap as interlayer coupling decreases, with more distinct electronic bands. Monolayer arsenic experiences the strongest quantum confinement, resulting in a direct or quasi-direct band gap depending on its phase, making it highly suitable for electronic and optoelectronic applications.[154] Puckered arsenene has an indirect bandgap of 0.831 eV, but its bandgap can transition from indirect to direct when subjected to external strain or an electric field. The α-arsenene nanomaterial became a semi-metal when an out-of-plane strain was applied to it. Additionally, a direction-dependent effective mass of electrons was observed during this process.[155] The band gap shifts from indirect to direct when uni-axial tensile and compressive strain is applied to β-arsenene. The transition from semiconducting to metallic behaviour in arsenene occurs at a compressive strain of 12%.[156] By adding an external electric field, the energy gap could be adjusted and its magnitude could be changed. Band inversion is attainable by the use of electric fields that run in a transverse direction.[151] When an electric field with a strength of roughly 4.2 V nm^{-1} was applied, a change from indirect to direct energy gap could be detected. Furthermore, when an electric field with a

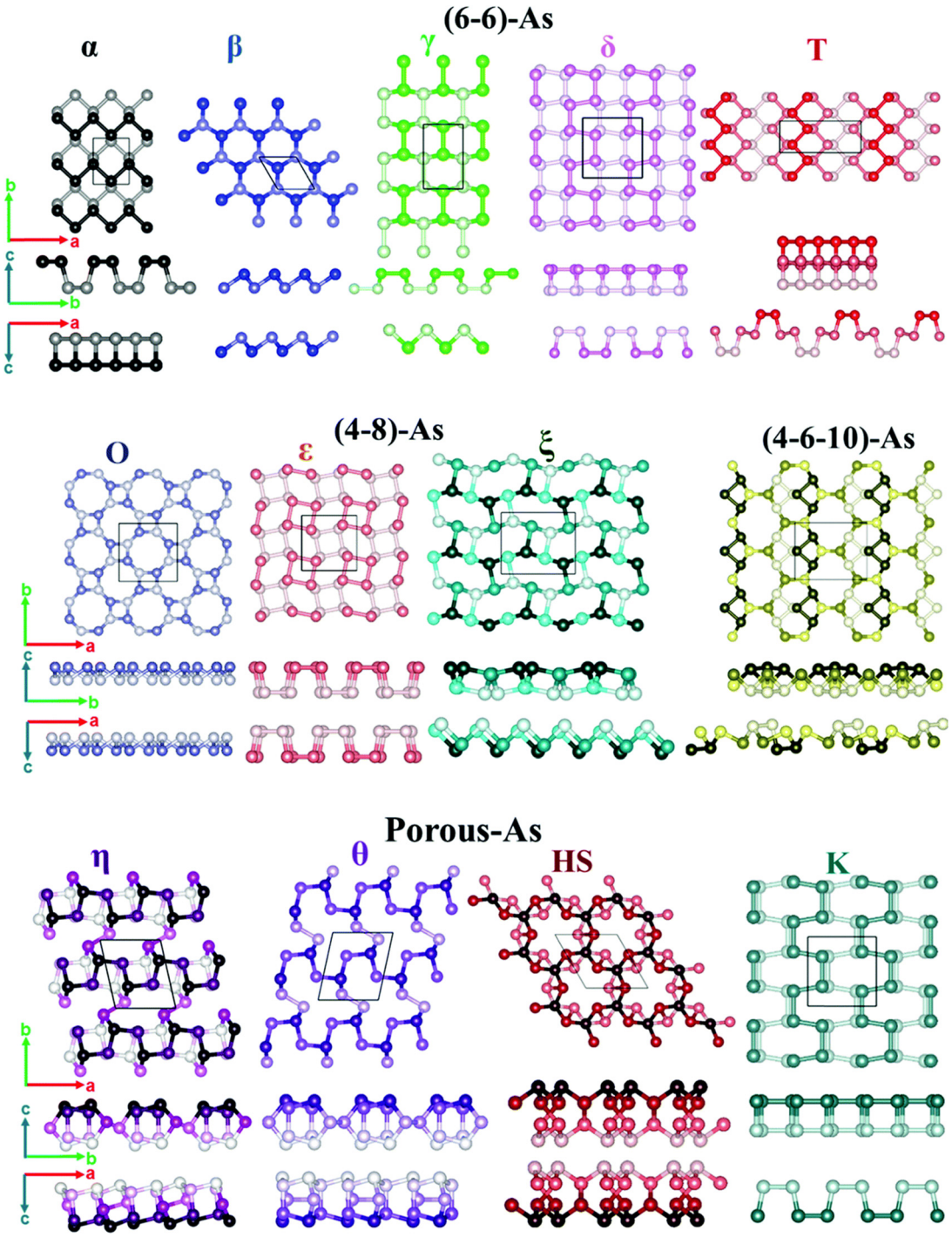

Fig. 22 Arsenene monolayer allotropes in top and side views, reproduced from ref. 134 with permission from RSC publication, copyright 2018.

strength of approximately 1 V A^{-1} was applied, a change from semiconductor to metal could be seen.[150,156] The interaction of pure arsenene with metals demonstrated a severe hybridization of the band structure, which led to the conversion of arsenene's electronic nature. The Mg–, Ni–, Pb–, Pd–, Pt–, and Zn–arsenene systems exhibit nonmagnetic semiconductor behavior, while the Al–, Cu–, Li–, and Na–arsenene systems display metallic behavior. Notably, Co– and V–arsenene systems exhibit magnetic metallic behavior, whereas Au–, Cr–, Mn–, and Ti–arsenene systems emerge as magnetic semiconductors.[157] The binding of biomolecules can modulate the bandgap, enabling detection of biomolecules through changes in its electronic properties.

Arsenene exhibits high carrier mobility comparable to other 2D materials like phosphorene. The mobility can vary depending on the phase and the structural configuration of the monolayer.

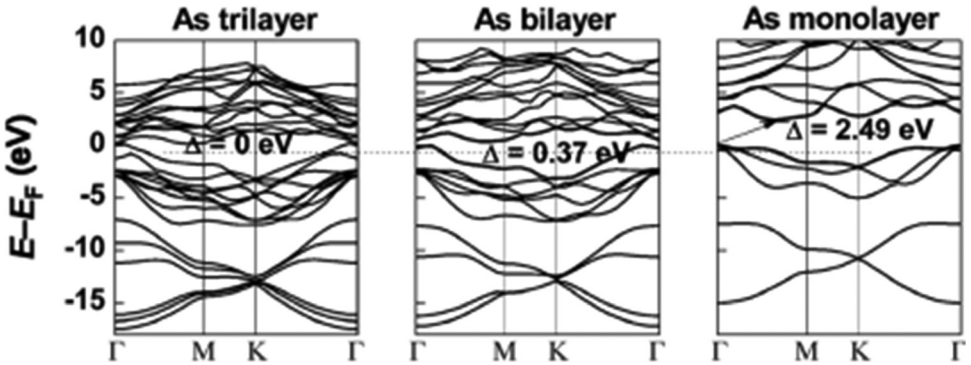

Fig. 23 Electronic band structures of trilayer, bilayer and monolayer gray arsenic, reproduced from ref. 154 with permission from John Wiley and Sons, copyright 2015.

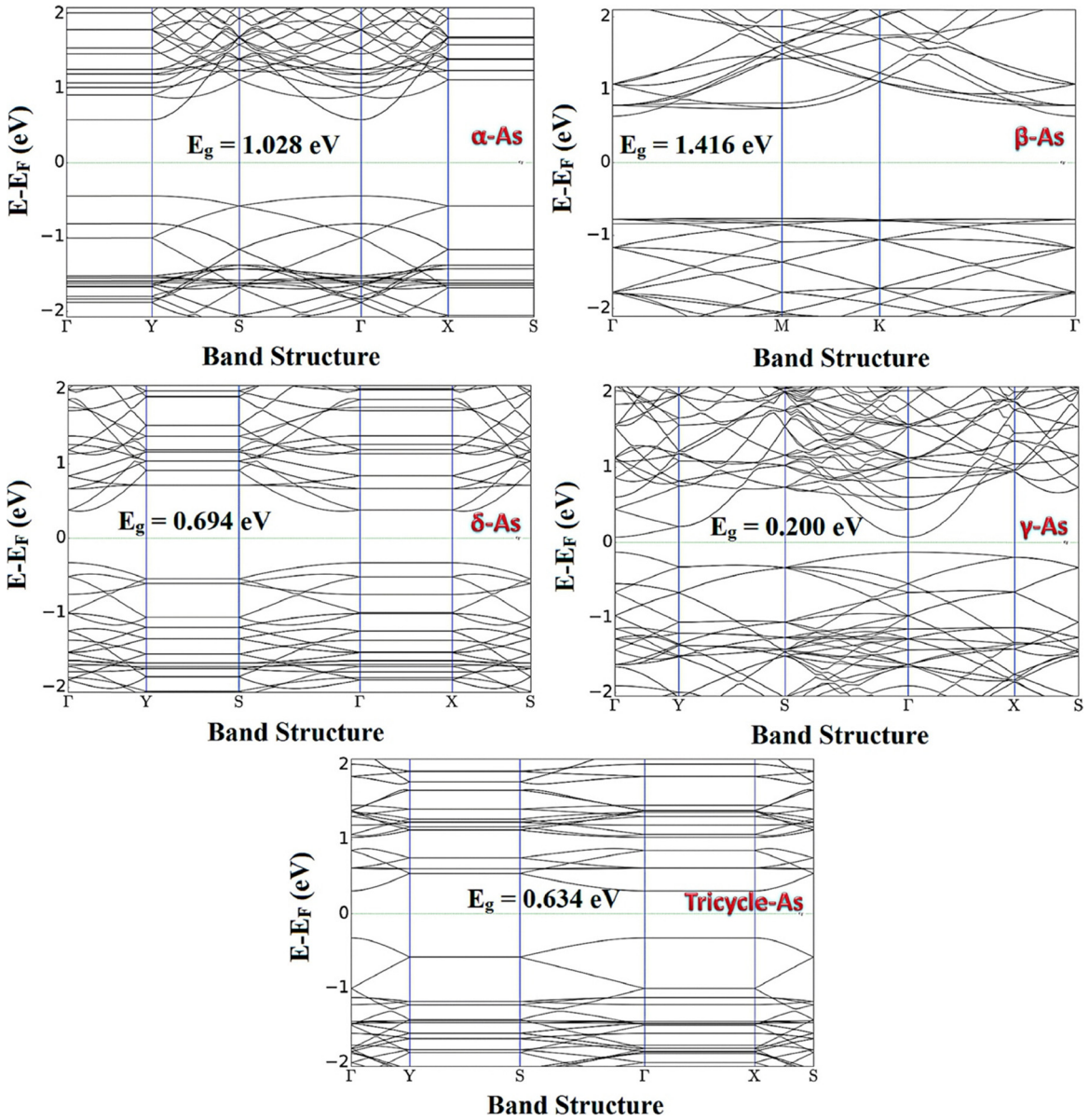

Fig. 24 Electronic band structures of allotropes of arsenene, reproduced from ref. 148 with permission from Elsevier, copyright 2022.

Table 3 Allotropes of arsenene and the bandgaps exhibited based on different levels of theories

Allotrope of arsenene	Range of bandgap observed (in eV)			
	GGA	HSE	GW	Expt
Alpha	0.72[134]	1.028[148]	—	—
Beta	1.58[134]	1.416[148]	2.47[148]	2.38[146]
Del	0.50[134]	0.649[148]	—	—
Gamma	0.79[134]	0.200[148]	—	—
Tricycle	0.61[134]	0.634[148]	—	—

GGA – Generalized Gradient Approximation theory, HSE – Heyd–Scuseria–Ernzerhof theory and GW – GW Approximation.

The structural anisotropy in arsenene allotropes plays a critical role in determining their carrier transport properties (Fig. 24). This anisotropy, which arises due to differences in atomic bonding along various crystal directions, leads to anisotropic carrier mobility. The mobility for holes (p-type) is reported to be up to highest on the order of 10^3 cm^2 V^{-1} s^{-1} in certain phases, which is favorable for high-speed electronic devices.[134] Experimentally, gray arsenic nanoflakes show thickness-dependent electrical resistance. For instance, a 10 nm thick gray arsenic nanoflake exhibited an electrical conductivity of about 3.5×10^3 S m^{-1}, highlighting its potential as a contact electrode material.[158] Black arsenic nanoflake-based FETs have demonstrated p-type behavior, with a carrier mobility of 51 cm^2 V^{-1} s^{-1} and a current on/off ratio of 10^5 at $V_{ds} = -1$ V.[159] These electronic properties of arsenene are useful in biosensing, stemming from its high sensitivity to changes in its electronic structure upon interaction with biomolecules. These properties enable arsenene to act as an efficient transducer in biosensors (Table 3).

4.2.3. Optical properties. The optical properties of arsenene are highly intriguing due to its unique electronic structure and the tunability of its bandgap through external factors such as strain, doping, and electric fields. These properties make arsenene a promising candidate for applications in optoelectronics and photonics. Arsenene has an energy gap close to the visible spectrum that is susceptible to change as a result of factors like as electric fields, strain, and the number of layers.[160] In addition to this, polarized light has the ability to alter the electrical and optical energy gaps. When light is polarized in the *y* direction, the allotrope of β-arsenene, which exhibits direction-oriented optical characteristics, is able to absorb light in the solar domain. In the visible to ultraviolet range of the electromagnetic spectrum, arsenene exhibits strong optical absorption.[161] The optical absorption of arsenene is enhanced due to strong quantum confinement effects in its 2D form. The absorption coefficient can be as high as 10^5 cm^{-1}, which is promising for applications in solar cells and photodetectors. When arsenene is subjected to electromagnetic fields, however, the indirect character of the energy gap in arsenene causes the substance to have a poor light-emitting efficiency. Enhancing the optical transition and extending the optical window into the infrared region may be accomplished by the use of defects, chemical decoration, doping, and adsorption.[162,163] Like many 2D materials, arsenene exhibits strong excitonic effects due to reduced screening in two dimensions. This leads to tightly bound exciton states, which enhance the optical absorption at specific wavelengths and are useful in designing excitonic devices for quantum computing or high-efficiency photovoltaics. The dielectric function of arsenene shows strong peaks in the UV region, indicating significant optical transitions. The refractive index of arsenene also varies with the energy of incident photons, which is essential for designing optical interference or evanescent field-based biosensing. Vishnoi *et al.* conducted experimental studies on liquid-exfoliated arsenene nanosheets and nanodots. The nanosheets exhibited a bandgap of approximately 2.3 eV, while the nanodots displayed blue photoluminescence (PL) in the 400–460 nm range, indicating their potential for light-emitting applications.[146] When biomolecules bind to arsenene, they can alter its surface properties through charge transfer, adsorption-induced strain, or local dielectric changes. These interactions modify the material's bandgap, exciton recombination dynamics, or surface states, leading to measurable changes in PL. For example, the quenching of PL intensity may occur due to non-radiative energy transfer to the adsorbed biomolecules, while a shift in the PL wavelength can indicate changes in the bandgap or exciton localization caused by the binding event. These alterations provide a sensitive, real-time, and label-free mechanism to detect specific biomolecular interactions.

4.2.4. Mechanical properties. The mechanical properties of arsenene, particularly its anisotropic elastic modulus, are influenced by its buckled structure. For monolayer arsenene, studies report elastic modulus values around 27–30 N m^{-1}, which, while lower than graphene, are still substantial for potential applications in flexible electronics. This mechanical flexibility, coupled with anisotropic stiffness, makes arsenene a promising material for nanoelectronics and sensor technologies.[164] Keckik *et al.* reported that the calculated in-plane stiffness values of different phases of arsenene reveal interesting mechanical properties. For the buckled structure arsenene (b-As), the in-plane stiffness is isotropic with a value of $C = 58$ N m^{-1}. In contrast, for w-As (wash board structure allotrope), the stiffness exhibits strong directionality due to its structure, with $C_x = 20$ N m^{-1} and $C_y = 55$ N m^{-1}. Poisson's ratio further highlights the mechanical anisotropy of arsenene phases. For b-As, Poisson's ratio is uniform at $\nu_x = 0.21$, whereas for w-As, it exhibits directionality with $\nu_{xy} = 0.33$ and $\nu_{yx} = 0.91$, emphasizing the structural differences between the two. This indicates that different arsenene allotropes have unique mechanical responses, making them suitable for various flexible electronic and nanoelectronic applications.[153] Arsenene's electronic properties can be tuned by applying strain. Uniaxial and biaxial strains affect its bandgap and carrier mobility. For example, a transition from semiconductor to metal has been observed under strain conditions.[165] The application of strain, both in-plane and out-of-plane, significantly alters the geometric and mechanical characteristics of arsenene. Without strain, hole mobility dominates due to the lower effective hole mass, but strains exceeding 2% reverse this trend. Out-of-plane strain influences the buckling height, while in-plane strain alters lattice constants

and other structural parameters.[155] Tensile and compressive strains reveal unique transitions in arsenene. α-arsenene displays superior stretchability, with a 1% uniaxial strain inducing an indirect-to-direct bandgap transition[154] and compressive strain over 10% leading to a semiconductor-to-metal transformation.[150] Similarly, β-arsenene undergoes an indirect-to-direct bandgap change with 4% biaxial strain while maintaining its honeycomb geometry.[150] Larger compressive strains in α-arsenene and λ-arsenene result in semiconductor-to-metal transitions, with λ-arsenene additionally showing a direct-to-indirect bandgap shift under uniaxial strain above 12%.[156] Notably, certain strains can induce a shift from topologically trivial to nontrivial phases in arsenene nanostructures.[166] Defects, both inherent and induced, significantly influence arsenene's mechanical properties. Point defects like single and double vacancies, as well as Stone–Wales (SW) defects, are commonly observed. The SW defects, in particular, have been shown to exhibit thermodynamic stability, affecting the structural and mechanical resilience of the material. These factors underscore the tunability of arsenene's properties through strain engineering and defect control.[167]

4.3. Applications of arsenene

Arsenene's potential as a biosensor is heavily supported by theoretical studies, which provide detailed insights into its interaction with biomolecules. Density functional theory (DFT) calculations have been extensively used to explore arsenene's electronic, chemical, and mechanical properties in the context of biosensing.[168] These studies provide insights into how arsenene might interact with biological molecules (like proteins, DNA, glucose, *etc.*). Although theoretical studies have shown great potential for arsenene in biosensing, experimental studies are still in their early stages due to challenges in material synthesis, stability, and characterization. DFT is a powerful computational tool widely used in biosensing studies to investigate the interaction between biomolecules and sensor materials at the atomic level. Its ability to model electron density makes it particularly useful for analyzing how biological molecules, such as enzymes, proteins, and DNA, interact with nanoscale sensor surfaces, such as 2D materials, including arsenene, graphene, and others.[169] DFT helps in predicting the adsorption energies, charge transfer, and binding affinities between biomolecules and nanomaterials. This is crucial in biosensing because the sensitivity of a biosensor is often linked to how effectively the target biomolecule interacts with the sensor surface. By analyzing how different modifications (*e.g.*, functionalization and doping) to 2D materials affect their electronic and chemical properties, DFT can aid in the design of more sensitive and selective biosensors.[170] DFT is used to explore changes in the electronic structure of materials when biomolecules bind to the sensor surface, which is key to understanding the sensing mechanism. For instance, the conductance or current changes in a 2D material-based biosensor due to biomolecule adsorption can be predicted using DFT calculations.[171] DFT has also been applied to study the interaction between DNA strands and nanomaterials. The adsorption energies and electronic changes observed through DFT can help develop highly selective DNA biosensors for detecting genetic mutations or pathogens.[172] In certain biosensors, enzymes that react with specific gases or toxins are immobilized on nanomaterial surfaces. DFT is used to simulate how these interactions occur and how the sensor's properties change, which is essential for real-time monitoring of environmental pollutants or harmful substances in medical diagnostics.

4.3.1. Detection of nucleobases. The study conducted by Nagarajan *et al.* into the adsorption of nucleobases, namely adenine (A), guanine (G), thymine (T), cytosine (C), and uracil (U), on ε-arsenene nanosheets holds significant implications for the field of biosensing. In this study, various factors were studied when allowing the adsorption of nucleobases on ε-arsenene nanosheets. Negative adsorption energy shows that the process of adsorption is exothermic while negative charge transfer shows that the charge moves from the nanosheet to nucleobases where the nanosheet acts as the donor. The electrical properties were also seen to change after adsorption. The utilization of ε-arsenene nanosheets as a sensing platform has been proposed for the detection of nucleobases, which are crucial constituents of DNA and RNA. The comprehension of the adsorption characteristics of nucleobases on ε-arsenene nanosheets can facilitate the creation of biosensors that exhibit elevated selectivity and sensitivity. The precise interactions that occur between nanosheets and nucleobases can be utilized for the purpose of devising sensors that possess the ability to detect and differentiate various nucleobases or sequences of DNA/RNA. The utilization of ε-arsenene nanosheets enables a label-free detection strategy, whereby the adsorption of nucleobases onto the surface of the nanosheets can elicit alterations in their electronic properties or energy band gap. These alterations are capable of being identified and quantified, thereby facilitating the direct identification of nucleobases without necessitating supplementary labelling or amplification procedures. The relevance of ε-arsenene nanosheets in the adsorption of nucleobases is particularly notable in the context of DNA/RNA sequencing. The acquisition of significant genetic information for applications such as disease diagnostics, personalized medicine, and genetic research can be achieved through the sequencing of DNA/RNA. The integration of ε-arsenene nanosheets into sequencing devices or platforms presents a promising avenue for the detection of nucleobases during the sequencing process, thereby offering a novel approach. The findings have the potential to enhance label-free nucleobase detection, selective sensing, and facilitate DNA/RNA sequencing.[173]

4.3.2. Detection of vomiting agents. The exploration of gamma arsenene nanosheets (GAs) as a sensing medium for vomiting agents is covered in another study by Nagarajan *et al.* The diphenyl-chloroarsine (DA) and diphenylcyanoarsine (DC) molecules, which are the vomiting agents, were employed as sensing substrates for GA nanosheets, which were shown to have semiconductor nature and a band gap of 1.39 eV. The interaction of vomiting agents on GA nanosheets was examined using band gap fluctuation, charge transfer, and

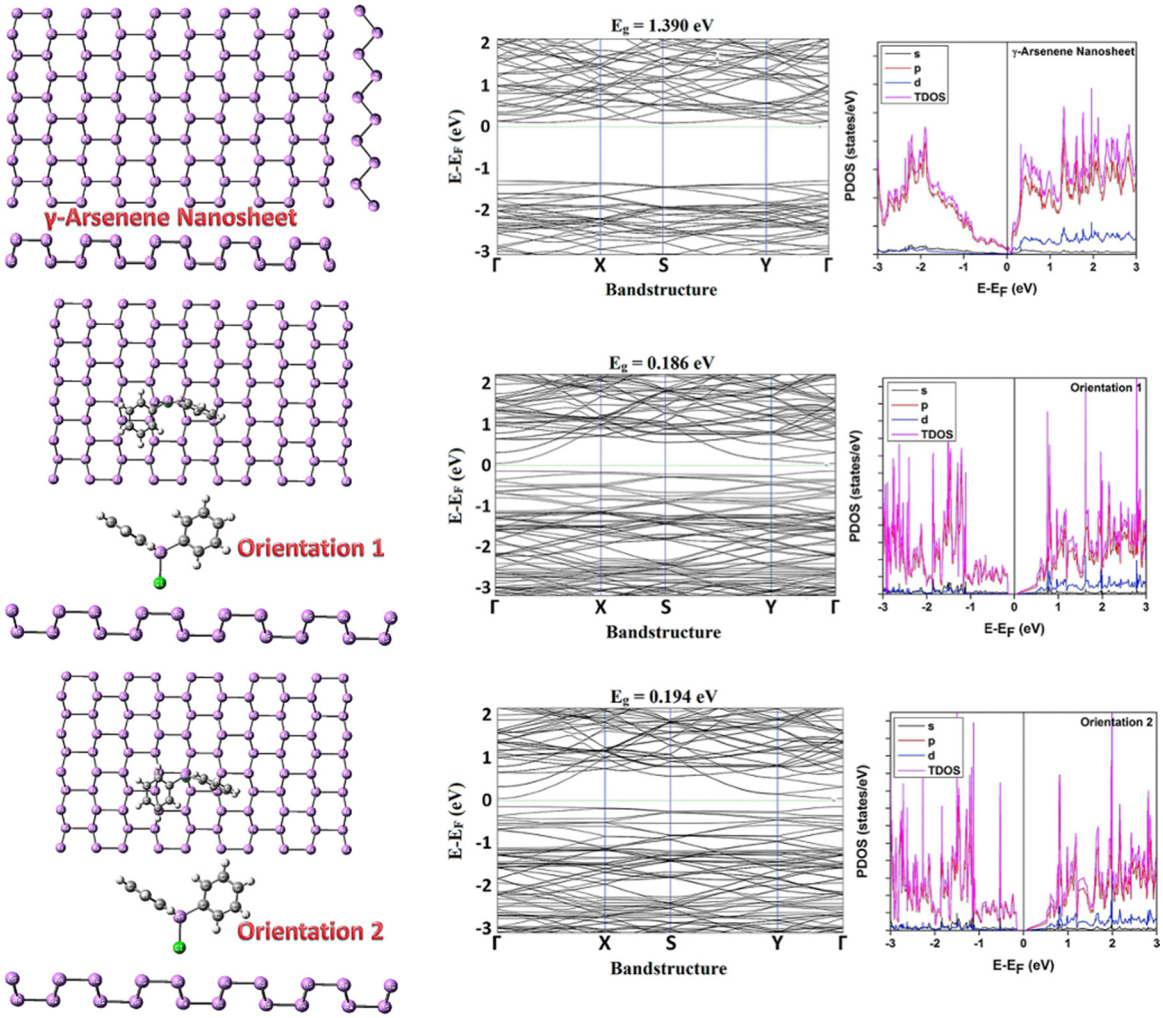

Fig. 25 Various orientations in which DA and DC adsorb onto GA and their respective pDOS and band structure maps, reproduced from ref. 174 with permission from Elsevier, copyright 2020.

adsorption energy. The projected-density of states spectrum and band structure analysis both revealed alterations in the electronic properties of GA nanosheets. Only three locations, namely the bridge, top, and valley sites, show significant diphenyl-chloroarsine and diphenylcyanoarsine adsorption. The adsorption behaviour of the GA nanosheets was also investigated, and the basis set superposition error (BSSE) and the Boys-Bernadi counterpoise technique were used to calculate the adsorption energies. Charge transfer between the vomiting agents and gamma-arsenene sheets happens during the physisorption process, and it is shown that the average energy gap fluctuation is higher for diphenylcyanoarsine adsorption than diphenyl-chloroarsine adsorption. This may result in a notable adjustment to the conductivity of the gamma-arsenene nanosheet. The adsorption of molecules also modifies the energy bandgap value of the nanosheet. When compared to the density of states (DOS) spectrum of pristine gamma-arsenene nanosheets, the adsorption clearly demonstrates the variance in the peaks. In addition, the p-orbital of the arsenic atoms in the nanosheet was shown to hybridize with the target molecules. The change in the color gradient along the nanosheets brought about by the adsorption of target molecules may be used to determine the electron density of adsorbed GA nanosheets. Thus, the alteration in the electronic characteristics of nanosheets caused by the adsorption of diphenyl-chloroarsine and diphenylcyanoarsine based on the electron density, DOS spectrum, and band structure analyses was also observed (Fig. 25).[174]

4.3.3. Detection of pesticides. Bhuvaneshwari *et al.* study's target compounds, malathion and ethyl parathion, are members of a specific family of pesticides. Among the organophosphate insecticides, malathion is one of the least harmful comparatively and, when consumed by people, may turn into malaoxon. Another organophosphate used to treat pests including aphids, mites, moths, *etc.* is ethyl parathion. However, it also has the potential to inadvertently harm the lives of birds and bees, prohibiting their use in agriculture. Two-dimensional nanomaterials have been used as chemi-resistive-based sensors to detect these compounds. It is shown how ε-arsenene may be employed in this study by Bhuvaneshwari *et al.* to detect the

presence of malathion and ethyl parathion. For both malathion and ethyl parathion, the energy band gap value for the valley-site adsorption of the target molecule on ε-arsenene was significantly lower than that for the top-site adsorption, which can be explained by the closer distance of interaction between the sulfur atom of the target molecule and the arsenic atom of ε-arsenene. In order to get meaningful insight into the electron redistribution when the target molecule interacts with the base material, the electron difference density (EDD) of pristine ε-arsenene and target molecule adsorbed ε-arsenene is estimated. Due to electron transmission, the target molecules' adsorption on ε-arsenene changes the electron availability. The charge transmission that occurs between the target molecule and the primary structure, as well as its direction of traversal, may be investigated by exploring the charge transfer (Q). The pristine ε-arsenene and target molecule adsorbed ε-arsenene nanosheet's electronic characteristics and adsorption attributes were estimated. Based on the factors calculated, including the energy band gap, projected density of states (PDOS) spectrum, electron density, adsorption energy, charge transfer, and average energy gap analysis, ε-arsenene nanosheets may be used as a chemi-resistive-based detector for the target molecules malathion and ethyl parathion.[175]

4.3.4. Detection of volatile tuberculosis biomarkers. *Mycobacterium tuberculosis* (Mtb) is the bacterium that causes the infectious lung disease known as tuberculosis (TB). Primary

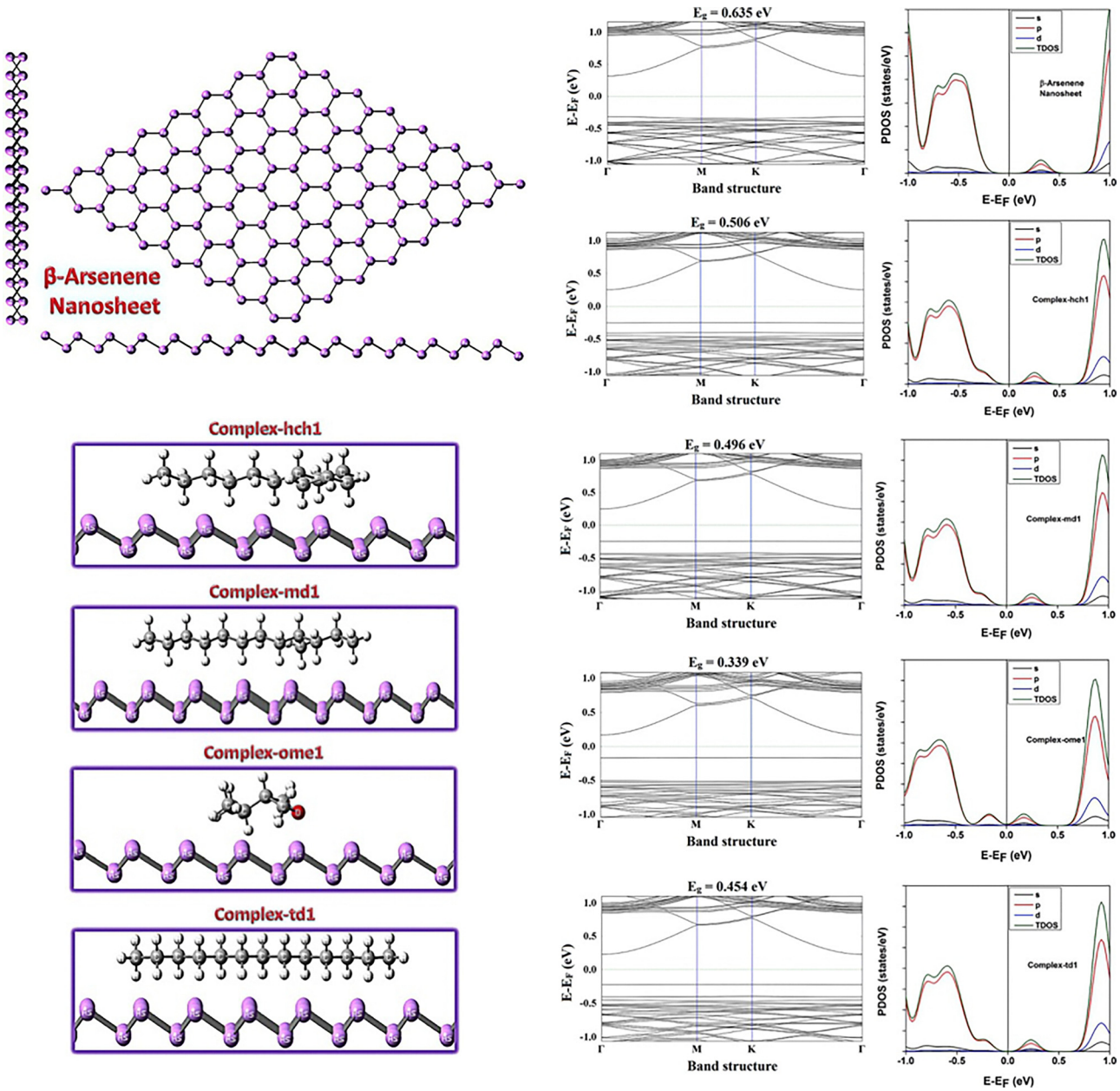

Fig. 26 pDOS and band structure maps of pristine beta-arsenene and beta-arsenene complexes with various TB biomarkers, reproduced from ref. 176 with permission from Elsevier, copyright 2021.

TB is mostly transferred by the sneeze or cough of the infected individual. Active TB may cause coughing, chest discomfort, bloody coughing, appetite loss, breathing trouble, exhaustion, and fever. Nagarajan *et al.* examined the absorption characteristics of four major volatile organic compounds (VOCs) as TB biomarkers such as hch1, md1, md2, ome1, and td1 on the beta-arsenene nanosheets as shown in Fig. 26. These VOCs are often related to the unique metabolism of Mtb and the host's response to infection.

Using the Atomistix Toolkit -VNL program, the electron density, band structure, and density of states were calculated. It has also been investigated how charge transfer, adsorption energy, and energy gap fluctuation relate to the adsorption characteristics of TB biomarkers. For the complexes hch1, md1, md2, ome1, and td1, the adsorption energy of TB biomarker VOCs following adsorption on beta-arsenene was measured. The range of 0.00–0.065 eV is discovered to represent the dispersion correction's (DFT-D3) effect on the estimation of the adsorption energy. The exothermic character of adsorption is shown by the computed values from adsorption energy, as evidenced from its negative values. The smaller magnitude of adsorption energy indicates physisorption, and the charge transfer analysis shows that beta-arsenene functions as an electron acceptor, while the TB biomarker VOCs act as electron donors. Beta-arsenene's electrical characteristics will alter as a result of the TB biomarker's adsorption. The average energy gap fluctuation may be used to estimate the second crucial component that guarantees the adsorption of TB biomarkers on beta-arsenene. The isolated beta-arsenene from the TB biomarker adsorbed beta–arsenene complex has an energy gap variation that ranges between 2.52 and 51.34%. The difference in the electrical characteristics of beta-arsenene caused by the adsorption of TB biomarkers is explained by the band structure analysis. Due to the TB biomarker's adsorption, peak maxima are seen in the beta-arsenene's conduction band and valence band. With the aid of transition state theory, the recovery period of beta-arsenene after the desorption of TB biomarkers is determined. It is discovered that the adsorption energy is a key factor in influencing how quickly beta-arsenene adsorbed at different sites would recover. When the TB biomarker was added, beta-arsenene's electrical characteristics changed, as seen from the band structure and PDOS spectrum. It is shown how beta-arsenene nanosheets may be utilized to qualitatively identify the presence of TB biomarker volatiles in TB patients' exhaled breath (Table 4).[176]

4.3.5. Drug delivery. Arsenene has the capability to undergo functionalization, which enables it to transport anticancer medications. Arsenene's functional groups can be altered to regulate the loading and release of medicines, so assuring targeted delivery to the tumour site. Targeted medication delivery can be achieved by altering the surface of arsenene with ligands or antibodies that specifically target cancer cell markers. This minimises the adverse impact on healthy tissues. Rosli *et al.* conducted a study on Janus nanomachines based on arsenene, which are composed of a layered structure. These nanomachines have a high loading capacity and were created by altering arsenene nanoparticles with platinum, resulting in the formation of As–Pt nanomotors. The synthesis and characterization of As–Pt nanomotors were effectively carried out using SEM, STEM, EDS, DLS, and XPS techniques. The propulsion tests showed rapid circular movement of As-Pt nanomotors using H_2O_2 as fuel, achieved through self-diffusiophoresis. Surprisingly, even with a very small amount of H_2O_2 (0.25%), these As–Pt nanomotors were able to move at a speed of 3 μm s^{-1}. In addition, it was discovered that As–Pt nanomotors are non-toxic at low concentrations, exhibit high cellular absorption into A549 cells, and show great potential for loading the medication doxorubicin (DOX). The DOX-loaded As–Pt nanomotors were seen to be successfully taken up by A549 cells, resulting in increased toxicity. This confirms that the

Table 4 Summary of theoretical arsenene-based biosensors and biomolecular interaction studies

No.	Target(s) studied	Main DFT/computational result/sensing indicator	Arsenene property leveraged	Notes	Study (Year)
1	DNA/RNA nucleobases (A, T, G, C, and U)	Adsorption energies: −0.34 to −0.46 eV, guanine strongest (−0.46 eV), charge transfer up to 0.03	Differential physisorption + charge transfer; bandgap modulation	ε-Arsenene shows selective nucleobase adsorption with slight DOS changes; guanine selectivity observed	Nagarajan *et al.* (2021)[173]
2	Vomiting agents (adamsite, chloropicrin, and diphenylchloroarsine)	Adsorption energies: −0.42 to −0.63 eV; charge transfer ∼0.04–0.09 e, bandgap reduction up to 0.27 eV	Strong physisorption; electronic conductivity changes; bandgap modulation	γ-Arsenene shows selective adsorption of toxic agents with measurable electronic responses; potential for chemical warfare agent detection	Swetha *et al.* (2020)[174]
3	Organophosphate pesticides: malathion and parathion	Adsorption energies: −0.45 to −0.58 eV, charge transfer ∼0.03–0.07 e, bandgap reduction up to 0.25 eV	Physisorption, charge transfer, bandgap sensitivity	ε-Arsenene shows selective adsorption of pesticides with detectable electronic property changes; potential for pesticide detection	Bhuvaneswari *et al.* (2020)[175]
4	Tuberculosis biomarker vapors (methyl nicotinate and methyl *p*-anisate)	Adsorption energies: −0.38 to −0.52 eV, charge transfer ∼0.02–0.05 e, bandgap reduction up to 0.21 eV	Physisorption, bandgap modulation, selective charge transfer	β-Arsenene selectively adsorbs TB biomarkers; measurable electronic changes suitable for sensing	Nagarajan *et al.* (2021)[176]
5	Acute promyelocytic leukemia (APL) nuclear proteins	Arsenene interacts preferentially with nuclear proteins *via* non-covalent binding; favorable binding energies	Biocompatibility; strong non-covalent biomolecular interactions; charge redistribution	Therapeutic study showing arsenene's biomolecular interaction capability; informs potential biosensor functionalization	Wang *et al.* (2020)[177]

As–Pt nanomotors are effective and biocompatible drug carriers for delivering DOX into human cells, which are easily internalized.[177]

5. Conclusions

To conclude, the exploration of the potential applications of phosphorene and arsenene in the field of biosensing presents fascinating opportunities for advancements in diagnostics and personalized therapy. The study's results indicate that the remarkable electrical, mechanical, and optical properties of 2D materials, combined with their elevated surface-to-volume ratios, render them highly appropriate for deployment in biosensing applications. Phosphorene, a monolayer allotrope of phosphorus, exhibits exceptional mobility of charge carriers, tunable bandgap, and significant light–matter interaction. As a consequence of this phenomenon, biosensors exhibit a significant enhancement in their signal-to-noise ratio, thereby resulting in augmentation of their sensitivity and specificity. The high chemical reactivity and capacity to form stable bonds with biomolecules make phosphorene a promising candidate for biosensor fabrication. Phosphorene exhibits particular utility in the realm of detecting minute molecules and proteins. Conversely, arsenene, a two-dimensional stratified material composed of arsenic atoms, exhibits equally remarkable properties. The tunability of its bandgap, high carrier mobility, and direct bandgap in the visible light range render it a highly promising contender for deployment in optical biosensing applications. A noteworthy attribute of arsenene is its chemical stability, which could potentially enhance the longevity and reliability of biosensors.

The amalgamation of phosphorene and arsenene with diverse nanomaterials and technologies has the potential to facilitate the development of hybrid biosensors that exhibit enhanced sensitivity, specificity, and multiplexing capabilities. The integration of 2D materials with microfluidic technologies has the potential to yield lab-on-a-chip devices that are capable of conducting intricate biological investigations. This would potentially expand the scope of diagnostic procedures that can be conducted at the point-of-care. Notwithstanding, significant challenges remain in the large-scale production, stability, and biocompatibility of phosphorene and arsenene. The existing methods of synthesis have not yet achieved full efficacy and controllability of the resulting products. Additionally, the environmental variability may pose a hindrance to the feasible application of such materials. An additional crucial aspect that necessitates further investigation pertains to ensuring the safety and compatibility of biological systems for interaction with humans.

Future research should focus on integrating plasmonic nanostructures with phosphorene and arsenene platforms to develop multimodal, hybrid biosensors capable of combining optical and electronic detection. Such plasmonic–2D material systems hold promise for intelligent sensor fusion, miniaturization, and multiplexed detection in clinical diagnostics. Additionally, novel approaches to enhancing the stability of these compounds and their biocompatibility should be explored. Furthermore, to fully maximize their potential, it is imperative to continue researching the fundamental characteristics of these materials, as well as their potential applications in biosensing. Phosphorene and arsenene represent a promising new frontier in the field of biosensor research and development. The unique attributes of these entities possess the capability to induce a significant transformation in this sector by facilitating the creation of diagnostic apparatus that exhibits heightened sensitivity, specificity, and reliability. Despite the challenges, the potential benefits justify the pursuit of further research and investment in this swiftly evolving field. As further research is conducted and a deeper comprehension of these intriguing materials is attained, it is plausible to anticipate a forthcoming era of advancements in biosensing technology. Should these innovations prove to be successful, their impact on healthcare and medicine could be substantial.

Conflicts of interest

All authors declare no conflicts of interest.

Data availability

This work is a review article and does not include any new experimental data. All data and materials discussed are obtained from previously published studies, cited accordingly, and reproduced with permission from the respective copyright holders. Full data supporting the conclusions of this review are available within the manuscript and the referenced literature.

References

1 A. P. Turner, Biosensors: sense and sensibility, *Chem. Soc. Rev.*, 2013, **42**(8), 3184–3196.
2 G. Selvolini and G. Marrazza, Sensor principles and basic designs, in *Fundamentals of Sensor Technology*, Woodhead Publishing, 2023, pp. 17–43.
3 S. P. Mohanty and E. Kougianos, Biosensors: A tutorial review, *IEEE potentials*, 2006, **25**(2), 35–40.
4 N. Bhalla, P. Jolly, N. Formisano and P. Estrela, Introduction to biosensors, *Essays Biochem.*, 2016, **60**, 1–8.
5 S. Wang, Y. Liu, A. Zhu and Y. Tian, In vivo electrochemical biosensors: Recent advances in molecular design, electrode materials, and electrochemical devices, *Anal. Chem.*, 2023, **95**(1), 388–406.
6 Z. L. Lei and B. Guo, 2D material-based optical biosensor: status and prospect, *Adv. Sci.*, 2022, **9**(4), 2102924.
7 P. Skládal, Piezoelectric biosensors: shedding light on principles and applications, *Microchim. Acta*, 2024, **191**(4), 184.
8 H. N. Abdelhamid, Calorimetric biosensors, in *Fundamentals of Biosensors in Healthcare*, Academic Press, 2025, pp. 359–372.

9 Z. Zhang, J. J. Hu, S. Lin, J. Wu, F. Xia and X. Lou, Field effect transistor biosensors for healthcare monitoring, *Interdiscip. Med.*, 2024, **2**(4), e20240032.
10 B. Bao, Y. Hua, R. Wang and D. Li, Quantum-Based Magnetic Field Sensors for Biosensing, *Adv. Quantum Technol.*, 2023, **6**(5), 2200146.
11 A. B. Dahlin, Size matters: problems and advantages associated with highly miniaturized sensors, *Sensors*, 2012, **12**(3), 3018–3036.
12 M. Pozzi, S. Jonak Dutta, M. Kuntze, J. Bading, J. S. Rüßbült, C. Fabig, M. Langfeldt, F. Schulz, P. Horcajada and W. J. Parak, Visualization of the high surface-to-volume ratio of nanomaterials and its consequences, *J. Chem. Educ.*, 2024, **101**(8), 3146–3155.
13 A. Vaseashta and D. Dimova-Malinovska, Nanostructured and nanoscale devices, sensors and detectors, *Sci. Technol. Adv. Mater.*, 2005, **6**(3–4), 312–318.
14 N. Yang, X. Chen, T. Ren, P. Zhang and D. Yang, Carbon nanotube based biosensors, *Sens. Actuators, B*, 2015, **207**, 690–715.
15 S. Noreen, M. B. Tahir, A. Hussain, T. Nawaz, J. U. Rehman, A. Dahshan, M. Alzaid and H. Alrobei, Emerging 2D-Nanostructured materials for electrochemical and sensing Application-A review, *Int. J. Hydrogen Energy*, 2022, **47**(2), 1371–1389.
16 M. C. Lemme, L. J. Li, T. Palacios and F. Schwierz, Two-dimensional materials for electronic applications, *MRS Bull.*, 2014, **39**(8), 711–718.
17 S. Su, Q. Sun, X. Gu, Y. Xu, J. Shen, D. Zhu, J. Chao, C. Fan and L. Wang, Two-dimensional nanomaterials for biosensing applications, *TrAC, Trends Anal. Chem.*, 2019, **119**, 115610.
18 A. Carvalho, M. Wang, X. Zhu, A. S. Rodin, H. Su and A. H. Castro Neto, Phosphorene: from theory to applications, *Nat. Rev. Mater.*, 2016, **1**(11), 1–6.
19 A. Vaidyanathan, M. Mathew, S. Radhakrishnan, C. S. Rout and B. Chakraborty, Theoretical insight on the biosensing applications of 2D materials, *J. Phys. Chem. B*, 2020, **124**(49), 11098–11122.
20 N. Rohaizad, C. C. Mayorga-Martinez, M. Fojtů, N. M. Latiff and M. Pumera, Two-dimensional materials in biomedical, biosensing and sensing applications, *Chem. Soc. Rev.*, 2021, **50**(1), 619–657.
21 A. E. Seitz, F. Hippauf, W. Kremer, S. Kaskel and M. Scheer, Facile storage and release of white phosphorus and yellow arsenic, *Nat. Commun.*, 2018, **9**(1), 361.
22 S. Minchin and J. Lodge, Understanding biochemistry: structure and function of nucleic acids, *Essays Biochem.*, 2019, **63**(4), 433–456.
23 V. Babrauskas, Phosphorus explosions, *Process Saf. Environ. Prot.*, 2017, **107**, 87–93.
24 R. Hultgren, N. S. Gingrich and B. E. Warren, The atomic distribution in red and black phosphorus and the crystal structure of black phosphorus, *J. Chem. Phys.*, 1935, **3**(6), 351–355.
25 L. Zhang, H. Huang, B. Zhang, M. Gu, D. Zhao, X. Zhao, L. Li, J. Zhou, K. Wu, Y. Cheng and J. Zhang, Structure and properties of violet phosphorus and its phosphorene exfoliation, *Angew. Chem.*, 2020, **132**(3), 1090–1096.
26 P. W. Bridgman, Two new modifications of phosphorus, *J. Am. Chem. Soc.*, 1914, **36**(7), 1344–1363.
27 D. Yin and Y. Yoon, Design strategy of two-dimensional material field-effect transistors: Engineering the number of layers in phosphorene FETs, *J. Appl. Phys.*, 2016, **119**(21), 214312.
28 J. Lu, J. Yang, A. Carvalho, H. Liu, Y. Lu and C. H. Sow, Light–matter interactions in phosphorene, *Acc. Chem. Res.*, 2016, **49**(9), 1806–1815.
29 R. Gusmao, Z. Sofer and M. Pumera, Black phosphorus rediscovered: from bulk material to monolayers, *Angew. Chem., Int. Ed.*, 2017, **56**(28), 8052–8072.
30 M. S. Islam, M. T. Islam and M. R. Hossain, Phosphorene: A novel nanomaterial revolutionizing biomedicine, *JCIS Open*, 2024, **16**, 100124.
31 S. Lin, Y. Chui, Y. Li and S. P. Lau, Liquid-phase exfoliation of black phosphorus and its applications, *FlatChem*, 2017, **2**, 15–37.
32 S. Ge, L. Zhang and Y. Fang, Photoluminescence mechanism of phosphorene quantum dots (PQDs) produced by pulsed laser ablation in liquids, *Appl. Phys. Lett.*, 2019, **115**(9), 092107.
33 W. Lu, H. Nan, J. Hong, Y. Chen, C. Zhu, Z. Liang, X. Ma, Z. Ni, C. Jin and Z. Zhang, Plasma-assisted fabrication of monolayer phosphorene and its Raman characterization, *Nano Res.*, 2014, **7**(6), 853–859.
34 L. Kou, C. Chen and S. C. Smith, Phosphorene: fabrication, properties, and applications, *J. Phys. Chem. Lett.*, 2015, **6**(14), 2794–2805.
35 S. Das, W. Zhang, M. Demarteau, A. Hoffmann, M. Dubey and A. Roelofs, Tunable transport gap in phosphorene, *Nano Lett.*, 2014, **14**(10), 5733–5739.
36 R. Gao, C. Jiang, D. Walker, H. Li and Z. Zheng, Molecular dynamics study on mechanical cleavage mechanisms of GaAs and experimental verification, *Ceram. Int.*, 2022, **48**(24), 36076–36083.
37 Y. Saito and Y. Iwasa, Ambipolar insulator-to-metal transition in black phosphorus by ionic-liquid gating, *ACS Nano*, 2015, **9**(3), 3192–3198.
38 L. Li, Y. Yu, G. J. Ye, Q. Ge, X. Ou, H. Wu, D. Feng, X. H. Chen and Y. Zhang, Black phosphorus field-effect transistors, *Nat. Nanotechnol.*, 2014, **9**(5), 372–377.
39 Z. Luo, J. Maassen, Y. Deng, Y. Du, R. P. Garrelts, M. S. Lundstrom, P. D. Ye and X. Xu, Anisotropic in-plane thermal conductivity observed in few-layer black phosphorus, *Nat. Commun.*, 2015, **6**(1), 8572.
40 Z. Yuan, D. Liu, N. Tian, G. Zhang and Y. Zhang, Structure, preparation and properties of phosphorene, *Acta Chim. Sin.*, 2016, **74**(6), 488.
41 J. O. Island, G. A. Steele, H. S. van der Zant and A. Castellanos-Gomez, Environmental instability of few-layer black phosphorus, *2D Mater.*, 2015, **2**(1), 011002.
42 A. E. Mag-isa, J. H. Kim, H. J. Lee and C. S. Oh, A systematic exfoliation technique for isolating large and pristine samples of 2D materials, *2D Mater.*, 2015, **2**(3), 034017.

43 Z. Guo, H. Zhang, S. Lu, Z. Wang, S. Tang, J. Shao, Z. Sun, H. Xie, H. Wang, X. F. Yu and P. K. Chu, From black phosphorus to phosphorene: basic solvent exfoliation, evolution of Raman scattering, and applications to ultrafast photonics, *Adv. Funct. Mater.*, 2015, **25**(45), 6996–7002.
44 P. Yasaei, B. Kumar, T. Foroozan, C. Wang, M. Asadi, D. Tuschel, J. E. Indacochea, R. F. Klie and A. Salehi-Khojin, High-quality black phosphorus atomic layers by liquid-phase exfoliation, *Adv. Mater.*, 2015, **27**(11), 1887–1892.
45 C. Huo, Z. Yan, X. Song and H. Zeng, 2D materials via liquid exfoliation: a review on fabrication and applications, *Sci. Bull.*, 2015, **60**(23), 1994–2008.
46 S. C. Dhanabalan, J. S. Ponraj, Z. Guo, S. Li, Q. Bao and H. Zhang, Emerging trends in phosphorene fabrication towards next generation devices, *Adv. Sci.*, 2017, **4**(6), 1600305.
47 Z. Yan, X. He, L. She, J. Sun, R. Jiang, H. Xu, F. Shi, Z. Lei and Z. H. Liu, Solvothermal-assisted liquid-phase exfoliation of large size and high quality black phosphorus, *J. Materiomics*, 2018, **4**(2), 129–134.
48 J. R. Brent, N. Savjani, E. A. Lewis, S. J. Haigh, D. J. Lewis and P. O'Brien, Production of few-layer phosphorene by liquid exfoliation of black phosphorus, *Chem. Commun.*, 2014, **50**(87), 13338–13341.
49 D. Hanlon, C. Backes, E. Doherty, C. S. Cucinotta, N. C. Berner, C. Boland, K. Lee, A. Harvey, P. Lynch, Z. Gholamvand and S. Zhang, Liquid exfoliation of solvent-stabilized few-layer black phosphorus for applications beyond electronics, *Nat. Commun.*, 2015, **6**(1), 8563.
50 W. Zhao, Z. Xue, J. Wang, J. Jiang, X. Zhao and T. Mu, Large-scale, highly efficient, and green liquid-exfoliation of black phosphorus in ionic liquids, *ACS Appl. Mater. Interfaces*, 2015, **7**(50), 27608–27612.
51 M. Bat-Erdene, M. Batmunkh, C. J. Shearer, S. A. Tawfik, M. J. Ford, L. Yu, A. J. Sibley, A. D. Slattery, J. S. Quinton, C. T. Gibson and J. G. Shapter, Efficient and fast synthesis of few-layer black phosphorus via microwave-assisted liquid-phase exfoliation, *Small Methods*, 2017, **1**(12), 1700260.
52 A. E. Castillo, C. D. Reyes-Vazquez, L. E. Rojas-Martinez, S. B. Thorat, M. Serri, A. L. Martinez-Hernandez, C. Velasco-Santos, V. Pellegrini and F. Bonaccorso, Single-step exfoliation and functionalization of few-layers black phosphorus and its application for polymer composites, *FlatChem*, 2019, **18**, 100131.
53 C. Shu, P. D. Zhou, P. D. Jia, H. Zhang, Z. Liu, W. Tang and X. Sun, Electrochemical exfoliation of two-dimensional phosphorene sheets and its energy application, *Chem. – Eur. J.*, 2022, **28**(49), e202200857.
54 A. Ambrosi, Z. Sofer and M. Pumera, Electrochemical exfoliation of layered black phosphorus into phosphorene, *Angew. Chem., Int. Ed.*, 2017, **56**(35), 10443–10445.
55 E. Kovalska, J. Luxa, T. Hartman, N. Antonatos, P. Shaban, E. Oparin, M. Zhukova and Z. Sofer, Non-aqueous solution-processed phosphorene by controlled low-potential electrochemical exfoliation and thin film preparation, *Nanoscale*, 2020, **12**(4), 2638–2647.
56 A. Ambrosi and M. Pumera, Exfoliation of layered materials using electrochemistry, *Chem. Soc. Rev.*, 2018, **47**(19), 7213–7224.
57 Y. Yang, H. Hou, G. Zou, W. Shi, H. Shuai, J. Li and X. Ji, Electrochemical exfoliation of graphene-like two-dimensional nanomaterials, *Nanoscale*, 2019, **11**(1), 16–33.
58 M. B. Erande, M. S. Pawar and D. J. Late, Humidity sensing and photodetection behavior of electrochemically exfoliated atomically thin-layered black phosphorus nanosheets, *ACS Appl. Mater. Interfaces*, 2016, **8**(18), 11548–11556.
59 X. Tang, W. Liang, J. Zhao, Z. Li, M. Qiu, T. Fan, C. S. Luo, Y. Zhou, Y. Li, Z. Guo and D. Fan, Fluorinated phosphorene: electrochemical synthesis, atomistic fluorination, and enhanced stability, *Small*, 2017, **13**(47), 1702739.
60 Z. Huang, H. Hou, Y. Zhang, C. Wang, X. Qiu and X. Ji, Layer-tunable phosphorene modulated by the cation insertion rate as a sodium-storage anode, *Adv. Mater.*, 2017, **29**(34), 1702372.
61 S. Yang, K. Zhang, A. G. Ricciardulli, P. Zhang, Z. Liao, M. R. Lohe, E. Zschech, P. W. Blom, W. Pisula, K. Müllen and X. Feng, A delamination strategy for thinly layered defect-free high-mobility black phosphorus flakes, *Angew. Chem.*, 2018, **130**(17), 4767–4771.
62 L. Zu, X. Gao, H. Lian, C. Li, Q. Liang, Y. Liang, X. Cui, Y. Liu, X. Wang and X. Cui, Electrochemical prepared phosphorene as a cathode for supercapacitors, *J. Alloys Compd.*, 2019, **770**, 26–34.
63 F. Luo, D. Wang, J. Zhang, X. Li, D. Liu, H. Li, M. Lu, X. Xie, L. Huang and W. Huang, Ultrafast cathodic exfoliation of few-layer black phosphorus in aqueous solution, *ACS Appl. Nano Mater.*, 2019, **2**(6), 3793–3801.
64 C. C. Mayorga-Martinez, N. Mohamad Latiff, A. Y. Eng, Z. Sofer and M. Pumera, Black phosphorus nanoparticle labels for immunoassays via hydrogen evolution reaction mediation, *Anal. Chem.*, 2016, **88**(20), 10074–10079.
65 X. Li, B. Deng, X. Wang, S. Chen, M. Vaisman, S. I. Karato, G. Pan, M. L. Lee, J. Cha, H. Wang and F. Xia, Synthesis of thin-film black phosphorus on a flexible substrate, *2D Mater.*, 2015, **2**(3), 031002.
66 J. B. Smith, D. Hagaman and H. F. Ji, Growth of 2D black phosphorus film from chemical vapor deposition, *Nanotechnology*, 2016, **27**(21), 215602.
67 J. L. Zhang, S. Zhao, C. Han, Z. Wang, S. Zhong, S. Sun, R. Guo, X. Zhou, C. D. Gu, K. D. Yuan and Z. Li, Epitaxial growth of single layer blue phosphorus: a new phase of two-dimensional phosphorus, *Nano Lett.*, 2016, **16**(8), 4903–4908.
68 Z. Yang, J. Hao, S. Yuan, S. Lin, H. M. Yau, J. Dai and S. P. Lau, Field-effect transistors based on amorphous black phosphorus ultrathin films by pulsed laser deposition, *Adv. Mater.*, 2015, **27**(25), 3748–3754.
69 Z. Wu, Y. Lyu, Y. Zhang, R. Ding, B. Zheng, Z. Yang, S. P. Lau, X. H. Chen and J. Hao, Large-scale growth of few-layer two-dimensional black phosphorus, *Nat. Mater.*, 2021, **20**(9), 1203–1209.

70 Y. Jing, X. Zhang and Z. Zhou, Phosphorene: what can we know from computations?, *Wiley Interdiscip. Rev.: Comput. Mol. Sci.*, 2016, **6**(1), 5–19.
71 A. Jain and A. J. McGaughey, Strongly anisotropic in-plane thermal transport in single-layer black phosphorene, *Sci. Rep.*, 2015, **5**(1), 8501.
72 A. Castellanos-Gomez, Black phosphorus: narrow gap, wide applications, *J. Phys. Chem. Lett.*, 2015, **6**(21), 4280–4291.
73 M. Wu, H. Fu, L. Zhou, K. Yao and X. C. Zeng, Nine new phosphorene polymorphs with non-honeycomb structures: a much extended family, *Nano Lett.*, 2015, **15**(5), 3557–3562.
74 J. Zhang, H. J. Liu, L. Cheng, J. Wei, J. H. Liang, D. D. Fan, P. H. Jiang and J. Shi, Thermal conductivities of phosphorene allotropes from first-principles calculations: a comparative study, *Sci. Rep.*, 2017, **7**(1), 4623.
75 A. N. Rudenko and M. I. Katsnelson, Quasiparticle band structure and tight-binding model for single-and bilayer black phosphorus, *Phys. Rev. B:Condens. Matter Mater. Phys.*, 2014, **89**(20), 201408.
76 A. Castellanos-Gomez, L. Vicarelli, E. Prada, J. O. Island, K. L. Narasimha-Acharya, S. I. Blanter, D. J. Groenendijk, M. Buscema, G. A. Steele, J. V. Alvarez and H. W. Zandbergen, Isolation and characterization of few-layer black phosphorus, *2D Mater.*, 2014, **1**(2), 025001.
77 M. Nehra, N. Dilbaghi, R. Kumar, S. Srivastava, K. Tankeshwar, K. H. Kim and S. Kumar, Catalytic applications of phosphorene: Computational design and experimental performance assessment, *Crit. Rev. Environ. Sci. Technol.*, 2024, **54**(3), 185–209.
78 A. Hashmi and J. Hong, Transition metal doped phosphorene: first-principles study, *J. Phys. Chem. C*, 2015, **119**(17), 9198–9204.
79 J. L. Luo, X. Zhu, L. Fan, F. Chen, C. M. Li, G. N. Li and Z. Q. Chen, Transition metal (TM= Cr, Mn, Fe, Co, Ni) doped phosphorene as anode material for lithium-ion batteries predicted from first-principle calculations, *Comput. Mater. Sci.*, 2020, **183**, 109877.
80 I. Khan and J. Hong, Manipulation of magnetic state in phosphorene layer by non-magnetic impurity doping, *New J. Phys.*, 2015, **17**(2), 023056.
81 L. Yang, W. Mi and X. Wang, Tailoring magnetism of black phosphorene doped with B, C, N, O, F, S and Se atom: a DFT calculation, *J. Alloys Compd.*, 2016, **662**, 528–533.
82 P. Srivastava, K. P. Hembram, H. Mizuseki, K. R. Lee, S. S. Han and S. Kim, Tuning the electronic and magnetic properties of phosphorene by vacancies and adatoms, *J. Phys. Chem. C*, 2015, **119**(12), 6530–6538.
83 T. Cao, X. Li, L. Liu and J. Zhao, Electric field and strain tunable electronic structures in monolayer Black Phosphorus, *Comput. Mater. Sci.*, 2016, **112**, 297–303.
84 G. H. Chen, Y. N. Chen, Y. W. Zhou, Y. L. Sun and E. J. Ye, Strain and electric field tunable electronic transport in armchair phosphorene nanodevice with normal-metal electrodes, *AIP Adv.*, 2020, **10**(10), 105012.
85 B. Sa, Y. L. Li, Z. Sun, J. Qi, C. Wen and B. Wu, The electronic origin of shear-induced direct to indirect gap transition and anisotropy diminution in phosphorene, *Nanotechnology*, 2015, **26**(21), 215205.
86 H. Liu, A. T. Neal, Z. Zhu, Z. Luo, X. Xu, D. Tománek and P. D. Ye, Phosphorene: an unexplored 2D semiconductor with a high hole mobility, *ACS Nano*, 2014, **8**(4), 4033–4041.
87 L. Li, J. Kim, C. Jin, G. J. Ye, D. Y. Qiu, F. H. Da Jornada, Z. Shi, L. Chen, Z. Zhang, F. Yang and K. Watanabe, Direct observation of the layer-dependent electronic structure in phosphorene, *Nat. Nanotechnol.*, 2017, **12**(1), 21–25.
88 X. Peng, Q. Wei and A. Copple, Strain-engineered direct-indirect band gap transition and its mechanism in two-dimensional phosphorene, *Phys. Rev. B:Condens. Matter Mater. Phys.*, 2014, **90**(8), 085402.
89 V. Tran, R. Soklaski, Y. Liang and L. Yang, Layer-controlled band gap and anisotropic excitons in few-layer black phosphorus, *Phys. Rev. B:Condens. Matter Mater. Phys.*, 2014, **89**(23), 235319.
90 H. Liu, A. T. Neal, Z. Zhu, Z. Luo, X. Xu, D. Tománek and P. D. Ye, Phosphorene: an unexplored 2D semiconductor with a high hole mobility, *ACS Nano*, 2014, **8**(4), 4033–4041.
91 H. Yuan, X. Liu, F. Afshinmanesh, W. Li, G. Xu, J. Sun, B. Lian, A. G. Curto, G. Ye, Y. Hikita and Z. Shen, Polarization-sensitive broadband photodetector using a black phosphorus vertical p–n junction, *Nat. Nanotechnol.*, 2015, **10**(8), 707–713.
92 K. Cho, J. Yang and Y. Lu, Phosphorene: An emerging 2D material, *J. Mater. Res.*, 2017, **32**(15), 2839–2847.
93 M. N. Brunetti, O. L. Berman and R. Y. Kezerashvili, Optical properties of anisotropic excitons in phosphorene, *Phys. Rev. B:Condens. Matter Mater. Phys.*, 2019, **100**(15), 155433.
94 M. Rohlfing and S. G. Louie, Electron-hole excitations and optical spectra from first principles, *Phys. Rev. B:Condens. Matter Mater. Phys.*, 2000, **62**(8), 4927.
95 J. M. Galicia Hernandez, H. N. Fernandez-Escamilla, J. Guerrero Sanchez and N. Takeuchi, Electronic and optical properties of the buckled and puckered phases of phosphorene and arsenene, *Sci. Rep.*, 2022, **12**(1), 20979.
96 A. S. Rodin, A. Carvalho and A. H. Castro Neto, Excitons in anisotropic two-dimensional semiconducting crystals, *Phys. Rev. B:Condens. Matter Mater. Phys.*, 2014, **90**(7), 075429.
97 L. Li, G. J. Ye, V. Tran, R. Fei, G. Chen, H. Wang, J. Wang, K. Watanabe, T. Taniguchi, L. Yang and X. H. Chen, Quantum oscillations in a two-dimensional electron gas in black phosphorus thin films, *Nat. Nanotechnol.*, 2015, **10**(7), 608–613.
98 N. Gillgren, D. Wickramaratne, Y. Shi, T. Espiritu, J. Yang, J. Hu, J. Wei, X. Liu, Z. Mao, K. Watanabe and T. Taniguchi, Gate tunable quantum oscillations in air-stable and high mobility few-layer phosphorene heterostructures, *2D Mater.*, 2014, **2**(1), 011001.
99 Q. Wei and X. Peng, Superior mechanical flexibility of phosphorene and few-layer black phosphorus, *Appl. Phys. Lett.*, 2014, **104**(25), 251915.

100 J. Y. Wang, Y. Li, Z. Y. Zhan, T. Li, L. Zhen and C. Y. Xu, Elastic properties of suspended black phosphorus nanosheets, *Appl. Phys. Lett.*, 2016, **108**(1), 013104.
101 Z. D. Sha, Q. X. Pei, Z. Ding, J. W. Jiang and Y. W. Zhang, Mechanical properties and fracture behavior of single-layer phosphorene at finite temperatures, *J. Phys. D: Appl. Phys.*, 2015, **48**(39), 395303.
102 J. W. Jiang and H. S. Park, Negative Poisson's ratio in single-layer black phosphorus, *Nat. Commun.*, 2014, **5**(1), 4727.
103 X. Cui, X. Tang, Y. Niu, L. Tong, H. Zhao, Y. Yang, G. Jin, M. Li and X. Han, Functional phosphorene: Burgeoning generation, two-dimensional nanotherapeutic platform for oncotherapy, *Coord. Chem. Rev.*, 2024, **507**, 215744.
104 J. R. Choi, K. W. Yong, J. Y. Choi, A. Nilghaz, Y. Lin, J. Xu and X. Lu, Black phosphorus and its biomedical applications, *Theranostics*, 2018, **8**(4), 1005.
105 V. Kumar, J. R. Brent, M. Shorie, H. Kaur, G. Chadha, A. G. Thomas, E. A. Lewis, A. P. Rooney, L. Nguyen, X. L. Zhong and M. G. Burke, Nanostructured aptamer-functionalized black phosphorus sensing platform for label-free detection of myoglobin, a cardiovascular disease biomarker, *ACS Appl. Mater. Interfaces*, 2016, **8**(35), 22860–22868.
106 S. Yan, B. Wang, Z. Wang, D. Hu, X. Xu, J. Wang and Y. Shi, Supercritical carbon dioxide-assisted rapid synthesis of few-layer black phosphorus for hydrogen peroxide sensing, *Biosens. Bioelectron.*, 2016, **80**, 34–38.
107 C. C. Mayorga-Martinez, Z. Sofer and M. Pumera, Binary phosphorene redox behavior in oxidoreductase enzymatic systems, *ACS Nano*, 2019, **13**(11), 13217–13224.
108 F. Shi, B. Wang, L. Yan, B. Wang, Y. Niu, L. Wang and W. Sun, In-situ growth of nitrogen-doped carbonized polymer dots on black phosphorus for electrochemical DNA biosensor of Escherichia coli O157: H7, *Bioelectrochemistry*, 2022, **148**, 108226.
109 H. Xu, J. Zheng, H. Liang and C. P. Li, Electrochemical sensor for cancer cell detection using calix [8] arene/polydopamine/phosphorene nanocomposite based on host–guest recognition, *Sens. Actuators, B*, 2020, **317**, 128193.
110 H. Liang, H. Xu, Y. Zhao, J. Zheng, H. Zhao, G. Li and C. P. Li, Ultrasensitive electrochemical sensor for prostate specific antigen detection with a phosphorene platform and magnetic covalent organic framework signal amplifier, *Biosens. Bioelectron.*, 2019, **144**, 111691.
111 Y. Chen, R. Ren, H. Pu, J. Chang, S. Mao and J. Chen, Field-effect transistor biosensors with two-dimensional black phosphorus nanosheets, *Biosens. Bioelectron.*, 2017, **89**, 505–510.
112 P. Li, D. Zhang, J. Liu, H. Chang, Y. E. Sun and N. Yin, Air-stable black phosphorus devices for ion sensing, *ACS Appl. Mater. Interfaces*, 2015, **7**(44), 24396–24402.
113 C. Zhang, H. Huang, J. Zhou, C. Hu, S. Li, D. Wei, Y. Tan and Y. Deng, A sensitive electrochemical aptasensor based on black phosphorus nanosheet for carbaryl detection, *Sci. Adv. Mater.*, 2022, **14**(12), 1836–1844.
114 Y. T. Yew, Z. Sofer, C. C. Mayorga-Martinez and M. Pumera, Black phosphorus nanoparticles as a novel fluorescent sensing platform for nucleic acid detection, *Mater. Chem. Front.*, 2017, **1**(6), 1130–1136.
115 C. C. Mayorga-Martinez, N. Mohamad Latiff, A. Y. Eng, Z. Sofer and M. Pumera, Black phosphorus nanoparticle labels for immunoassays via hydrogen evolution reaction mediation, *Anal. Chem.*, 2016, **88**(20), 10074–10079.
116 W. Gu, Y. Yan, X. Pei, C. Zhang, C. Ding and Y. Xian, Fluorescent black phosphorus quantum dots as label-free sensing probes for evaluation of acetylcholinesterase activity, *Sens. Actuators, B*, 2017, **250**, 601–607.
117 J. Peng, Y. Lai, Y. Chen, J. Xu, L. Sun and J. Weng, Sensitive detection of Carcinoembryonic antigen using stability-limited few-layer Black phosphorus as an electron donor and a reservoir, *Small*, 2017, **13**(15), 1603589.
118 W. Tao, X. Zhu, X. Yu, X. Zeng, Q. Xiao, X. Zhang, X. Ji, X. Wang, J. Shi, H. Zhang and L. Mei, Black phosphorus nanosheets as a robust delivery platform for cancer theranostics, *Adv. Mater.*, 2016, **29**, 1603276.
119 P. K. Sarswat, Y. K. Mishra and M. L. Free, Fabrication and response of alpha-hydroxybutyrate sensors for rapid assessment of cardiometabolic disease risk, *Biosens. Bioelectron.*, 2017, **89**, 334–342.
120 X. Meng, X. Wang, Z. Cheng, N. Tian, M. C. Lang, W. Yan, D. Liu, Y. Zhang and P. Wang, Photoluminescence lifetime of black phosphorus nanoparticles and their applications in live cell imaging, *ACS Appl. Mater. Interfaces*, 2018, **10**(37), 31136–31145.
121 H. U. Lee, S. Y. Park, S. C. Lee, S. Choi, S. Seo, H. Kim, J. Won, K. Choi, K. S. Kang, H. G. Park and H. S. Kim, Black phosphorus (BP) nanodots for potential biomedical applications, *Small*, 2016, **12**(2), 214–219.
122 C. Sun, L. Wen, J. Zeng, Y. Wang, Q. Sun, L. Deng, C. Zhao and Z. Li, One-pot solventless preparation of PEGylated black phosphorus nanoparticles for photoacoustic imaging and photothermal therapy of cancer, *Biomaterials*, 2016, **91**, 81–89.
123 J. B. Shao, C. F. Ni, P. F. Duan and Y. H. Jin, Preventive effects of different drugs on asymptomatic lower extremities deep venous thrombosis after artificial joint replacement: a mixed treatment comparison, *Am. J. Ther.*, 2019, **26**(1), e45–e53.
124 M. Seidl, G. Balazs and M. Scheer, The chemistry of yellow arsenic, *Chem. Rev.*, 2019, **119**(14), 8406–8434.
125 Y. Hu, J. Liang, Y. Xia, C. Zhao, M. Jiang, J. Ma, Z. Tie and Z. Jin, 2D arsenene and arsenic materials: fundamental properties, preparation, and applications, *Small*, 2022, **18**(9), 2104556.
126 S. Batool, M. Idrees, S. T. Han and Y. Zhou, 2D Layers of group VA semiconductors: fundamental properties and potential applications, *Adv. Sci.*, 2023, **10**(1), 2203956.
127 B. A. Hanedar, F. Ersan, T. Altalhi, M. Yagmurcukardes and B. Yakobson, Thickness-dependent piezoelecticity of black arsenic from few-layer to monolayer, *Solid State Commun.*, 2023, **368**, 115175.

128 O. Osters, T. Nilges, F. Bachhuber, F. Pielnhofer, R. Weihrich, M. Schöneich and P. Schmidt, Synthesis and identification of metastable compounds: Black arsenic—Science or fiction?, *Angew. Chem., Int. Ed.*, 2012, **51**(12), 2994.

129 A. Yoshiasa, M. Tokuda, M. Misawa, F. Shimojo, K. Momma, R. Miyawaki, S. Matsubara, A. Nakatsuka and K. Sugiyama, Natural arsenic with a unique order structure: potential for new quantum materials, *Sci. Rep.*, 2019, **9**(1), 6275.

130 R. Boča, P. Hajko, L. Benco, I. Benkovský and D. Faktor, Thin layers of grey arsenic: a molecular orbital study, *Czech. J. Phys.*, 1993, **43**(8), 813–819.

131 L. Kou, Y. Ma, X. Tan, T. Frauenheim, A. Du and S. Smith, Structural and electronic properties of layered arsenic and antimony arsenide, *J. Phys. Chem. C*, 2015, **119**(12), 6918–6922.

132 J. Yu, M. I. Katsnelson and S. Yuan, Tunable electronic and magneto-optical properties of monolayer arsenene: From GW 0 approximation to large-scale tight-binding propagation simulations, *Phys. Rev. B:Condens. Matter Mater. Phys.*, 2018, **98**(11), 115117.

133 P. Jamdagni, A. Thakur, A. Kumar, P. K. Ahluwalia and R. Pandey, Two dimensional allotropes of arsenene with a wide range of high and anisotropic carrier mobility, *Phys. Chem. Chem. Phys.*, 2018, **20**(47), 29939–29950.

134 J. Shah, W. Wang, H. M. Sohail and R. I. Uhrberg, Experimental evidence of monolayer arsenene: an exotic 2D semiconducting material, *2D Mater.*, 2020, **7**(2), 025013.

135 R. Zhou, N. Xu, R. Guo, G. Ling and P. Zhang, Preparation of arsenene and its applications in sensors, *J. Phys. D: Appl. Phys.*, 2021, **55**(16), 163002.

136 Y. Chen, C. Chen, R. Kealhofer, H. Liu, Z. Yuan, L. Jiang, J. Suh, J. Park, C. Ko, H. S. Choe and J. Avila, Black arsenic: a layered semiconductor with extreme in-plane anisotropy, *Adv. Mater.*, 2018, **30**(30), 1800754.

137 M. Zhong, Q. Xia, L. Pan, Y. Liu, Y. Chen, H. X. Deng, J. Li and Z. Wei, Thickness-dependent carrier transport characteristics of a new 2D elemental semiconductor: black arsenic, *Adv. Funct. Mater.*, 2018, **28**(43), 1802581.

138 H. Yun, S. Ghosh, P. Golani, S. J. Koester and K. A. Mkhoyan, Layer dependence of dielectric response and water-enhanced ambient degradation of highly anisotropic black As, *ACS Nano*, 2020, **14**(5), 5988–5997.

139 M. Eredia 2D materials: exfoliation in liquid-phase and electronics applications (Doctoral dissertation, Université de Strasbourg).

140 S. M. Beladi-Mousavi, A. M. Pourrahimi, Z. Sofer and M. Pumera, Atomically thin 2D-arsenene by liquid-phased exfoliation: toward selective vapor sensing, *Adv. Funct. Mater.*, 2019, **29**(5), 1807004.

141 R. Gusmão, Z. Sofer, D. Bouša and M. Pumera, Pnictogen (As, Sb, Bi) nanosheets for electrochemical applications are produced by shear exfoliation using kitchen blenders, *Angew. Chem.*, 2017, **129**(46), 14609–14614.

142 E. Kovalska, N. Antonatos, J. Luxa and Z. Sofer, ''Top-down'' arsenene production by low-potential electrochemical exfoliation, *Inorg. Chem.*, 2020, **59**(16), 11259–11265.

143 J. Sturala, Z. Sofer and M. Pumera, Coordination chemistry of 2D and layered gray arsenic: photochemical functionalization with chromium hexacarbonyl, *NPG Asia Mater.*, 2019, **11**(1), 42.

144 J. Zhao, C. Liu, W. Guo and J. Ma, Prediction on the light-assisted exfoliation of multilayered arsenene by the photoisomerization of azobenzene, *Nanoscale*, 2017, **9**(21), 7006–7011.

145 P. Vishnoi, M. Mazumder, S. K. Pati and C. R. Rao, Arsenene nanosheets and nanodots, *New J. Chem.*, 2018, **42**(17), 14091–14095.

146 H. S. Tsai, S. W. Wang, C. H. Hsiao, C. W. Chen, H. Ouyang, Y. L. Chueh, H. C. Kuo and J. H. Liang, Direct synthesis and practical bandgap estimation of multilayer arsenene nanoribbons, *Chem. Mater.*, 2016, **28**(2), 425–429.

147 R. Bhuvaneswari, V. Nagarajan and R. Chandiramouli, Recent advances in arsenene nanostructures towards prediction, properties, synthesis and applications, *Surf. Interfaces*, 2022, **28**, 101610.

148 S. Nahas, A. Bajaj and S. Bhowmick, Polymorphs of two dimensional phosphorus and arsenic: insight from an evolutionary search, *Phys. Chem. Chem. Phys.*, 2017, **19**(18), 11282–11288.

149 C. Kamal and M. Ezawa, Arsenene: Two-dimensional buckled and puckered honeycomb arsenic systems, *Phys. Rev. B:Condens. Matter Mater. Phys.*, 2015, **91**(8), 085423.

150 S. Mardanya, V. K. Thakur, S. Bhowmick and A. Agarwal, Four allotropes of semiconducting layered arsenic that switch into a topological insulator via an electric field: Computational study, *Phys. Rev. B*, 2016, **94**(3), 035423.

151 B. Zhang, H. Zhang, J. Lin and X. Cheng, First-principle study of seven allotropes of arsenene and antimonene: thermodynamic, electronic and optical properties, *Phys. Chem. Chem. Phys.*, 2018, **20**(48), 30257–30266.

152 D. Kecik, E. Durgun and S. Ciraci, Stability of single-layer and multilayer arsenene and their mechanical and electronic properties, *Phys. Rev. B*, 2016, **94**(20), 205409.

153 S. Zhang, Z. Yan, Y. Li, Z. Chen and H. Zeng, Atomically thin arsenene and antimonene: semimetal–semiconductor and indirect–direct band-gap transitions, *Angew. Chem., Int. Ed.*, 2015, **54**(10), 3112–3115.

154 C. Wang, Q. Xia, Y. Nie, M. Rahman and G. Guo, Strain engineering band gap, effective mass and anisotropic Dirac-like cone in monolayer arsenene, *AIP Adv.*, 2016, **6**(3), 035204.

155 P. Jamdagni, A. Thakur, A. Kumar, P. K. Ahluwalia and R. Pandey, Superior mechanical and electronic properties of novel 2D allotropes of As and Sb monolayers, *J. Phys. Chem. C*, 2019, **123**(44), 27214–27221.

156 Z. Cui, M. Wang, N. Lyu, S. Zhang, Y. Ding and K. Bai, Electronic, magnetism and optical properties of transition metals adsorbed puckered arsenene, *Superlattices Microstruct.*, 2021, **152**, 106852.

157 Y. Wang, P. Huang, M. Ye, R. Quhe, Y. Pan, H. Zhang, H. Zhong, J. Shi and J. Lu, Many-body effect, carrier mobility, and device performance of hexagonal arsenene and antimonene, *Chem. Mater.*, 2017, **29**(5), 2191–2201.

158 M. Zhong, Q. Xia, L. Pan, Y. Liu, Y. Chen, H. X. Deng, J. Li and Z. Wei, Thickness-dependent carrier transport characteristics of a new 2D elemental semiconductor: black arsenic, *Adv. Funct. Mater.*, 2018, **28**(43), 1802581.

159 Y. Xu, B. Peng, H. Zhang, H. Shao, R. Zhang and H. Zhu, First-principle calculations of optical properties of monolayer arsenene and antimonene allotropes, *Ann. Phys.*, 2017, **529**(4), 1600152.

160 D. Kecik, E. Durgun and S. Ciraci, Optical properties of single-layer and bilayer arsenene phases, *Phys. Rev. B*, 2016, **94**(20), 205410.

161 X. Zhou, W. Feng, F. Li and Y. Yao, Large magneto-optical effects in hole-doped blue phosphorene and gray arsenene, *Nanoscale*, 2017, **9**(44), 17405–17414.

162 X. Liu, L. Liu, L. Yang, X. Wu and P. K. Chu, Optical identification of topological defect types in monolayer arsenene by first-principles calculation, *J. Phys. Chem. C*, 2016, **120**(43), 24917–24924.

163 J. Guo, G. Liu and Z. Sun, Effect of Size Change on Mechanical Properties of Monolayer Arsenene, *J. Wuhan Univ. Technol., Mater. Sci. Ed.*, 2024, **39**(1), 206–212.

164 D. Guo, B. Shao, C. Li and Y. Ma, Theoretical insight into structure stability, elastic property and carrier mobility of monolayer arsenene under biaxial strains, *Superlattices Microstruct.*, 2016, **100**, 324–334.

165 H. Zhang, Y. Ma and Z. Chen, Quantum spin hall insulators in strain-modified arsenene, *Nanoscale*, 2015, **7**(45), 19152–19159.

166 K. Iordanidou, J. Kioseoglou, V. V. Afanas'Ev, A. Stesmans and M. Houssa, Intrinsic point defects in buckled and puckered arsenene: a first-principles study, *Phys. Chem. Chem. Phys.*, 2017, **19**(15), 9862–9871.

167 T. Van Mourik, M. Bühl and M. P. Gaigeot, Density functional theory across chemistry, physics and biology, *Philos. Trans. R. Soc., A*, 2014, **372**(2011), 20120488.

168 S. Dutta, S. Corni and G. Brancolini, Atomistic simulations of functionalized nano-materials for biosensors applications, *Int. J. Mol. Sci.*, 2022, **23**(3), 1484.

169 A. Vaidyanathan, M. Mathew, S. Radhakrishnan, C. S. Rout and B. Chakraborty, Theoretical insight on the biosensing applications of 2D materials, *J. Phys. Chem. B*, 2020, **124**(49), 11098–11122.

170 Z. Khoshbin, M. R. Housaindokht, M. Izadyar, M. R. Bozorgmehr and A. Verdian, Recent advances in computational methods for biosensor design, *Biotechnol. Bioeng.*, 2021, **118**(2), 555–578.

171 G. Chellasamy, E. Varathan, K. Sekar, S. Venkateswarlu, S. Govindaraju and K. Yun, Single-atom catalysts for biosensing: Progress in theoretical and mechanistic understanding, *Coord. Chem. Rev.*, 2024, **502**, 215606.

172 V. Nagarajan, S. Sarvaka and R. Chandiramouli, Adsorption studies of nucleobases on ε-arsenene nanosheet based on first-principles research, *J. Mol. Graphics Modell.*, 2021, **103**, 107827.

173 B. Swetha, V. Nagarajan, A. Soltani and R. Chandiramouli, Novel gamma arsenene nanosheets as sensing medium for vomiting agents: A first-principles research, *Comput. Theor. Chem.*, 2020, **1185**, 112876.

174 R. Bhuvaneswari, V. Nagarajan and R. Chandiramouli, Novel ε-arsenene nanosheets for sensing toxic malathion and parathion–a first-principles approach, *Comput. Theor. Chem.*, 2020, **1190**, 112995.

175 V. Nagarajan, S. Sundar and R. Chandiramouli, Interaction studies of tuberculosis biomarker vapours on novel beta arsenene sheets–A DFT insight, *Comput. Theor. Chem.*, 2021, **1205**, 113426.

176 X. Wang, Y. Hu, J. Mo, J. Zhang, Z. Wang, W. Wei, H. Li, Y. Xu, J. Ma, J. Zhao and Z. Jin, Arsenene: a potential therapeutic agent for acute promyelocytic leukaemia cells by acting on nuclear proteins, *Angew. Chem.*, 2020, **132**(13), 5189–5196.

177 A. H. Woomer, T. W. Farnsworth, J. Hu, R. A. Wells, C. L. Donley and S. C. Warren, Phosphorene: synthesis, scale-up, and quantitative optical spectroscopy, *ACS Nano*, 2015, **9**(9), 8869–8884.